Aus dem Institut für Schlaganfall- und Demenzforschung
der Ludwig-Maximilians-Universität München
Klinik der Universität München
Direktor: Prof. Dr. med. Martin Dichgans

HDAC9-related alterations to NF-κB-signalling in atherogenic inflammation

Dissertation
zum Erwerb des Doktorgrades der Medizin
an der Medizinischen Fakultät der
Ludwig-Maximilians-Universität München

vorgelegt von

Thomas Alexander Campbell-James, MPH

aus Bielefeld

Jahr
2025

Mit Genehmigung der Medizinischen Fakultät der
Ludwig-Maximilians-Universität zu München

Berichterstatter:	Prof. Dr. med. Martin Dichgans
Mitberichterstatter:	PD Dr. Roland Kälin
	Prof. Dr. Thomas Pfefferkorn
	Prof. Dr. Lars Kellert
Mitbetreuung durch den promovierten Mitarbeiter:	Dr. rer. nat. Yaw Asare
Dekan:	Prof. Dr. med. Thomas Gudermann
Tag der mündlichen Prüfung:	10.07.2025

In loving memory of my “Oma”, Gerda Paula Stegmaier

The majority of results presented in this dissertation were previously published in:

Asare Y, **Campbell-James TA**, Bokov Y, Yu LL, Prestel M, El Bounkari O, Roth S, Megens RTA, Straub T, Thomas K, Yan G, Schneider M, Ziesch N, Tiedt S, Silvestre-Roig C, Braster Q, Huang Y, Schneider M, Malik R, Haffner C, Liesz A, Soehnlein O, Bernhagen J, Dichgans M. **Histone Deacetylase 9 Activates IKK to Regulate Atherosclerotic Plaque Vulnerability.** *Circulation Research.* 2020 Aug 28;127(6):811-823[1].

1. Table of Contents

2. Abstract

Background: Atherosclerosis – the leading cause of morbidity and premature mortality worldwide and a driver of healthcare costs – is a chronic inflammatory arterial disease underlying most primary clinical manifestations of CVD. GWAS have associated elevated *HDAC9*-expression with LAS and other atherosclerotic complications. It plays a prominent role in driving pro-atherogenic vascular inflammation, atheroprogression and plaque vulnerability. Previous research confirmed HDAC9-dependent p65-phosphorylation at ser468 and ser536, activating NF-κB-signalling. However, the exact link between HDAC9 and NF-κB – including potential for therapeutic targeting – requires further investigation.

Methods: To explore interactions between HDAC9 and NF-κB-signalling, along with their mechanistic role and downstream effects, wild type and *Hdac9*-depleted samples were generated from murine BMDMs, HEK293 cells and HUVECs. Depending on the experimental setup, *HDAC9* was knocked down or co-transfected with an NF-κB signalling component. The samples were then employed for protein complex immunoprecipitation, kinase activity assays, TNFα-stimulation or ELISAs.

Results: Interactions were identified for HDAC9 with IKKα and IKKβ in both HEK293 cells and HUVECs, establishing a crucial link between HDAC9 and pro-atherogenic inflammation. Further, IKKα and IKKβ were demonstrated to undergo HDAC9-mediated deacetylation. Heightened HDAC9-mediated kinase activity was revealed for IKKβ, enhancing p65-phosphorylation at ser536. HDAC9-depletion in HUVECs did not affect TNFα-stimulated p65-phosphorylation at ser276, diverging from findings for both ser468 and ser536. IKKβ-inhibition significantly reduced Ccl2-secretion in wild type BMDMs, whilst showing no effect in *Hdac9*-depleted samples, suggesting a non-additive mechanistic overlap between HDAC9 and IKKβ.

Conclusion: HDAC9 interacts with NF-κB-signalling via IKKα and IKKβ, resulting in their deacetylation. HDAC9 enhances IKKβ kinase activity, stimulating pro-atherogenic downstream NF-κB-activity. Specific inhibition of HDAC9's catalytic domain and the identified interactions may offer promising therapeutic strategies in atherosclerosis, heightening selectivity and reducing off-target effects.

3. Zusammenfassung

Hintergrund: Atherosklerose, die weltweit führende Ursache für Morbidität sowie vorzeitige Mortalität und ein Treiber von Gesundheitskosten, ist eine für viele primäre klinische Manifestationen von CVD ursächliche chronisch entzündliche Arterienerkrankung. GWAS assoziierten zuvor erhöhte *HDAC9*-Expression mit LAS und anderen atherosklerotischen Komplikationen. HDAC9 spielt eine zentrale Rolle bei pro-atherogener vaskulärer Entzündung, Atheroprogression und Plaquevulnerabilität. Frühere Ergebnisse bestätigen eine HDAC9-abhängige Phosphorylierung von p65 an ser468 und ser536, die eine Aktivierung der NF-κB-Signalübertragung zur Folge hat. Der genaue Zusammenhang zwischen HDAC9 und NF-κB, sowie das therapeutische Potenzial, bleiben aber weiterhin unklar.
Methoden: Zur Untersuchung von Interaktionen zwischen HDAC9 und NF-κB, sowie deren mechanistische Rolle und nachgeschaltete Folgeeffekte, wurden wildtyp und *Hdac9*-depletierte Proben aus murinen BMDMs, HEK293-Zellen und HUVECs erzeugt. *HDAC9* wurde entweder herunterreguliert oder mit einer Signalkomponente von NF-κB ko-transfiziert. Proben wurden für Protein-Komplex-Immunpräzipitation, Kinase-Aktivitätsassays, TNFα-Stimulation oder ELISAs eingesetzt.
Ergebnisse: In HEK293-Zellen und HUVECs wurden Interaktionen für HDAC9 mit IKKα und IKKβ nachgewiesen, die den Zusammenhang zwischen HDAC9 und pro-atherogener Inflammation entscheidend herstellen. IKKα und IKKβ wurden in Anwesenheit von HDAC9 deacetyliert. Eine erhöhte HDAC9-vermittelte Kinaseaktivität von IKKβ verstärkte die Phosphorylierung von p65 an ser536. Im Kontrast zu Ergebnissen für ser468 und ser536, beeinflusste die Depletion von HDAC9 in HUVECs die TNFα-stimulierte Phosphorylierung von p65 an ser276 nicht. Hinweisgebend für einen nicht-additiven mechanistischen Overlap von HDAC9 und IKKβ, reduzierte die Inhibition von IKKβ die Ccl2-Sekretion in wildtyp-BMDMs, während sie in *Hdac9*-depletierten Proben keine Wirkung zeigte.
Fazit: HDAC9 interagiert mit NF-κB via IKKα und IKKβ, was zu deren Deacetylierung führt. HDAC9 erhöht die Kinaseaktivität von IKKβ und stimuliert pro-atherogene NF-κB-Aktivität. Selektive katalytische Hemmung von HDAC9 und der identifizierten Interaktionen könnte neuartige therapeutische Strategien zur Eindämmung von Atherosklerose ermöglichen und Off-Target-Effekte reduzieren.

4. Introduction

4.1. Ischaemic stroke

4.1.1. Overview

Accounting for 11.6% of global mortality and 5.7% of disability-adjusted life years (DALYs), stroke is the second most common cause of premature death and the third leading cause of combined death and disability worldwide[2]. In 2019, there were 12.2 million global incident cases and at 25 years of age, the global lifetime risk for stroke approximates 24.9% in both men and women, with the majority of lifetime risk – 18.3% – falling on ischaemic stroke[2,3].

At 7.63 million incident cases in 2019 – 64.2% of all global incidence of stroke in that year – ischaemic stroke is the most common form[2]. It is defined as an episode of neurological dysfunction caused by hypoxia-induced cell death in the central nervous system[4]. Ischaemic stroke accounts for half of all stroke-related deaths worldwide and is also dominant in Germany, which faced 225,531 cases in 2019[2,5]. With an ageing population, incidence and the substantial associated economic burden are set to rise. In 2017, Germany's stroke-induced healthcare expenditures and productivity losses amounted to €17.6 billion – 0.54% of its GDP[6].

Ischaemic strokes are typically thromboembolic in nature, whereby an atherosclerotic plaque ruptures, resulting in distal embolisation of cerebral vasculature[7]. Globally and in Germany, a fifth of ischaemic stroke cases are attributed to large artery atherosclerosis[8,9]. This subcategory of ischaemic stroke, Large Artery Stroke (LAS), is defined as a complete occlusion or significant stenosis (of at least 50% in diameter) of a major brain artery or branch cortical artery, with presumed atherosclerotic aetiology[10].

Advances in treatment and risk factor control are thought to explain a global 34.0% reduction in ischaemic stroke's age-standardised mortality between 1990 and 2019, with steeper declines in developed countries[2,11–13]. Recent studies of modifiable risk factors – including hypertension, smoking, elevated blood levels of low-density lipoprotein (LDL) cholesterol and a lack of physical activity and diabetes – imply

significant preventability of the condition: 85.7% to 91.5% of global DALYs caused by ischaemic stroke are attributed to modifiable risk factors[2,10]. Besides age, sex, race and other non-modifiable risk factors, interest in genetic determinants is increasingly gaining traction[14]. Figure 1 categorises the different types of ischaemic stroke by aetiology.

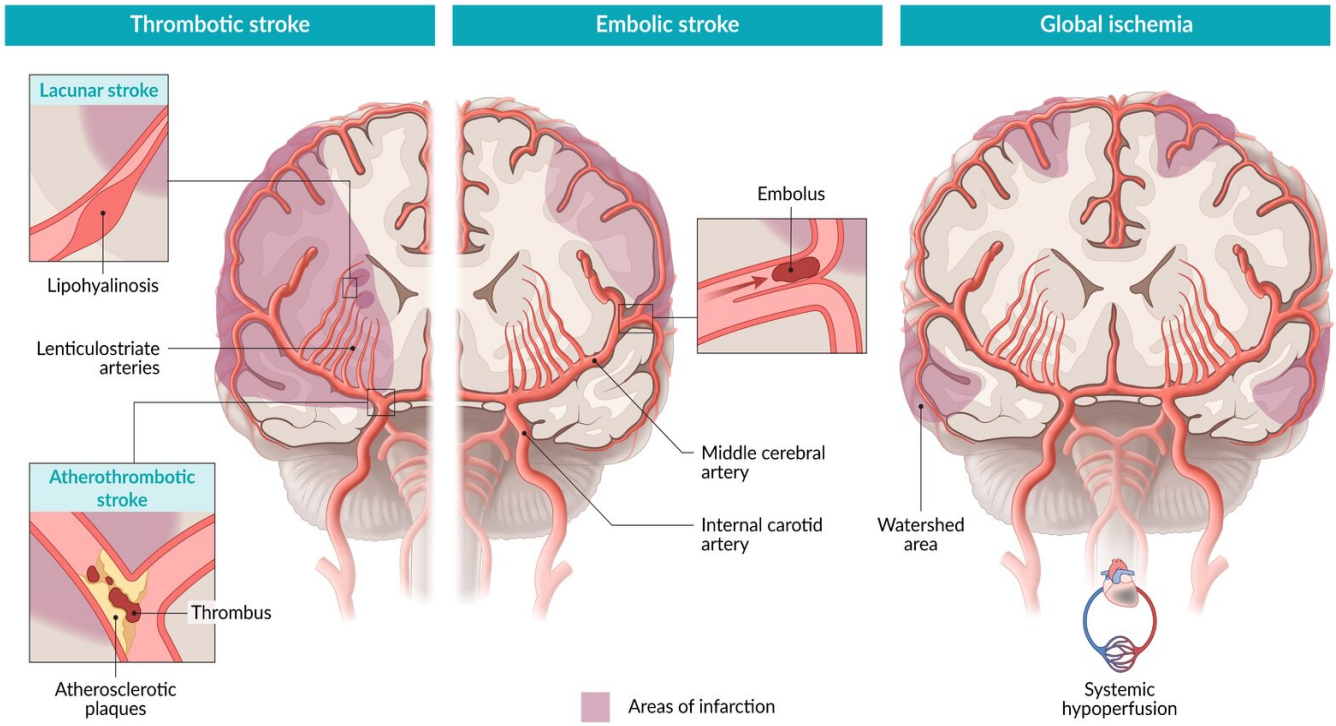

Figure 1: Types of ischaemic stroke

Ischaemic strokes are typically thromboembolic in nature. Rupture of ulcerated and stenotic atherosclerotic plaques results in distal embolization of cerebral vasculature. Large arteries are most commonly affected (LAS), with the Middle Cerebral Artery being the most prominent example. In thrombotic stroke, the source of the thrombus is located in the arteries supplying blood to the brain. Characteristically, culprit atherosclerotic plaques are located in the Internal Carotid Artery immediately distal to the bifurcation from the Common Carotid Artery. Intracranial atherosclerosis is sometimes also observed. Embolic stroke is characterised by debris originating from other parts of the body, such as ruptured thrombi from the left atrium following atrial fibrillation (cardioembolic stroke). Hypoxia induces cell death in the central nervous system, whereby resulting neurological dysfunction depends on the area of primary arterial occlusion[7]. Figure from Amboss GmbH (2023)[15].

4.1.2. The rs2107595-risk locus as a genetic determinant of ischaemic stroke

Advances in technology are assisting continuous knowledge expansion surrounding ischaemic stroke's genetic determinants. Various single-gene disorders associated with LAS have been identified via gene sequencing, including Fabry and sickle cell disease, while a genome-wide association study (GWAS) approximated LAS' genetic heritability at 40.3%[14,16,17]. GWAS allow for the definition of common genetic variants

– usually defined as having an allele frequency of at least 0.5% – by comparing the frequency of variants between predetermined phenotypes. Single nucleotide polymorphisms (SNPs) are the most common form of variant[16]. The first stroke GWAS, conducted using European ancestry data, identified the SNP rs2107595, an intergenic risk variant between *HDAC9* and *TWIST1* on chromosome 7p21.1, as the strongest risk variant for LAS. Each allele copy increased risk by 40%[16,18]. This finding was confirmed by the MEGASTROKE-collaboration, which conducted a transancestral meta-analysis of GWAS among 521,612 individuals, identifying rs2107595 to obtain genome-wide significance for stroke, ischaemic stroke and LAS at an odds ratio of 1.21[19]. The MEGASTROKE-results are depicted in Figure 2. Demonstrating a gene-dosage effect and implying a specificity for *HDAC9*-transcription, rs2107595 was then associated with elevated *HDAC9*-expression levels in murine peripheral blood mononuclear cells, but not with increased mRNA-levels of its other two neighbouring contenders, *TWIST1* and *FERD3L*[16,20]. The findings were confirmed in human blood-derived macrophages[21].

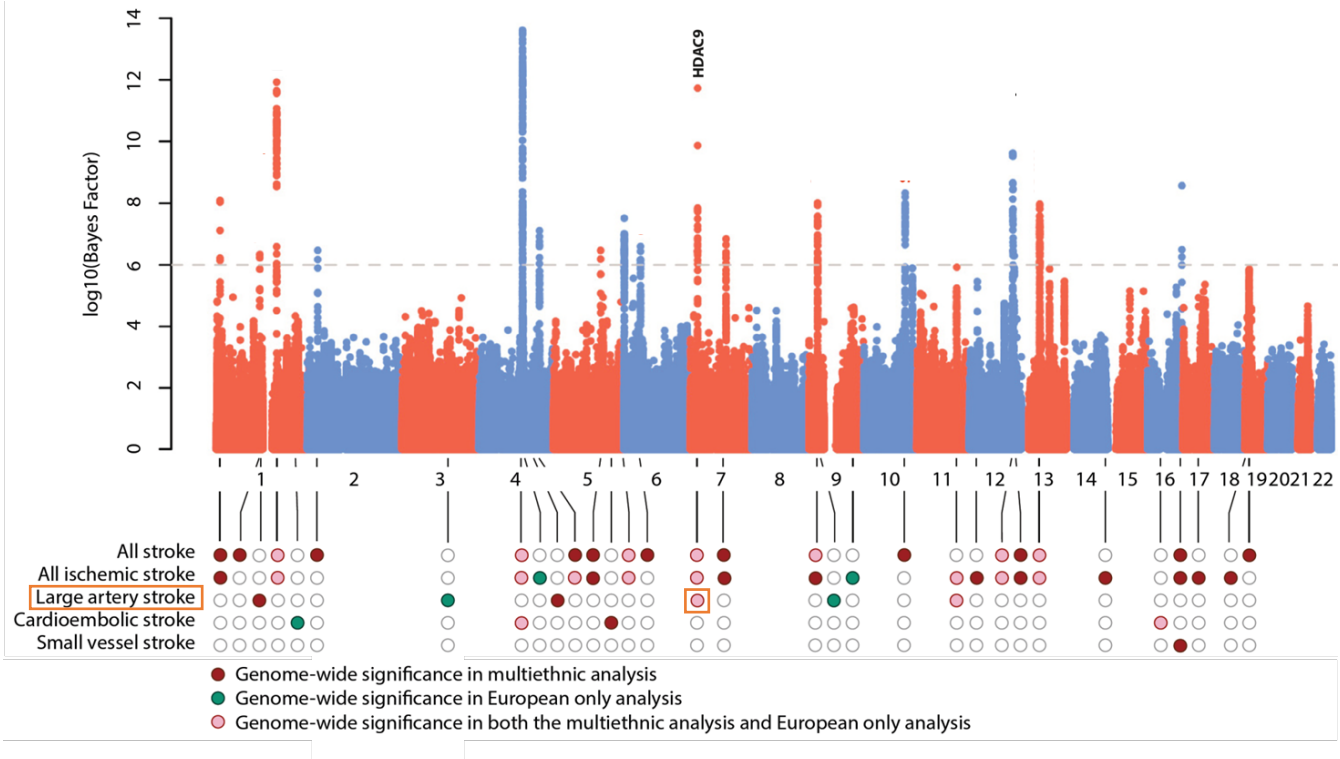

Figure 2: HDAC9 is a major risk locus for large artery atherosclerotic stroke

Manhattan plot visualising the findings of a transancestral meta-analysis of GWAS conducted by the MEGASTROKE-collaboration among 521,612 individuals. HDAC9 was identified as the strongest risk locus for LAS. rs2107595 further obtained genome-wide significance for stroke and ischaemic stroke. Figure adapted from Malik et al. (2018)[19].

Leading to the suspicion of a role in atherosclerosis, the variant was further identified in various GWAS as a common risk locus in coronary artery disease (CAD), myocardial infarction, peripheral artery disease (PAD), atherosclerotic aortic calcification and Moyamoya, a disease involving stenotic carotids[22–27]. Immunohistochemical evidence associating the SNP with carotid intima-media thickness and the presence of carotid plaque further strengthened the hypothesis that rs2107595 increases the risk for ischaemic stroke via pro-atherogenicity[23]. This theory was underlined by research conducted in our group, finding *HDAC9*-deficiency to attenuate murine atherosclerotic plaque size and formation[20].

In summary, rs2107595 is the lead SNP for LAS. It results in elevated *HDAC9*-expression and plays a role in various other atherosclerotic complications. However, notwithstanding the overwhelming evidence associating HDAC9 with LAS, arterial inflammation and atherogenesis, the exact mechanism remains unclear.

4.2. Atherosclerosis

4.2.1. Overview

Atherosclerosis is a chronic inflammatory arterial disease involving both an innate and adaptive immune response[28,29]. Pathogenically, it underlies most primary clinical manifestations of cardiovascular disease (CVD) – ischaemic stroke, CAD and PAD, in particular – making it the leading cause of global premature mortality and morbidity and a driver of rising healthcare costs worldwide[11,28,30–32]. Notwithstanding treatment-related global declines in vascular mortality, 35.3% of Germany's deaths in 2019 were linked to CVD, while the global burden attributable to modifiable risk factors increases continuously[11,31,33].

Atherosclerosis is exacerbated by various modifiable risk factors, including arterial hypertension and elevated blood levels of LDL[11,28,34]. The chronic inflammatory process is characterised by an expansion of the tunica intima via the formation of plaques protruding into the arterial lumen[28,35].

4.2.2. Atherogenesis

Atherosclerosis typically develops in the arterial wall at specific predilection sites: arches and bifurcations of medium-sized to large vessels of the arterial system exposed to shear stress and disturbed laminar blood flow[35,36]. The ensuing endothelial injury leads to subendothelial accumulation of LDL, its intimal retention and subsequent oxidation to oxLDL[37,38]. oxLDL triggers the endothelial secretion of adhesion molecules and chemokines, resulting in increased endothelial permeability and leukocyte infiltration into the intima – monocytes in particular – and further induces the transformation of accumulating intimal monocytes into macrophages[28,39,40]. The pro-inflammatory environment, heightened by the continued secretion of various pro-inflammatory chemokines, including MIF, CXCL1 and CCL2, drives further monocyte recruitment[41]. This leads to the development of 'fatty streaks', an early subendothelial lesion comprised predominantly of foam cells – macrophages that have taken up oxLDL via phagocytosis – and T-cells[28,40,42].

Characterised by a progressing fibrous cap, these early lesions mature into fibroatheromatous plaques. This follows macrophage-mediated migration of smooth muscle cells (SMCs) from the tunica media to the intima, intimal SMC- and collagen-accumulation, intimal calcification and the development of a necrotic core comprised of accumulated apoptotic cell debris and extracellular cholesterol[28,42,43].

4.2.3. Complications

As fibroatheromatous plaques progress in advanced stages of atherosclerosis, clinical manifestations become increasingly likely. Plaque growth-induced luminal narrowing may result in a limitation of blood flow and downstream ischaemia. The risk for complicative plaque rupture increases[44]. Intrinsically, rupture-prone plaque vulnerability is aggravated by fibrous cap thinning – through the depletion of SMCs and collagen – and an expansion of the lipiduous necrotic core induced by lesional macrophage and other cell death[45,46]. Extrinsically, hypertension and high velocity blood flow augment the risk of plaque rupture, particularly in the lesion's shoulder

regions[28,47]. Plaque rupture – the predominant cause of thrombosis – leads to blood's exposure to thrombogenic plaque material, collagen and lipids in the necrotic core, resulting in clotting and eventual downstream thrombotic vessel occlusion[47–49]. Most plaque ruptures remain silent with autopsy data indicating that 9% of healthy, asymptomatic individuals display ruptured plaques in their coronaries[47,50]. Some clinical manifestations of atherosclerotic plaque rupture, such as myocardial infarction, are acute and catastrophic. Haemodynamically significant thrombotic luminal stenosis of cerebral arteries can culminate in ischaemic LAS[51]. The pathogenesis of atherosclerosis and its complications is depicted in Figure 3.

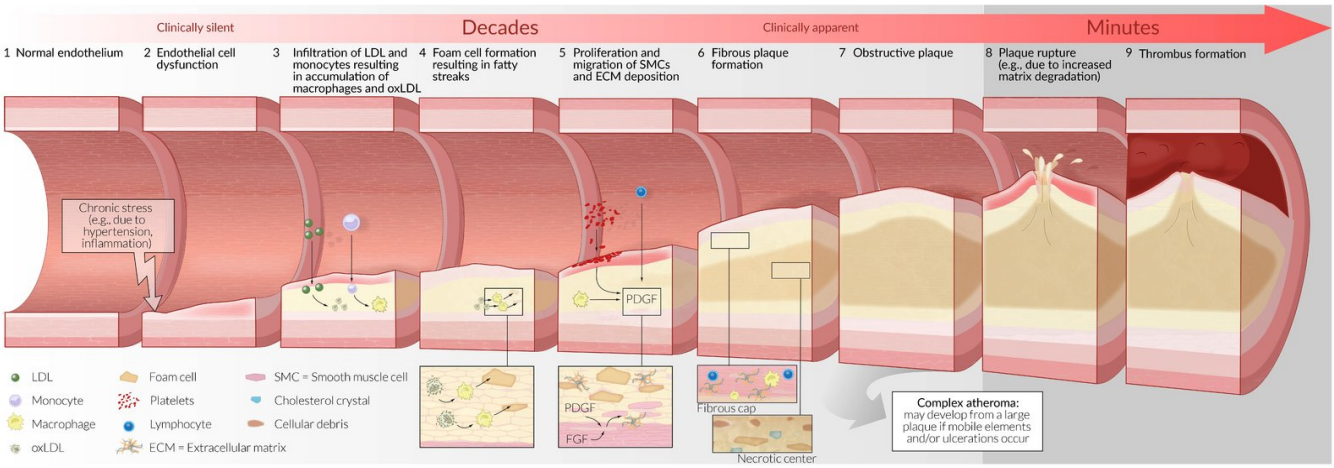

Figure 3: Schematic illustration of atherogenesis

Healthy arterial endothelium progresses towards dysfunction due to exposure to chronic stress, induced by the likes of arterial hypertension and chronic inflammation. Ensuing endothelial injury permits LDL and monocytes to infiltrate the intima and accumulate as macrophages and oxLDL. Macrophages then take up oxLDL via phagocytosis and transform into foam cells, resulting in fatty streaks. Stimulated by growth factors like PDGF and FGF, SMCs proliferate and migrate from the tunica media towards the intima, depositing extracellular matrix components. Surrounded by a stable fibrous cap, a lipid necrotic core develops, comprised of accumulated apoptotic cell debris and extracellular cholesterol. The plaque grows over decades, with increasing clinical apparency due to the luminal obstruction of blood flow. Plaque rupture can lead to rapid thrombus formation, potentially resulting in acute clinical events. Figure from Amboss GmbH (2024)[52].

4.3. Histone deacetylases

4.3.1. Overview and classification

Eucaryotic cells' genetic information is organised in nucleic chromosomes. These are ordinarily found in the form of compact structures containing deoxyribonucleic acid (DNA) wrapped around histones, which serve as key controllers of gene expression[53,54]. Their N-terminal domains contain positively charged amino acids –

prominently, lysine and arginine – allowing for chromatin condensation by binding with DNA's negatively charged backbone. This compacts the DNA – thereby effectively suppressing gene transcription – and can be regulated by reversible post-translational modifications (PTMs). These include acetylation, phosphorylation and methylation[53–55]. In particular, epigenetic mechanisms resulting in the acetylation and deacetylation of histones' lysine residues – conducted by histone acetyltransferases (HATs) and histone deacetylases (HDACs) respectively – have been identified as fundamental to transcriptional regulation. Whereas histone-acetylation by HATs decompacts the DNA – via removal of a lysine residue's positive charge to promote gene transcription – HDAC-induced histone deacetylation has the opposite effect. This results in suppression of gene transcription[54,55]. Figure 4 depicts the processes of histone-acetylation and deacetylation by HATs and HDACs.

However, beyond interactions with histones to suppress transcription, HDACs' ability to deacetylate target proteins has other far-reaching regulatory effects. Their deacetylation of non-histone proteins' lysine residues typically modulates protein-protein interactions (PPIs), target proteins' activation-status and enzymatic activity, depending on the lysine residue in question[56,57]. Mass spectrometry has identified 3,600 acetylation sites on 1750 proteins involved in regulating cell cycle, nuclear translocation and a range of other cellular processes[58]. Both in- and outside the nucleus, HDACs interact with various important non-histone substrate proteins, including transcription factor p53, α-tubulin and oestrogen receptor α[56,57,59]. Due to their extensive regulatory effects, HDACs have been identified to play a role in oncogenesis for various types of cancer – often characterised by the regulation of inflammatory and immune pathways – and, among others, various cardiovascular, neurological and immunological diseases[60–70].

18 different HDACs have been identified in humans, which are divided into four classes. These are based on the zinc-dependence of their enzymatic activity and the conservation of a deacetylase domain. Enzymatic activity of classes I, IIa, IIb and IV is Zn^{2+}-dependent, in contrast to class III – known as sirtuins – whose enzymatic activity is dependent on the availability of cofactor NAD^+. Sirtuins are not typically categorised as classical histone deacetylases[60,69,71].

Class I HDACs are ubiquitously expressed nuclear proteins and – due to their characteristic role as histone modifiers – are predominantly involved in cell proliferation and survival. This is explained by their strong deacetylase activity and subcellular nucleic localisation[69,71]. HDAC3 provides an exception, being able to shuttle between the nucleus and cytoplasm. Shuttling facilitates the mediation of other HDACs' deacetylase activity – particularly that of class II HDACs – as multiprotein complexes are formed to confer transcriptional co-repression[69,72].

Expression of the remaining classes of HDACs typically exhibits characteristic tissue-specificity[64,72,73]. Class II HDACs maintain a conserved deacetylase domain with reduced activity compared to members of class I. They are subdivided into the classes IIa and IIb[69]. Class IIb and IV HDACs are primarily expressed in the kidneys, liver and heart and, at a subcellular level, predominantly localised in the cytoplasm and nucleus respectively[64,73].

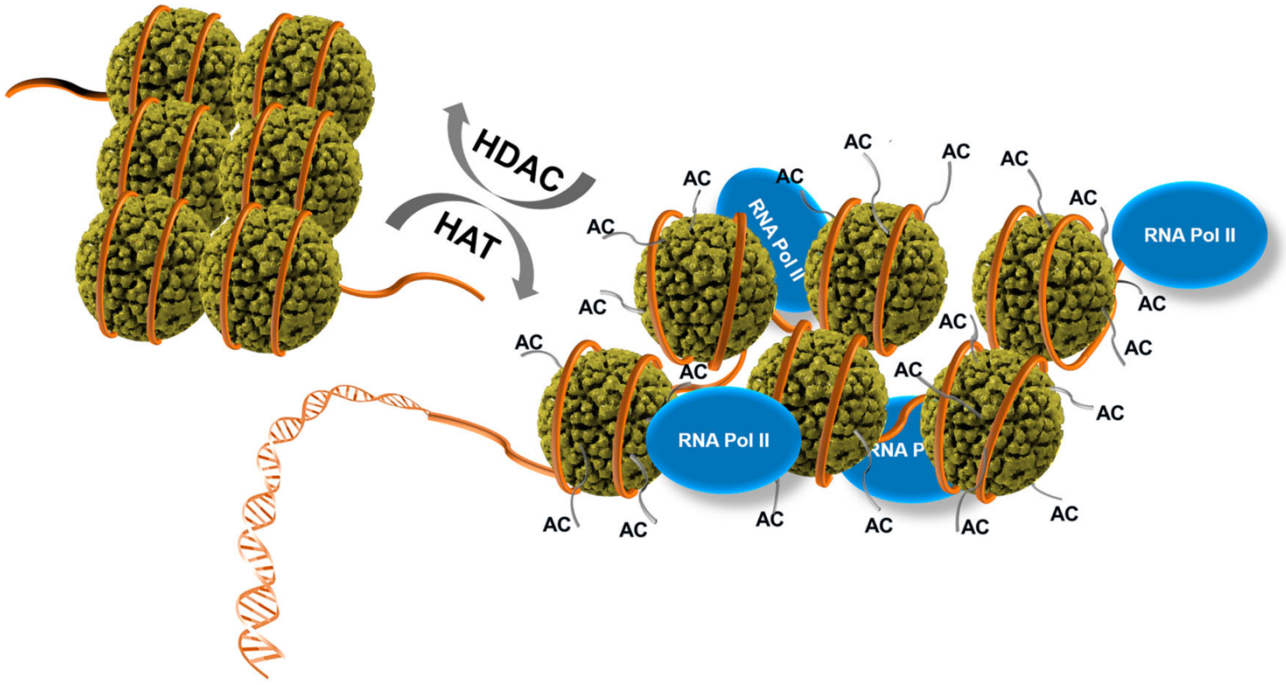

Figure 4: HDACs and HATs regulate gene expression via histone acetylation

HATs acetylate (AC) histones' lysine residues, resulting in an open chromatin configuration that facilitates the attachment of RNA polymerase II (RNA Pol II) for gene expression. Conversely, HDACs remove acetyl groups, resulting in a compact chromatin structure repressing gene expression. Figure from Park et al. (2020)[69].

4.3.2. Class IIa histone deacetylases

HDAC9 is grouped into the class IIa family, which also includes HDAC4, HDAC5 and HDAC7[69]. Members of class IIa are characteristically expressed cerebrally and in cardiac and skeletal muscles[74,75]. At a subcellular level, this family of HDACs shuttles between the nucleus – where they typically act as repressors of myocyte enhancer factor-2 (MEF2)-dependent transcription – and the cytoplasm. Their N-terminal domain enables interactions with transcription factors while nuclear export signals in their C-terminal domain regulate subcellular localisation. Shuttling of class IIa HDACs from the nucleus to the cytoplasm is induced by phosphorylation of specific serine residues and subsequent binding of chaperone 14-3-3 proteins[64,76,77]. Subcellular transport out of the nucleus prevents class IIa HDACs from functioning as transcriptional repressors, thereby inducing gene expression[60,64,78]. HDAC4, HDAC5 and HDAC7 are deemed dependent on the formation of large nucleic multiprotein complexes to establish deacetylase activity. These include the transcription co-repressors SMRT and N-CoR as well as HDAC3, which was found to confer the totality of deacetylase activity associated with the complexes[64,72]. In select cases, class IIa HDACs may conversely recruit transcriptional co-activators to stimulate gene expression[79–81]. In summary, class IIa HDACs modulate transcription, usually via repression and independent of their intrinsic HDAC-activity. This often involves binding large nucleic, enzymatically active multiprotein complexes containing transcription co-factors and other HDACs[64,72].

4.3.3. Histone deacetylase 9 (HDAC9)

Research into HDAC9 – a member of the family of class IIa HDACs – is gaining traction. Due to its critical role in regulating transcription, cell differentiation and proliferation, it has been associated with several diseases ranging from various cancers to intracranial aneurysms[82–87]. It further promotes angiogenesis by stimulating endothelial cell sprouting and is associated with obesity-related metabolic disease, downregulating adipocyte differentiation and reducing glucose tolerance and insulin sensitivity[88–91]. Critically for this study, HDAC9 has been associated with

atherosclerosis and ischaemic stroke and has also been found to regulate pro-inflammatory responses[1,16–20,60,91].

HDAC9 demonstrates tissue-specific expression. Typically, said tissue-specificity is defined as brain, skeletal myocytes and peripheral blood cells[73,75,87]. However, HDAC9 also shows significant expression in cells relevant to atherosclerosis, including macrophages, endothelial and SMCs[23,87,88,91,92].

HDAC9 plays a prominent role in a range of tissue-specific physiological processes – both in the cytoplasm, via interaction with other non-histone proteins, and the nucleus, where it typically functions as a transcription repressor[87]. Phosphorylation of its ser223 and ser253-residues is hypothesised to result in its transportation from the nucleus to the cytoplasm, facilitated by the binding of chaperone 14-3-3 proteins[75]. This prevents HDAC9's nucleic interaction with MEF2, a transcription factor involved in cell division and differentiation, regulating myogenesis in skeletal and cardiac muscles, angiogenesis and other forms of development[93–95]. While HDAC9's binding of MEF2 in the nucleus represses MEF2-mediated transcription, said effect is reduced when HDAC9 shuttles into the cytoplasm[96]. Further, HDAC9's function as a repressor of MEF2-mediated transcription is independent of its intrinsic enzymatic activity[87,97–99].

HDAC9 maintains its enzymatic function via the conservation of its deacetylase domain, as seen in other class IIa HDACs. However, while these exhibit reduced enzymatic activity, HDAC9 has been found to deacetylate both histones and non-histone proteins[75,96,100]. HDAC9's endogenous interaction with TANK-binding kinase 1 (TBK1) via its deacetylase domain was identified in mouse peritoneal macrophages. Here, direct HDAC9-mediated deacetylation of TBK1's lysine residue lys241 heightened kinase activity, leading to an enhanced antiviral innate immune response[100].

HDAC9-involvement in further immunological processes indicates a prominent role as a driver of inflammation. In a model of murine colitis – an inflammatory bowel disease displaying a 12-fold increase of locally expressed HDAC9 – its inhibition prevented or reduced case severity. *Hdac9*-deletion reproduced similar results and

was associated with increased suppressive Foxp3^{+}-regulatory T cell-function (T_{reg})[101]. HDAC9 is exported from the nucleus upon T_{reg}-activation, which is thought to be necessary for optimal T_{reg}-function[62]. At a molecular level, HDAC9 establishes a functional complex with FOXP3, a transcriptional repressor and regulator of T_{reg}-function and development[102]. In summary, HDAC9 has been linked to inflammation via the enhancement of innate immune responses and its interaction with crucial regulators to modulate immune cell function.

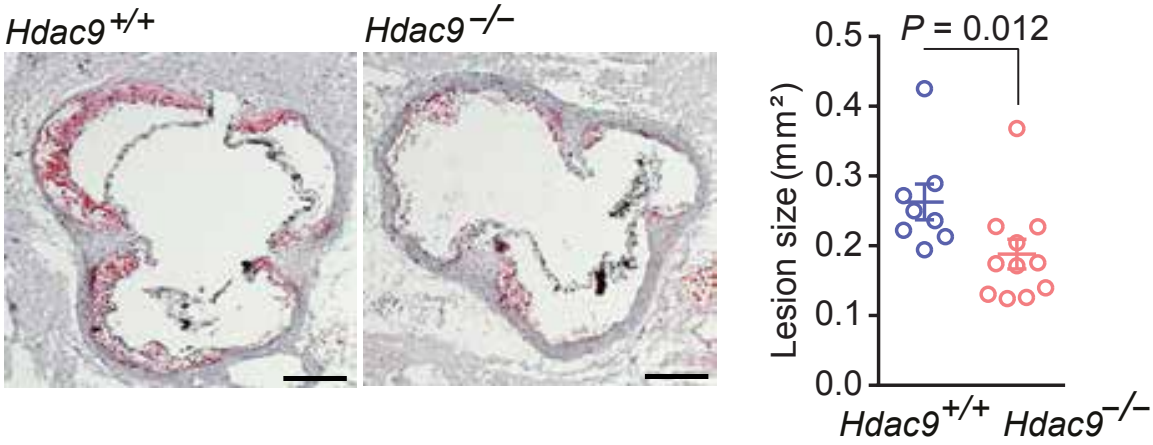

Figure 5: *Hdac9*-deficiency reduces aortic root lesion size

Experimental outline: Lethally irradiated Apoe$^{-/-}$ mice were reconstituted with bone marrow from either *Hdac9*$^{-/-}$ *Apoe*$^{-/-}$ (*Hdac9*$^{-/-}$ BM) or *Hdac9*$^{+/+}$*Apoe*$^{-/-}$ (*Hdac9*$^{+/+}$ BM) mice and fed a Western-type diet for 11 weeks to induce advanced atherosclerosis. **Left:** Representative images of Oil-Red-O stained aortic root lesion. Scale bars, 200 µm. **Right:** Quantification of lesion sizes. Figure adapted from Asare et al. (2020)[1].

4.3.4. HDAC9's pro-inflammatory role in atherosclerosis

Various GWAS have associated *HDAC9* with atherosclerosis, a chronic inflammatory arterial disease[16,18,19,22–27]. Our group previously linked rs2107595 – a risk allele at *HDAC9* – to elevated mRNA-expression of *HDAC9* in two atherosclerosis-relevant cells: macrophages and human peripheral blood mononuclear cells. The findings were emphasised by a gene-dosage effect[20,21]. The risk allele was also associated with elevated plasma levels of HDAC9 in patients with CAD[103]. *HDAC9*-expression is upregulated in human atherosclerotic plaques, with our group replicating the finding in an *Hdac9*-deficient murine model displaying reduced atherosclerotic plaque size and formation[20,23]. *Hdac9*-upregulation in macrophages is atherogenic via the repression of cholesterol efflux and generation of alternatively activated, pro-

inflammatory macrophages[91]. Further, HDAC9 partly mediates oxLDL-cell viability suppression and cell apoptosis via TNFα-expression in HUVECs[104].

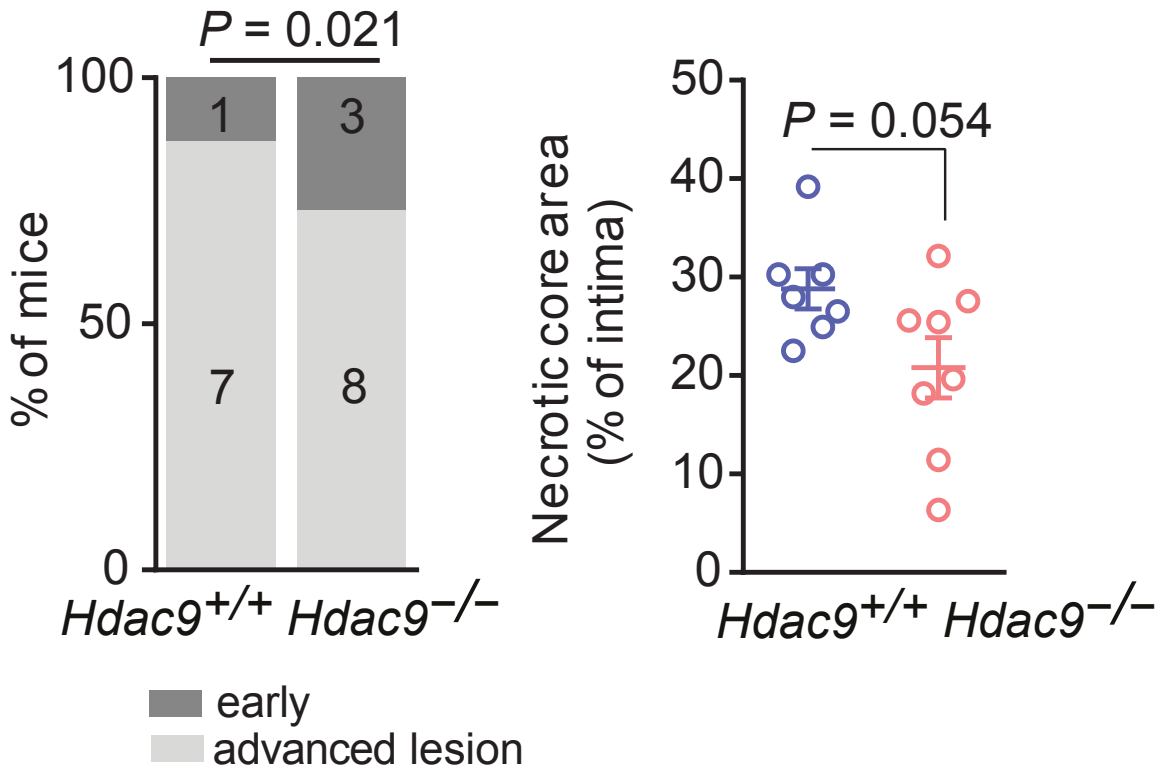

Figure 6: *Hdac9*-deficiency reduces lesion development

Experimental outline: Lethally irradiated *Apoe*$^{-/-}$ mice were reconstituted with bone marrow from either *Hdac9*$^{-/-}$ *Apoe*$^{-/-}$ (*Hdac9*$^{-/-}$ BM) or *Hdac9*$^{+/+}$*Apoe*$^{-/-}$ (*Hdac9*$^{+/+}$ BM) mice and fed a Western-type diet for 11 weeks to induce advanced atherosclerosis. **Left:** Classification of atherosclerotic lesions into early and advanced via Masson-trichrome staining. **Right:** Quantification of necrotic core area as a percentage of the tunica intima. Figure adapted from Asare et al. (2020)[1].

Prior to this study, our group was able to solidify the link between HDAC9 and vascular inflammation. HDAC9 was shown to promote pro-inflammatory responses and increase atherosclerotic plaque vulnerability. Compared to control bone marrow, aortic root lesion size and lesion development were reduced in lethally irradiated *Apoe*$^{-/-}$ atherosclerotic mice that had been reconstituted with *Hdac9*$^{-/-}$ *Apoe*$^{-/-}$-bone marrow. Further, haematopoietic *Hdac9*-deficiency was shown to attenuate multiple characteristics of atherosclerotic plaque vulnerability: necrotic core and intimal macrophage area were both reduced while fibrous cap thickness was increased. Finally, *Hdac9*-deficienct bone marrow-derived macrophages (BMDMs) displayed reduced TNFα-induced mRNA-expression and secretion of various pro-atherogenic cytokines and chemokines. Our group's discoveries – summarised in Figures 5 to 7

– are indicative of HDAC9's role in vascular inflammation, suggesting promotion of atherosclerotic plaque vulnerability and pro-inflammatory responses via the haematopoietic vascular compartment[1]. However, the exact link between HDAC9 and vascular inflammation and its potential as a therapeutic target require further exploration.

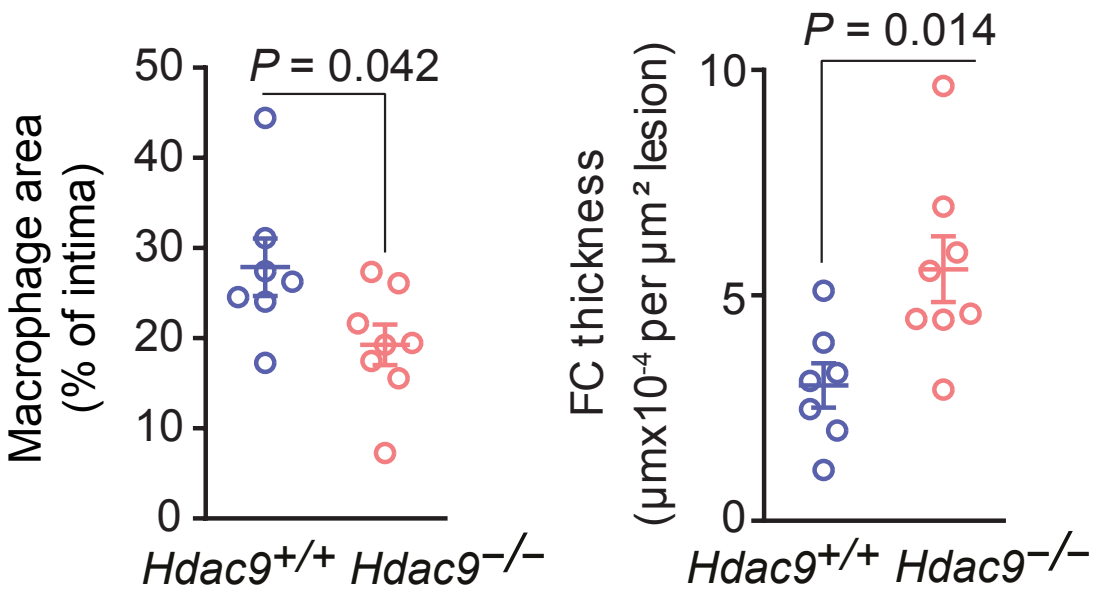

Figure 7: *Hdac9*-deficiency attenuates atherosclerotic plaque vulnerability

Experimental outline: Lethally irradiated *Apoe*$^{-/-}$ mice were reconstituted with bone marrow from either *Hdac9*$^{-/-}$ *Apoe*$^{-/-}$ (*Hdac9*$^{-/-}$ BM) or *Hdac9*$^{+/+}$*Apoe*$^{-/-}$ (*Hdac9*$^{+/+}$ BM) mice and fed a Western-type diet for 11 weeks to induce advanced atherosclerosis. **Left:** Quantification of macrophage area as a percentage of the tunica intima. **Right:** Quantification of fibrous cap thickness. Figure adapted from Asare et al. (2020)[1].

4.3.5. HDAC9 as a therapeutic target

HDAC-involvement in the pathogenesis of various diseases – including oncological, cardiovascular, immune and neurological conditions – is well-studied and established[60–70]. Thus, interest in their potential as therapeutic targets is high.

HDACs boast ubiquitarian relevance in tissue-specific development and physiological processes, and predictably, their genetic deletion typically results in dramatic phenotypes that are incompatible with life. Full deletion of genes coding for

all class I HDACs, as well as HDAC4 and HDAC7 from the class IIa-family, result in early or embryonic murine lethality. However, genetic ablation of HDAC5 or HDAC9 is viable in mice, though – due to their role in cardiomyocyte development – prone to cardiac hypertrophy and other cardio-anatomical abnormalities[63,64,70].

As an alternative, interest in pharmacological inhibition of HDACs is gaining traction. Their generally better tolerability is hypothesised to result from incomplete inactivation, the transient nature of their mechanistic action and their inhibition of enzymatic activity whilst leaving transcriptional co-repressor complexes intact[64]. Some broad-spectrum HDAC-inhibitors are already clinically implemented in the treatment of select lymphomas and myelomas[105]. Further, carboxylic acids with inhibitory effects on HDACs, such as valproic acid, are used in the treatment of epilepsy and for mood stabilisation in bipolar disorder[106,107]. Some HDAC-inhibitors' adverse effect profiles suggest contraindication for atherosclerosis, exacerbating murine oxLDL-uptake and expression of atherosclerosis-relevant genes in atherosclerotic mice[108].

To date, selective inhibition of HDAC9 or other specific class IIa-isoforms remains to be developed, with target selectivity proving challenging. Notably, TMP195 – a first-in-class selective competitive inhibitor of the class IIa HDAC-family – stands out as a promising development and has recently been demonstrated *in vivo* to reduce tumour burden and metastasis in breast and colorectal cancer via macrophage modulation[109–111]. Its promising candidacy as an anti-inflammatory treatment was therefore – in parallel to this study – a central pillar of our group's research into the link between HDAC9 and atherosclerosis[1].

4.4. Nuclear factor kappa-light-chain-enhancer of activated B cells (NF-κB)

4.4.1. Overview

NF-κB is a family of major pro-inflammatory transcription factors. It is a significant regulator of chronic inflammation – including pro-atherogenic inflammation – and its dysregulation is involved in a range of inflammatory processes ranging from

oncogenesis to autoimmunity[112–115]. Responsible for the transcriptional regulation of over 160 genes for cytokines, chemokines and adhesion molecules, it consists of five proteins collectively modulating immune and inflammatory signalling, apoptosis and cell proliferation: p50, p52, p65 (RelA), c-Rel and RelB. These DNA-binding subunits form complexes of homo- and heterodimers, whereby positive gene regulation depends on the binding of p65, c-Rel or RelB due to their Transactivation Domains (TADs)[113,116,117]. The most common complex – often abbreviated as NF-κB – is a heterodimer comprised of p50 and p65. It is kept inactive by interaction with inhibitor of kappa B (IκB), which expresses nuclear export signals and prevents NF-κB's nuclear translocation. The most abundant isoform is inhibitor of kappa B alpha (IκBα)[113,116,117].

The IκB kinase-complex (IKK) is a significant regulator of NF-κB-activity, directing transcription in a target gene-specific manner[118–120]. It consists of two structurally similar catalytic subunits – IκB kinase alpha (IKKα) and IκB kinase beta (IKKβ) – and a non-catalytic regulatory subunit, IκB kinase gamma (IKKγ/NEMO)[121–123]. IKKγ/NEMO-dimers are required for TNFα-induced NF-κB-activity and confer stability to the IKK-complex, thus keeping IKKα and IKKβ inactive[116,124,125]. Pro-inflammatory stimulation results in IKKγ/NEMO's interaction with other upstream NF-κB signalling components, leading to a conformational change of the IKK-complex, thus permitting IKKα and IKKβ to phosphorylate downstream targets, such as IκBα[116,125].

4.4.2. The signalling pathway

A diverse range of endo- and exogenous stimuli lead to NF-κB-activation, which occurs via two characteristic signalling cascades regulating two distinct sets of target genes: the canonical and the non-canonical pathways[116].

Canonical NF-κB-activation relies on upstream IKK-activation and IκB-degradation. The canonical pathway is induced by numerous extracellular ligands. The cytokine TNFα is well-studied, next to Lipopolysaccharide (LPS), though a plethora of further stimuli result in ligation of an equally diverse set of receptors[113,116]. TNFα – which

regulates inflammation in various diseases, including pro-atherogenic responses in atherosclerosis – is bound by Tumor necrosis factor receptor 1 (TNFR1)[116,126]. TNFR1 then recruits TNF receptor associated factor 2 (TRAF2) and Receptor-interacting protein (RIP) via an adapter protein – Tumor necrosis factor receptor type 1-associated death domain protein (TRADD)[127]. TRAF5 is also recruited as both TRAF2 and TRAF5 are jointly required for IKK-activation[116]. RIP1 – an RIP-isoform essential for IKK- and NF-κB-activation – oligomerises[116,128]. Though IKK-activation is independent of RIP1's kinase activity, its oligomerisation is characterised by its scaffolding function that facilitates the recruitment of further proteins to the complex. These include Mitogen-activated protein kinase kinase kinase 7 (TAK1) and – importantly – IKKγ/NEMO[116,129–132]. TAK1 – which activates IKKβ via phosphorylation – has been found to be critical for IKK-mediated NF-κB-activation[116,133,134]. For IKKγ/NEMO, induced proximity models reveal its oligomerisation to be essential for canonical IKK-activation, as it facilitates IKK's autophosphorylation, described below[116,131,135]. Both the activation of IKKα and that of NF-κB are diminished when IKKβ-deficient cells are stimulated with TNFα, indicating canonical signalling's principal reliance on IKKβ-activity[136]. However, a supportive if not dominant function for IKKα in TNFα- and IL-1-stimulated canonical signalling is also increasingly described, with IKKα playing a prominent role in NF-κB-activation, nuclear translocation as well as ser468- and ser536-phosphorylation[116,134,137,138].

IKKα and IKKβ are activated via (auto-)phosphorylation of their activation loops[135,139]. In turn, activated IKK phosphorylates downstream IκB-proteins – typically IκBα – resulting in polyubiquitination and subsequent ubiquitin-mediated proteasomal degradation of IκB[116,140–142]. Thus, IκB-degradation – an intermediary milestone in canonical signalling – is oftentimes described to hinge on IKKβ-induced phosphorylation. Yet, deficiency of either IKKα or IKKβ has also been found not to affect IκBα-phosphorylation, indicating potential redundance of both[116,122,138,143,144].

Following IKKβ-mediated proteolysis of IκBα, the remaining transcriptionally active p65:p50-heterodimers are released to translocate freely into the nucleus[116,142]. Here, NF-κB binds to DNA via its Rel homology domain (RHD) and functions as a co-activator for the expression of various pro-inflammatory, atherogenic TNFα-target

genes. Examples of such NF-κB-dependent target genes include the adhesion molecules ICAM-1 and VCAM-1 and the cytokines IL-1β, IL-12 and CCL2[113] .

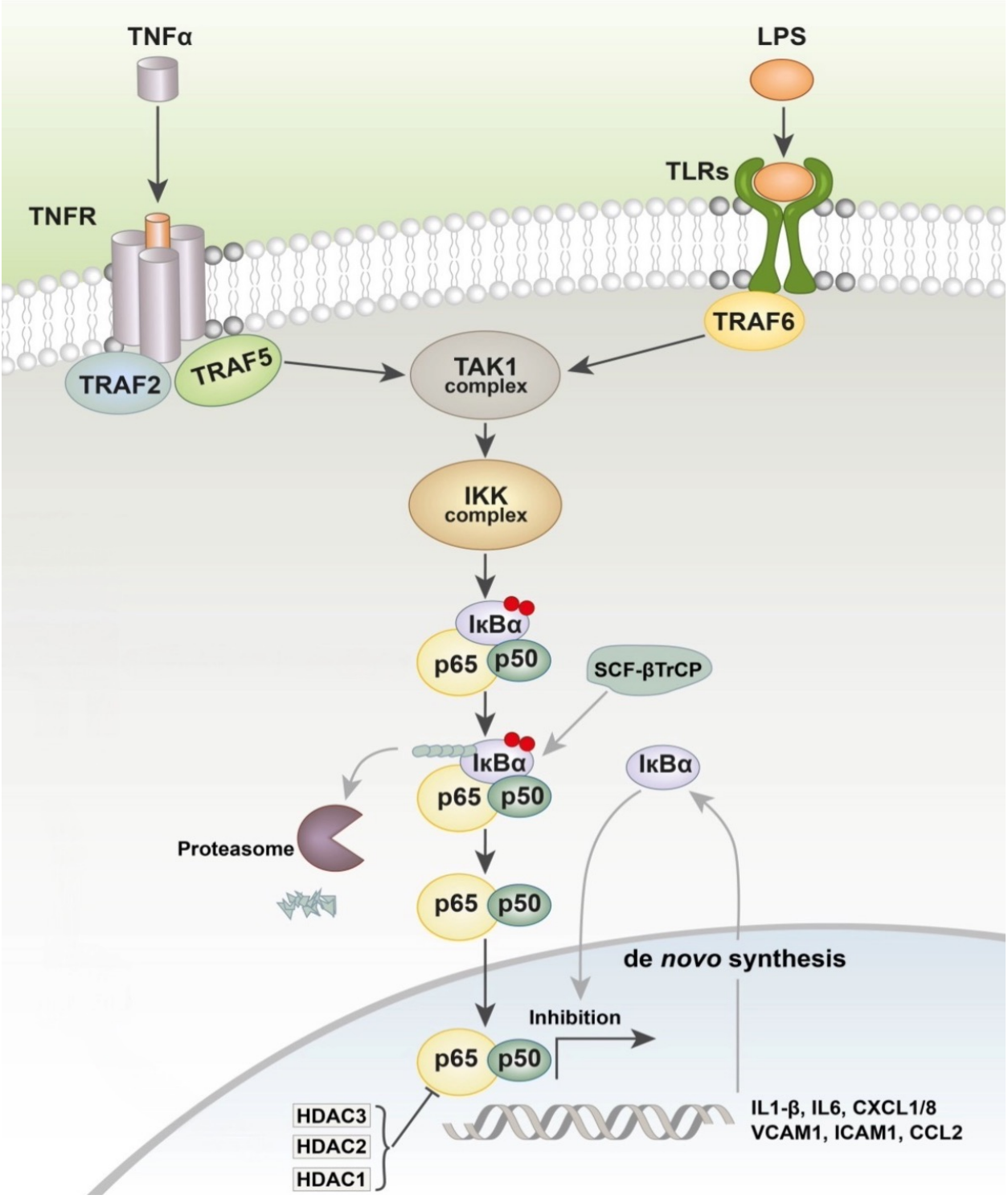

Figure 8: Schematic representation of canonical NF-κB-signalling

Canonical signalling is induced by numerous external stimuli. This includes TNFα, which binds to TNFR. A cascade is induced, whereby TRAFs, TAK1 and other proteins oligomerise. This activates the IKK-complex, which comprises the catalytic subunits IKKα and IKKβ and a regulatory subunit, IKKγ/NEMO. IKK phosphorylates downstream IκBα, which undergoes proteasomal degradation. This enables NF-κB's release to undergo nuclear translocation, where it transactivates TNFα-target genes, including VCAM-1 and CCL2. Both de-novo synthesis of IκB-α and interaction of NF-κB with class I HDACs can repress NF-κB-mediated transcription. Adapted from Asare et al. (unpublished).

To prevent its dysregulation, NF-κB's transcriptional activity is scrutinised by negative feedback mechanisms. Termination of NF-κB-dependent transcription is induced via p65's interaction with co-repressors, such as HDAC1 and HDAC2[145]. NF-κB-dependent IκBα-transcription also represents a negative feedback loop, ending NF-κB 's transcriptional activity. Here, NF-κB and newly synthesised IκBα form a complex undergoing prompt nuclear export, whereby the process is stimulated by HDAC3's prior deacetylation of p65[146–148].

Non-canonical NF-κB-signalling is associated with lymphoid malignancies and does not involve the phosphorylation of p65 or IκBα. Here, NF-κB-inducing kinase (NIK) and IKKα facilitate the processing of p100 to p52 and subsequent activation of p52/RelB-dimers in an IKKγ-independent manner[116,144,149]. Prominent examples of non-canonical kinases include RSK1, GSK3β, TBK1 and IKKε[150–152]. Though IKKε belongs to the family of IκB kinases, it forms complexes distinct to those of IKKα, IKKβ and IKKγ/NEMO and plays a secondary role in NF-κB-activation[153,154].

4.4.3. Post-translational modifications to NF-κB pathway proteins

Member proteins of the NF-κB signalling pathway may undergo various regulatory PTMs. Critically for this study, phosphorylation and acetylation may modulate NF-κB signalling proteins' enzymatic activity, the quality of their interactions with other cascade components, transcription co-factors and crosstalk with non-NF-κB signalling pathway proteins[119,155]. For example, class I HDACs have been found to regulate p65's transcriptional activity via deacetylation[145,146,156].

4.4.3.1. IKKα and IKKβ

Most research exploring PTMs to the IKK-complex has focussed on phosphorylation. IKK was shown to be inactivated when incubated with protein phosphatase 2A (PP2A) and the effect was extinct when PP2A was inhibited[118,141]. For IKKβ, autophosphorylation of serine residues ser177 and ser181 in the activation loop of

the kinase domain has been deemed essential for kinase activation by pro-inflammatory stimuli[123,135,141,157]. For IKKα, both autophosphorylation and NIK-dependent hetero-phosphorylation of serine residues ser176 and ser180 in its kinase domain activation loop result in activation[139,141,144]. However, though important for IKKα-activation, its phosphorylation is lesser so the target for pro-inflammatory stimuli, compared to IKKβ[135,141]. Further, in contrast to IKKβ, the phosphorylation of IKKα is not critical for canonical NF-κB-activation[135,158].

Acetylation of both IKKα and IKKβ's catalytic domains has also been found to mediate alterations in kinase activity. YopJ, a bacterial protein with acetyltransferase activity and an inhibitory effect on NF-κB-activity, was shown to inactivate both IKKα and IKKβ via acetylation. This delays phosphorylation within their activation loops and thus the kinases' activation[122,159]. Subsequent mass spectrometry identified the acetylation domains as threonine residues located between the previously mentioned phosphorylation domains: thr179 for IKKα and thr180 for IKKβ. In summary, acetylation of IKKα and IKKβ's catalytic domains attenuates kinase activity, thus preventing kinase activation and phosphorylation of IκBα in response to pro-inflammatory stimuli[122].

4.4.3.2. p65

PTMs of p65 are subject to ongoing interest. Phosphorylation can result in reduced affinity for IκBα – thereby promoting p65's translocation to the nucleus – and transactivation, an increased rate of transcription factor-dependent gene expression. However, NF-κB-activity can also be inhibited, depending on specific kinase and residue-involvement. The *barcode hypothesis* proposes a selective target gene-expression mediated by specific kinases, each conferring different effects on NF-κB's transcriptional activity via phosphorylation of distinct residues[119]. Thus, the identification of specific downstream phosphorylation sites within the NF-κB pathway can indicate changes in upstream kinase activity and triangulate evidence to assist kinase identification.

Phosphorylation of p65 at ser536 is mediated by kinases IKKα, IKKβ, RSK1 and TBK1 – with IKKε sustaining basal phosphorylation[150]. Phosphorylation of ser536 facilitates p65's binding of DNA, stimulating NF-κB's transcriptional activity. Similarly, phosphorylation at ser276 results in co-activation – here, involved kinases include mitogen- and stress-activated protein kinase 1 (MSK1), protein kinase A (PKAc) and proviral integration site for Moloney murine leukemia virus-1 (PIM1)[117,119,160–162].

Phosphorylation of ser468 – located in p65's transactivation domain – is associated with negative feedback during activated NF-κB-signalling and thus presents an exception to the rule. It results in p65's ubiquitination and eventual proteasomal degradation, leading to the selective termination of NF-κB-dependent transcriptional activity[163]. Ser468's basal phosphorylation is associated with glycogen synthase kinase-3 beta (GSK3β) and IKKβ, following canonical TNFα-stimulation[151,164]. Early evidence also suggests ser468-phosphorylation by IKKα and IKKε[138,152].

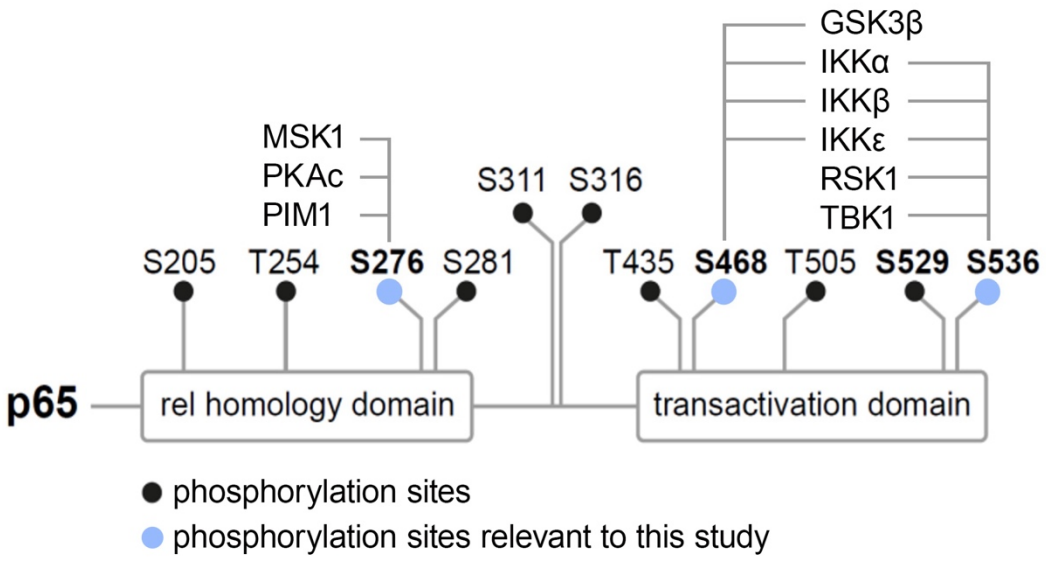

Figure 9: Schematic representation of p65's phosphorylation sites and relevant kinases

p65 consists of two domains: the Rel homology Domain (RHD), facilitating nucleic binding of DNA, and the transactivation domain (TAD), responsible for positive gene regulation. Depicted are each domain's serine (S) and threonine (T) residues, acting as distinct phosphorylation sites. Relevant to this study are ser276, ser468 and ser536. Kinases involved in phosphorylating ser276 include MSK1, PKAc and PIM1[160–162]. GSK3β, IKKα, IKKβ and IKKε phosphorylate ser468[138,151,152,164]. IKKα, IKKβ, IKKε, RSK1 and TBK1 phosphorylate ser536[150]. Figure reconstructed from Asare et al. (unpublished) and Christian et al. (2016)[119] to graphically include kinases.

p65's transcriptional activity is also regulated via its acetylation status, whereby most evidence points towards class I HDACs negatively regulating TNFα-stimulated NF-κB-dependent gene expression[145,146]. HDAC1 and HDAC2 act as co-repressors,

suppressing TNF-α-induced gene expression. Inhibition of their deacetylase activity exhibits the opposite effect[145]. Nucleic deacetylation by HDAC3 was found to reduce the duration of NF-κB-activity by promoting binding of p65 to IκBα, thus activating nuclear export[146]. Recently, HDAC3 was found to exhibit co-activating properties in IL-1-signalling by removing inhibitory acetylation at p65's lysine residues lys122, lys123, lys314 and lys315[156]. Acetylation of lys314 and lys310 also prominently regulates NF-κB target gene-transcription[165,166]. Interestingly, p65's acetylation at lys310 is regulated by prior phosphorylation of ser276 and ser536: joint phosphorylation and acetylation enhance NF-κB's transcriptional activity[167].

4.4.3.3. HDAC9-relevance to post-translational modifications in NF-κB pathway

Paving the way for this study, our research group previously provided early evidence on PTMs to p65, linking NF-κB to HDAC9-mediated pro-atherogenicity. TNFα-stimulation in three different atherosclerosis-relevant cell types identified HDAC9 to promote p65's phosphorylation at ser468 and ser536. In HUVECs, siRNA-mediated *HDAC9*-depletion reduced TNFα-stimulated phosphorylation levels at both ser468 and ser536 compared to *SCR* siRNA control. The findings are depicted in Figure 10.

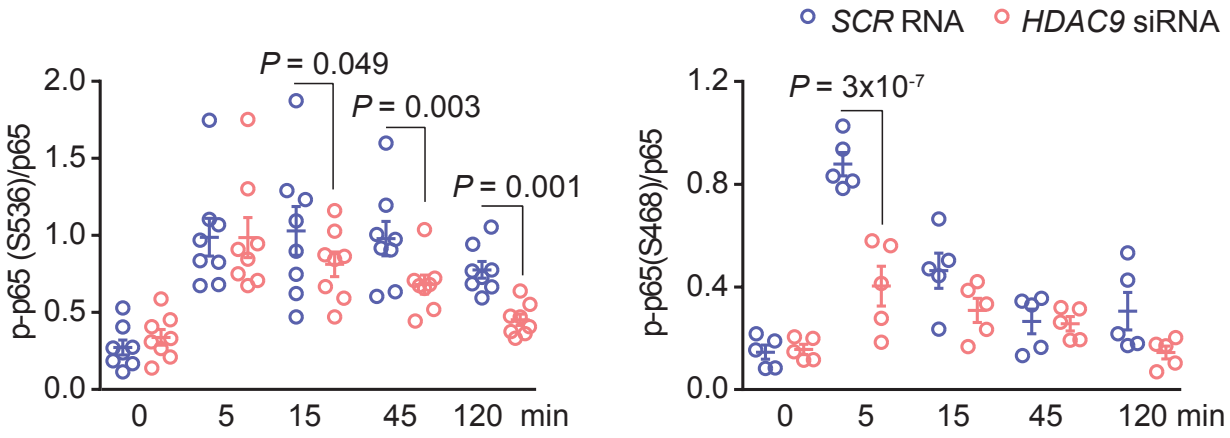

Figure 10: HDAC9-depletion reduces phosphorylation of ser468 and ser536

Experimental outline: HUVECs previously co-transfected with *HDAC9* siRNA or *SCR* siRNA control were left untreated or stimulated with TNFα for 5 to 120 minutes. Total p65 and levels of site-specific phosphorylation were visualised via immunoblotting with either anti-p65, anti-p-p65 (ser536) or anti-p-p65 (ser468). **Left:** Quantification of relative phosphorylation at ser536 in HDAC9-depleted samples normalised to total p65 versus control. Phosphorylation was most significantly reduced at 120 minutes (n=8). **Right:** Quantification of relative phosphorylation at ser468 in HDAC9-depleted samples normalised to total p65 versus control. Phosphorylation was significantly reduced at 5 minutes (n=5). Figure adapted from Asare et al. (2020)[1].

4.5. Aims of this study

Due to NF-κB's critical role in atherogenesis and the overlap between HDAC9's gene expression in inflammation and NF-κB-dependent canonical transcriptional responses, NF-κB-signalling was hypothesised to mediate pro-atherogenic downstream effects of HDAC9[1,113]. It was further hypothesised that one or more interactions between HDAC9 and key components of the NF-κB signalling cascade facilitate said pro-atherogenic effects. A schematic representation of the hypothesis is provided in Figure 11.

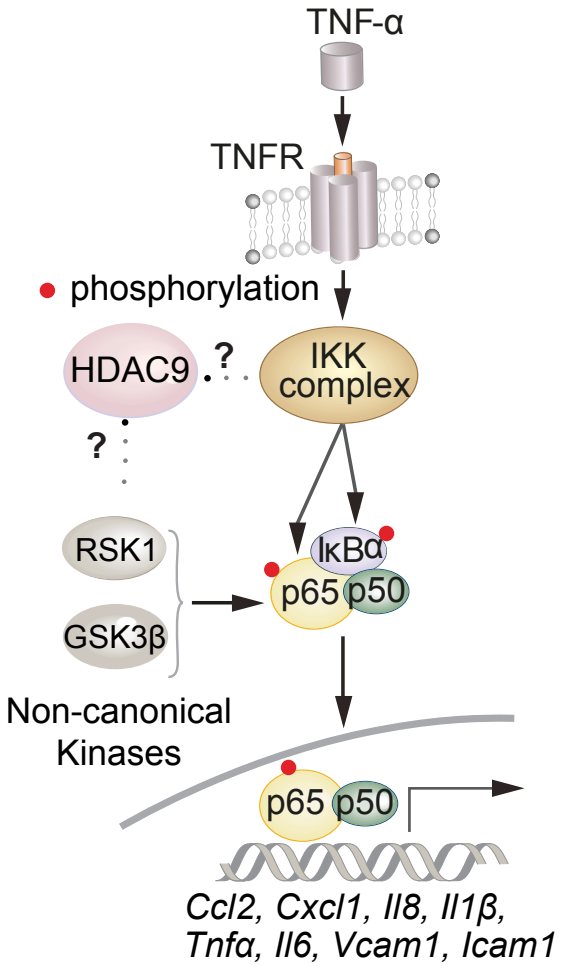

Figure 11: Schematic representation of hypothesis

Hypothesis: NF-κB-signalling mediates pro-atherogenic downstream effects of HDAC9. Leading to increased phosphorylation of p65's ser468 and ser536-residues, HDAC9 interacts either directly with one or more key components of the canonical NF-κB signalling cascade or indirectly via one or more non-canonical kinases. Figure adapted from Asare et al. (2020)[1].

Exploration of HDAC9's potential as a therapeutic target in atherogenic inflammation requires prior understanding of the mechanisms linking the two.

Thus, the aims of this study were defined as follows:

1. To clarify HDAC9's role in atherogenesis via screening for and identification of its potential interaction partners within the NF-κB signalling pathway

2. To explore the mechanistic role of HDAC9's interaction with NF-κB-signalling

3. To investigate downstream effects of HDAC9 in the NF-κB signalling pathway

5. Materials and Methods

5.1. Materials

5.1.1. Instruments

Instrument	**Company**
Block Heater SHT100D	Stuart Scientific, United Kingdom
Cooling room, 4°C	Viessmann, Germany
DynaMag-2 Magnet Stand	Invitrogen, USA
Fusion Fx7	Vilber, France
Heracell 240i CO2 Incubator	Thermo Fisher Scientific, USA
Heratherm Compact Microbiological Incubator	Thermo Fisher Scientific, USA
IKA KMO 2 basic IKAMAG stirrer	IKA-Werke, Germany
iMark Microplate Absorbance Reader	Bio-Rad, USA
Liquid nitrogen tank, -153°C	Thermo Fisher Scientific, USA
Megafuge 16R Centrifuge	Thermo Fisher Scientific, USA
Microscope, Eclipse TS100	Nikon, Japan
Millipore Q-Pod (for ddH_2O)	Merck, Germany
Mini-PROTEAN Tetra Cell Casting Stand/Clamps	Bio-Rad, USA
Mini-PROTEAN Tetra Vertical Electrophoresis Cell	Bio-Rad, USA
Mini Trans-Blot Module	Bio-Rad, USA
Mr. Frosty freezing container	Thermo Fisher Scientific, USA
NanoDrop 1000 Spectrophotometer	Thermo Fisher Scientific, USA
Nucleofector I Device	Lonza, Switzerland
PeqPower300 (electrophoresis power supply)	PeqLab, Germany
PowerPac HC (electrophoresis power supply)	PeqLab, Germany
Refrigerator, -20°C	Siemens, Germany
Refrigerator, -80°C	Thermo Fisher Scientific, USA
Rotating wheel, rotator 2-1175	neoLab, Germany
ST5 rocking shaker	Ingenieurbüro CAT, Germany
TC20 Automated Cell Counter	Bio-Rad, USA
Vortex-Genie 2	Scientific Industries, USA
Water bath 1003	Ges. für Labortechnik, Germany

5.1.2. Consumables

Material	**Company**
6-well plate	Thermo Fisher Scientific, USA
96-well plate	Sigma-Aldrich, Germany
Cell culture dish (100 mm)	Thermo Fisher Scientific, USA
Cell culture dish (150 mm)	Thermo Fisher Scientific, USA
Cell scraper	Corning, USA
Cell strainer (40 µm)	Corning, USA
Cryocial (2.0 ml)	Thermo Fisher Scientific, USA
Falcon tube (15 ml)	Corning, USA
Falcon tube (50 ml)	Corning, USA
Immun-Blot PVDF Membrane, Roll	Bio-Rad, USA
Millex Syringe Filter Unit, PVDF, 0.22 µm	Merck Millipore, USA
T75 cell culture flask	Thermo Fisher Scientific, USA
Thick blot filter paper	Bio-Rad, USA
TipOne Pipette Tips (10 µl – 1000 µl)	Starlab, Germany

5.1.3. Reagents and solutions

Reagent	**Company**
Accutase cell detachment solution	Sigma-Aldrich, Germany
Agar-agar	Sigma-Aldrich, Germany
Ampicillin	Thermo Fisher Scientific, USA
APS	Thermo Fisher Scientific, USA
ATP disodium salt hydrate	Sigma-Aldrich, Germany
BSA	Sigma-Aldrich, Germany
Cell lysis buffer (10x)	Cell Signaling Technology, USA
Collagen G	Merck Millipore, USA
cOmplete, EDTA-free Protease Inhibitor Cocktail	Roche, Switzerland
DH5α bacteria	Inst. f. Stroke and Dementia Res., Germany
DMEM	Thermo Fisher Scientific, USA
DMSO	Roth, Germany
DTT	Sigma-Aldrich, Germany
Dynabeads Protein A	Invitrogen, USA
Dynabeads Protein G	Invitrogen, USA
Endothelial Cell Growth Medium	Promocell, Germany

Ethanol 99%	Roth, Germany
FBS	Thermo Fisher Scientific, USA
Glycine	Sigma-Aldrich, Germany
“Immobilon” Chemiluminescent HRP Substrate	Merck Millipore, USA
Isoflurane	Sigma-Aldrich, Germany
Isopropanol	Sigma-Aldrich, Germany
KCl	Roth, Germany
KH_2PO_4	Roth, Germany
Kinase buffer (10x)	Cell Signaling Technology, USA
Laemmli protein sample buffer (4x)	Bio-Rad, USA
LCM (L929 conditioned medium)	Dr. Yaw Asare, Germany
Methanol >99%	Roth, Germany
MG-132	Cell Signaling Technology, USA
NaCl	Roth, Germany
Na_2HPO_4	Sigma-Aldrich, Germany
“NuPAGE” LDS Sample Buffer (4X)	Invitrogen, USA
OPTI-MEM reduced serum medium	Thermo Fisher Scientific, USA
Peptone	Roth, Germany
PhosSTOP Phosphatase Inhibitor Cocktail Tablets	Roche, Switzerland
“Pierce” BCA Protein Assay	Thermo Fisher Scientific, USA
“Pierce” BSA Protein Standard	Thermo Fisher Scientific, USA
PMSF	Roche, Switzerland
Precision Plus Protein Blotting Standards	Bio-Rad, USA
Recombinant NFκB p65 protein	Active Motif, USA
“Rotiphorese” Acrylamide/Bis-Solution, 30%	Roth, Germany
RPMI 1640 medium	Thermo Fisher Scientific, USA
SDS	Sigma-Aldrich, Germany
TEMED	Roth, Germany
TNFα (human)	Thermo Fisher Scientific, USA
TNFα (mouse)	Thermo Fisher Scientific, USA
TPCA-1	Abcam, United Kingdom
“Trizma“ Tris base	Sigma-Aldrich, Germany
Trypan blue solution	Sigma-Aldrich, Germany
Trypsin-EDTA (0.25%), phenol red	Thermo Fisher Scientific, USA
“Tween 20” Polysorbate 20	Sigma-Aldrich, Germany
Yeast extract	Roth, Germany

5.1.4. Cells

Cells	**Supplier**
BMDMs (*Hdac9*$^{+/+}$ *Apoe*$^{-/-}$)	Inst. f. Stroke and Dementia Res., Germany
BMDMs (*Hdac9*$^{-/-}$ *Apoe*$^{-/-}$)	Inst. f. Stroke and Dementia Res., Germany
HEK 293	ATCC, USA
HUVEC	Promocell, Germany

5.1.5. Buffers and solutions

Listed in order of mention in methods. 10x solutions denote stock solutions. If not described otherwise, 1x solutions were prepared by diluting a higher concentration stock solution with the appropriate amount of ddH_2O.

10x Phosphate buffer saline (for 5 l, pH: 7.4)		
Substance	Amount	Supplier
Na_2HPO_4	58,75 g	Sigma-Aldrich, Germany
NaCl	400 g	Roth, Germany
KCl	10 g	Roth, Germany
KH_2PO_4	10 g	Roth, Germany
ddH_2O	to 5 l	

BMDM growth medium (approx. 20 ml)		
Substance	Amount	Supplier
RPMI 1640	15 ml	Thermo Fisher Scientific, USA
FBS	2 ml	Thermo Fisher Scientific, USA
LCM (L929 conditioned medium)	3 ml	Dr. Yaw Asare, Germany
Gentamicin	20 µl	Thermo Fisher Scientific, USA

HEK293 cell medium (approx. 500 ml)		
Substance	Amount	Supplier
DMEM	450 ml	Thermo Fisher Scientific, USA
FBS	50 ml	Thermo Fisher Scientific, USA
Gentamicin	500 µl	Thermo Fisher Scientific, USA

Enriched endothelial cell growth medium (approx. 500 ml)		
Substance	Amount	Supplier
EC growth medium	450 ml	Promocell, Germany
FBS	50 ml	Thermo Fisher Scientific, USA
Gentamicin	500 µl	Thermo Fisher Scientific, USA

LB medium (for 500 ml, pH: 7.0)		
Substance	Amount	Supplier
Yeast extract	2.5 g	Roth, Germany
Peptone	5 g	Roth, Germany
NaCl	2.5 g	Roth, Germany

LB agar (for 500 ml, pH: 7.0)		
Substance	Amount	Supplier
Yeast extract	2.5 g	Roth, Germany
Peptone	5 g	Roth, Germany
Agar-agar	7.5 g	Sigma-Aldrich, Germany
NaCl	2.5 g	Roth, Germany

1x Cell lysis buffer (for 10 ml)		
Substance	Amount	Supplier
10x Cell Lysis Buffer	1 ml	Cell Signaling Technology, USA
ddH_2O	9 ml	
Protease inhibitor	1 tablet	Roche, Switzerland
Phosphatase inhibitor	1 tablet	Roche, Switzerland

SDS sample buffer (for 10 ml)		
Substance	Amount	Supplier
4x NuPAGE LDS Sample Buffer	2.5 ml	Invitrogen, USA
DTT (1 M)	1.25 ml	Sigma-Aldrich, Germany
ddH_2O	6.25 ml	
Protease inhibitor	1 tablet	Roche, Switzerland
Phosphatase inhibitor	1 tablet	Roche, Switzerland

10% APS (for 500 ml)		
Substance	Amount	Supplier
APS	50 mg	Thermo Fisher Scientific, USA
ddH_2O	to 500 ml	

Lower Tris 4x (for 1 l)		
Substance	Amount	Supplier
Tris base	181.7 g	Sigma-Aldrich, Germany
SDS	4 g	Sigma-Aldrich, Germany
ddH_2O	to 1 l	

Upper Tris 4x (for 1 l)		
Substance	Amount	Supplier
Tris base	60.6 g	Sigma-Aldrich, Germany
SDS	4 g	Sigma-Aldrich, Germany
ddH_2O	to 1 l	

7.5% lower gel (for 2 gels, 1mm depth)		
Substance	Amount	Supplier
ddH_2O	5.9 ml	
Lower Tris	3 ml	
Acrylamide	3 ml	Roth, Germany
APS	100 µl	Thermo Fisher Scientific, USA
Temed	10 µl	Roth, Germany

Upper gel (for 2 gels, 1mm depth)		
Substance	Amount	Supplier
ddH_2O	2.9 ml	
Upper Tris	1 ml	
Acrylamide	0.6 ml	Roth, Germany
APS	45 µl	Thermo Fisher Scientific, USA
Temed	4.5 µl	Roth, Germany

10x running buffer (for 5 l)		
Substance	Amount	Supplier
Tris base	150 g	Sigma-Aldrich, Germany
Glycine	720 g	Sigma-Aldrich, Germany
SDS	50 g	Sigma-Aldrich, Germany
ddH_2O	to 5 l	

10x blotting buffer (for 5 l)		
Substance	Amount	Supplier
Tris base	150 g	Sigma-Aldrich, Germany
Glycine	720 g	Sigma-Aldrich, Germany
ddH_2O	to 5 l	

10x TBS-T (for 5 l)		
Substance	Amount	Supplier
Tris base	60.57 g	Sigma-Aldrich, Germany
NaCl	87.66 g	Roth, Germany
Tween 20	50 ml	Sigma-Aldrich, Germany
ddH_2O	to 5 l	

5% BSA blocking buffer (for 500 ml)		
Substance	Amount	Supplier
BSA	25 g	Sigma-Aldrich, Germany
1x TBS-T	to 500 ml	

5.1.6. Kits

Kits	**Company**
DuoSET ELISA, Mouse CCL2/HE/MCP-1	R&D Systems, USA
DuoSET ELISA, Mouse CXCL1/KC	R&D Systems, USA
DuoSET ELISA, Mouse TNF-α	R&D Systems, USA
HUVEC Nucleofector Kit	Lonza, Switzerland
NucleoBond Xtra Midi Plus	Macherey-Nagel, Germany
Pierce BCA Protein Assay	Thermo Fisher Scientific, USA
PolyFect Transfection Reagent Kit	Qiagen, Netherlands

5.1.7. cDNA-clones and siRNA

Clone	**Company**
FLAG-HDAC9 cDNA	Dr. Matthias Prestel, Germany
FLAG cDNA	Dr. Matthias Prestel, Germany
GFP cDNA	Lonza, Switzerland

HA-IKKβ cDNA	InvivoGen, USA
HA-IKKα cDNA	InvivoGen, USA
HA-IKKγ/NEMO cDNA (Addgene plasmid #13512)	Prof. Kun-Liang Guan, USA
HA-IκB-α cDNA (Addgene plasmid #21985)	Prof. Warner Greene, USA
HA-RSK1 (Addgene plasmid #13841)	Prof. John Blenis, USA
HA-GSK3 cDNA (Addgene plasmid #14753)	Dr. Jim Woodgett, Canada
ON-TARGETplus nontargeting SCR siRNA	Horizon Discovery, United Kingdom
ON-TARGETplus SMARTpool *HDAC9* siRNA	Horizon Discovery, United Kingdom
T7-IKKε cDNA (Addgene plasmid #27238)	Prof. Tom Maniatis, USA

5.1.8. Antibodies

Antibody	**Company**
Anti-acetyl lysine	Abcam, United Kingdom
Anti-FLAG (M2) mAb	Sigma-Aldrich, Germany
Anti-GFP mAB (3E6)	Thermo Fisher Scientific, USA
Anti-HA (C29F4) Rabbit mAb	Cell Signaling Technology, USA
Anti-mouse IgG HRP	Agilent Dako, USA
Anti-p65	Santa Cruz, USA
Anti-p-p65 (ser276)	Invitrogen, USA
Anti-p-p65 (ser468)	Cell Signaling Technology, USA
Anti-p-p65 (ser536)	Cell Signaling Technology, USA
Anti-rabbit IgG HRP	Agilent Dako, USA
Anti-T7 (D9E1X) Rabbit mAb	Cell Signaling Technology, USA

5.1.9. Software

Software	**Company**
Graphpad Prism 7.0	Graphpad Software Inc., USA
Image J 1.47v	Wayne Rasband, USA
Microplate Manager Software 6	Bio-Rad, USA
Microsoft Excel	Microsoft Corporation, USA

5.2. Methods

5.2.1. Primary cell culture

5.2.1.1. Isolation of murine bone marrow-derived macrophages (BMDMs)

Animal experiments were ethically approved by the Institutional Animal Care Committee of the government of Upper Bavaria (ROB-55.2-2532.Vet_02-14-187) and the sacrifice of mice for these experiments were performed in line with best practice principles. Murine BMDMs were isolated from the *Hdac9*$^{+/+}$ *Apoe*$^{-/-}$ and *Hdac9*$^{-/-}$ *Apoe*$^{-/-}$ mice. These had been generated beforehand by crossing Eric Olson's *Hdac9*$^{-/-}$ mouse model with an *Apoe*$^{-/-}$ model, as previously described[20,63]. Prior to sacrifice, mice were sedated with isoflurane (Sigma-Aldrich, Germany). Sacrifice was performed by cervical dislocation, after which the lower extremities and abdomen were disinfected with 80% ethanol (Roth, Germany). Following abdominal midline cutaneous incision, the femurs and tibiae were exposed by pushing aside and removing surrounding tissue. After severing the femurs at the level of the hip, both ends of the femurs and tibiae were resected, thus exposing the bone marrow. This was flushed out using ice-cold 1x PBS. The BMDMs were then resuspended in 1x PBS and underwent filtration through a 40 µm cell strainer (Corning, USA), after which the suspension was centrifuged at 500 g for 10 minutes (Thermo Fisher Scientific, USA). The cell pellet was then resuspended in BMDM growth medium and the suspension transferred for culture in 150 mm cell culture dishes (Thermo Fisher Scientific, USA). 3 ml L929 conditioned medium (LCM) was added on each of the following two days. Harvesting took place after the 7th day in culture. After gentle washing of the BMDMs with PBS, a cell scraper (Corning, USA) was cautiously used to reduce adherence to the cell culture dishes' surface. Pending automated cell count, described below, 1 million cells were then transferred to each well of a 6-well plate (Thermo Fisher Scientific, USA). The BMDMs were given 24 hours to adhere in an LCM-free BMDM growth medium whilst microbiologically incubated at 37°C (Thermo Fisher Scientific, USA). They were then used to measure cytokine excretion in ELISA experiments.

5.2.1.2. Cell cultivation, count and cryopreservation

Beyond BMDMs, HEK293 cells (ATCC, USA) and HUVECs (Promocell, Germany) were also employed.

HEK293 cells (Thermo Fisher Scientific, USA) between the passages 4 and 15 were cultured for later plasmid DNA transfection in preparation of protein complex immunoprecipitation and kinase activity assay experiments. They were cultivated at 37°C (Thermo Fisher Scientific, USA) in T75 cell culture flasks (Thermo Fisher Scientific, USA) containing HEK293 cell medium, described above. Passaging at a ratio of between 1:2 and 1:5 was performed once a confluence of 90% was attained. First, the HEK293 cell medium was replaced with 5 ml Trypsin-EDTA (Thermo Fisher Scientific, USA) to reduce cell adherence to the flask. Following three minutes of incubation and short agitation, the solution containing the cells was transferred to a falcon tube (Corning, USA) for centrifugation at 1200 rpm for 5 minutes (Thermo Fisher Scientific, USA). Depending on the cell count, the HEK293 cells were distributed to 2 to 5 new flasks. If needed for experiments, they were transferred to 100 mm cell culture dishes (Thermo Fisher Scientific, USA), whereby 6 million HEK293 cells per cell culture dish were allowed to settle for 24 hours prior to transfection.

HUVECs (Promocell, Germany) between the passages 5 and 8 were cultured for transfection of plasmid DNA, *HDAC9*-silencing siRNA or non-targeting siRNA to facilitate protein complex immunoprecipitation and TNFα-stimulation experiments. Plated on T75 cell culture flasks (Thermo Fisher Scientific, USA), the cells were cultivated at 37°C in enriched endothelial cell growth medium (Thermo Fisher Scientific, USA), which was replaced every 48 hours. To promote cell adherence, container surfaces were coated with Collagen G (Merck Millipore, USA), previously diluted 1:100 in 1x PBS and passed through a 0.2 µm syringe-driven filter (Merck Millipore, USA). Once they had attained a confluence of 100%, the HUVECs were passaged at a ratio of between 1:2 and 1:10, depending on cell count. Here, Accutase (Sigma-Aldrich, Germany) was used for cell detachment and the above-described steps for HEK293 cells were maintained. For protein complex

immunoprecipitation experiments, 3 million HUVECs were plated on 150 mm cell culture dishes (Thermo Fisher Scientific, USA). For TNFα-stimulation experiments, 1 million cells were used for each well of a 6-well plate (Thermo Fisher Scientific, USA). Container surfaces were coated with diluted collagen G, as described above.

Cells were counted with an automated cell counter (Bio-Rad, USA). Here, 10 µl of a suspension containing the cells in question was dissolved 1:1 in 10 µl Trypan blue solution (Sigma-Aldrich, Germany). The average of three automated cell counts was calculated for subsequent use.

To accommodate future experiments and in cases where cells no longer were needed, HEK293 cells and HUVECs underwent cryopreservation. Here, they were brought out of adherence using the steps described above. They were then centrifuged at 500 g for 10 minutes (Thermo Fisher Scientific, USA). The supernatant was replaced with DMSO (Roth, Germany) – a freezing medium – and the cell suspension transferred into a cryovial (Thermo Fisher Scientific, USA). The vial was stored overnight at -80°C in a freezing container (Thermo Fisher Scientific, USA) before transfer to a liquid nitrogen tank (Thermo Fisher Scientific, USA), in which cells were preserved at -153°C. When required for experiments, cryopreserved cells were thawed on ice, the DMSO removed rapidly post-centrifugation and the cells brought into culture under above-described conditions.

5.2.1.3. Plasmid DNA preparation and transfection

Both HEK293 cells and HUVECs were transiently co-transfected with plasmid DNA for later protein complex immunoprecipitation. HUVECs were also transfected with siRNA for TNFα-stimulation experiments.

For protein complex immunoprecipitation, HEK293 cells and HUVECs were transiently co-transfected with *FLAG-HDAC9* (Dr. Matthias Prestel, Germany) or *FLAG* alone control (Dr. Matthias Prestel, Germany) and one component of the NF-κB signalling pathway: *HA-IKKα* (InvivoGen, USA), *HA-IKKβ* (InvivoGen, USA), *HA-*

IKKγ/NEMO (gift from Prof. Kun-Liang Guan, USA), *HA-IκBα* (gift from Prof. Warner Greene, USA), *HA-RSK1* (gift from Prof. John Blenis, USA), *HA-GSK3β* (gift from Dr. Jim Woodgett, Canada) or *T7-IKKε* (gift from Prof. Tom Maniatis, USA)[168–172].

Plasmids were prepared using the NucleoBond Xtra Midi Plus kit (Macherey-Nagel, Germany). Here, 1 µl of the aforementioned plasmid DNA samples was added to competent DH5α bacteria (Institute for Stroke and Dementia Research, Germany), incubated on ice for 30 minutes and heat-shocked at 42°C for 90 seconds. 250 µl LB medium (described above) was added. The solution was incubated at 37°C for 30 minutes (Thermo Fisher Scientific, USA) before being transferred uniformly onto an LB agar plate (described above) and incubated at 37°C overnight. Two clones were then picked from the agar plate and incubated at 37°C for 6 hours in a solution of 4 ml LB medium containing 4 µl Ampicillin (Thermo Fisher Scientific, USA). Subsequently, the kit's protocol was followed. The bacteria suspension was centrifuged at 4.000 g and 4°C over 45 minutes, the supernatant removed and the pellet resuspended and incubated for 5 minutes, at room temperature, in 4 ml kit-enclosed RES Buffer. 8 ml LYS Buffer was added to lyse the bacteria. The lysate was then added to the kit-enclosed column filter pretreated with 12 ml EQU buffer and 8 ml NEU buffer. 5 ml EQU buffer was added on top of the lysate and the eluate was collected below the column. 3.5 ml isopropanol was added and the solution centrifuged at 15.000 g and 4°C over 30 minutes. The supernatant was removed and the pellet resuspended in 70% ethanol (Roth, Germany) before being centrifuged at 15.000 g and room temperature for 5 minutes. The supernatant was removed and the pellet allowed to dry. The plasmid pellet was then resuspended in 300 µl ddH_2O and, using spectrophotometry, the concentration of plasmid DNA was quantified by Nanodrop (Thermo Fisher Scientific, USA).

For co-transfection in HEK293 cells, 6 million cells – plated a day prior to transfection – were cumulatively provided with 8.5 µg of plasmid DNA: 4 µg of either *FLAG-HDAC9* or *FLAG* alone control, 4 µg of one of the aforementioned NF-κB signalling components and, for control of transfection quality, 0.5 µg of *GFP* (Lonza, Switzerland). The plasmids were diluted in 300 µl OPTI-MEM medium (Thermo Fisher Scientific, USA) along with 80 µl of Polyfect transfection reagent (Qiagen,

Netherlands), agitated and incubated at room temperature for 10 minutes. The solution was then distributed uniformly when applied to the cells, prior to overnight incubation at 37°C. Following use of a microscope (Nikon, Japan) to verify green fluorescence as a surrogate for the transfection of *GFP*, the cells were lysed and the lysate used for protein complex immunoprecipitation.

For plasmid DNA co-transfection in HUVECs, 3 million cells per sample were passaged two days in advance. Due to the significant amount of highly concentrated cell lysate required for protein complex immunoprecipitation, the protocol provided by the HUVEC Nucleofector Kit (Lonza, Switzerland) was modified to accommodate pooling of samples. Transfected over three cycles, a total of 15 µg of plasmid DNA was used per sample: 6.75 µg of either *FLAG-HDAC9* or *FLAG* alone control, 6.75 µg of either *HA-IKK*α or *HA-IKK*β and 1.5 µg kit-enclosed *GFP*. In each culture dish, HUVECs – which had previously been washed with 1x PBS, brought out of adherence by Accutase (Sigma-Aldrich, Germany), centrifuged at 200 g for 10 minutes (Thermo Fisher Scientific, USA) and resuspended in 100 µl kit-enclosed nucleofector solution – thus received 5 µg of plasmid material. The cell/DNA suspension was then transferred to a transfection cuvette and underwent electroporation in the Nucleofector Device (Lonza, Switzerland), with the latter set to programme A-034. Three corresponding samples were pooled and transferred to a 150 mm collagen G-coated cell culture dish (Thermo Fisher Scientific, USA). The cells were left to incubate in enriched endothelial cell growth medium at 37°C overnight. Transfection quality was verified for GFP using a microscope and the cells were lysed ahead of protein complex immunoprecipitation.

5.2.1.4. siRNA transfection in HUVECs for TNFα-stimulation

For TNFα-stimulation experiments, 1 million HUVECs per sample were passaged two days ahead of siRNA transfection. The steps outlined in the protocol provided by the HUVEC Nucleofector Kit (Lonza, Switzerland) were followed. The preparatory steps mirrored those of plasmid DNA transfection in HUVECs, at the end of which the cells were resuspended in 100 µl kit-enclosed nucleofector solution. 100 pmol of

either predesigned ON-TARGETplus SMARTpool human *HDAC9* siRNA (Horizon Discovery, United Kingdom) or nontargeting ON-TARGETplus *SCR* siRNA control (Horizon Discovery, United Kingdom) were added and the cell/RNA suspension underwent electroporation in the Nucleofector Device (Lonza, Switzerland) set to programme A-034. Following transfer to a collagen G-coated 6-well plate (Thermo Fisher Scientific, USA) containing endothelial cell growth medium for a total volume of 1.5 ml in each well, the cells were allowed to recuperate for 48 hours. They were then stimulated with 20 ng/ml human TNFα (Thermo Fisher Scientific, USA) at time intervals of between 0 and 120 minutes. Stimulation was interrupted by aspiration of the TNFα-containing medium and two cycles of subsequent washing with 1x PBS, after which the cells were lysed.

5.2.1.5. Lysis

Whole cell lysate was required for both protein complex immunoprecipitation and immunoblotting following TNFα-stimulation. To prevent proteasomal degradation of proteins ahead of and throughout protein complex immunoprecipitation, HEK293 cells and HUVECs were incubated for 60 minutes with 1μM MG-132 (Cell Signaling Technology, USA), a proteasome inhibitor. After two washing cycles with 1x PBS, the cells were incubated for 5 minutes at 4°C with 500 µl 1x cell lysis buffer. Using a cell scraper (Corning, USA) to harvest, the cells were gently brought out of adherence from the surface of the cell culture dish (Thermo Fisher Scientific, USA) and transferred to an eppendorf vial. Using a pipette to homogenise the lysate, the cell material was resuspended before the whole cell lysate was centrifuged for 10 minutes at 14.000 g and with a temperature of 4°C (Thermo Fisher Scientific, USA). The supernatant was then transferred to a new vial and underwent protein concentration measurement, described below.

Whole cell lysate from HUVECs was harvested for TNFα-stimulation experiments. Here, the supernatant containing TNFα was removed from the wells of the 6-well plate (Thermo Fisher Scientific, USA) and the cells washed twice with 1x PBS. To maintain the effect from TNFα-stimulation, the cells were immediately incubated at

4°C with 100 µl LDS sample buffer (Invitrogen, USA) over 5 minutes. Following the above-described protocol, they were then brought out of adherence, homogenised, centrifuged and underwent protein concentration measurement.

5.2.2. Protein methods

5.2.2.1. Concentration measurement

To ensure the use of equal amounts of protein in subsequent experiments, sample protein concentrations were determined. These were measured by Bradford Protein Assay using the Pierce BCA Protein Assay Kit (Thermo Fisher Scientific, USA) and colorimetry. Following preliminary dilution of kit-enclosed BSA standards in ddH_2O (Merck, Germany) to attain standard concentrations of between 0 µg/ml to 2000 µg/ml, 10 µl of either (diluted) standard or sample were pipetted into a 96-well plate (Sigma-Aldrich, Germany). This was followed by 200 µl of working reagent, a 1:50 solution of the kit-enclosed Substrates A and B. It was ensured that all samples faced equal amounts of light exposure. Following 20-minute incubation of the probes at 37°C (Thermo Fisher Scientific, USA), a microplate absorbance reader (Bio-Rad, USA) was employed for colorimetry, whereby a samples' absorbance at a wavelength of 595 nm was plotted against the standard curve of a duplicated series of BSA standard. Total protein concentrations were calculated using Microplate Manager Software 6 (Bio-Rad, USA) and Microsoft Excel (Microsoft Corporation, USA). Samples were then immediately used in protein complex immunoprecipitation experiments or stored in a laboratory refrigerator at -80°C (Thermo Fisher Scientific, USA) for later use.

5.2.2.2. Protein complex immunoprecipitation

Whole cell lysate samples obtained from HEK293 cells (ATCC, USA) or HUVECs (Promocell, Germany) previously transfected with *FLAG-HDAC9* or *FLAG* alone control alongside one of various NF-κB signalling components were used for protein complex immunoprecipitation experiments. Derived from their respective total protein

concentration, the whole cell lysates were further diluted in 1x cell lysis buffer to attain equal total protein weights of 250 µg for HEK293 cells or 100 µg for HUVECs and 500 µL per sample. To inhibit serine proteases, 1 mM PMSF (Roche, Switzerland) was added to the 1x cell lysis buffer immediately prior to dilution. The samples were then incubated at 4°C overnight on a rotating wheel (neoLab, Germany) for conjugation with 10 µg of a primary antibody, either anti-FLAG (Sigma-Aldrich, Germany), anti-HA (Cell Signaling Technology, USA) or anti-T7 (Cell Signaling Technology, USA). Next, depending on isotope-specificity, 50 µL of either Protein A or G Dynabeads (Invitrogen, USA) were placed in an eppendorf vial equivalent to the number of samples. For pre-clearing, the Dynabeads were placed on a magnetic stand (Invitrogen, USA), the supernatant was removed and the magnetic beads washed three times with 100 µL cell lysis buffer. Each 500 µL sample was then resuspended into the respective eppendorf vial containing the magnetic beads. The sample suspensions were incubated over 2 hours at 4°C on a rotating wheel (neoLab, Germany), thereby initiating immunoprecipitation. Following incubation, the samples' cell lysate was discarded using the magnetic stand and the remaining magnetic pellets then kept on ice between five washing cycles. In the first three cycles, the pellet was resuspended in low salt washing buffer – 200 µL 1x cell lysis buffer with 150 nM NaCl (Roth, Germany). High salt washing buffer, containing 200 µL 1x cell lysis buffer and 250 nM NaCl (Roth, Germany), was used to resuspend the pellet in the last two cycles. Between each washing cycle, the washing buffer was collected and discarded using the magnetic stand. After the final washing cycle, the antigen-antibody complexes were eluted by resuspending the magnetic sample pellets in 40 µl SDS sample buffer. For input samples, which did not undergo immunoprecipitation and amounted to the 5% equivalent of initial total protein weight, 10 µl SDS sample buffer was used. The samples were then agitated for 30 seconds using a vortex (Scientific Industries, USA) and boiled for 10 minutes at 70°C in a block heater (Stuart Scientific, United Kingdom). Finally, the samples were placed on the magnetic stand, enabling the transfer of the supernatant with the antigen-antibody complexes for electrophoresis.

5.2.2.3. *Kinase activity assay*

Kinase activity assays were conducted using whole cell lysate of HEK293 cells or HUVECs previously transfected with *HA-IKKβ* and *FLAG-HDAC9* or *FLAG* alone control. Cell lysis, using pooled material from three and six 150 mm cell culture dishes (Thermo Fisher Scientific, USA) for HEK293 cells and HUVECs respectively, and protein complex immunoprecipitation were performed as described above. Either anti-FLAG (Sigma-Aldrich, Germany) or anti-HA (Cell Signaling Technology, USA) was used. The magnetically immunoprecipitated protein complexes were washed following the previously described washing process, whereby three washing cycles performed with 4°C cold 1x cell lysis buffer were followed by three washing cycles with 4°C cold 1x kinase buffer (Cell Signaling Technology, USA). The immunoprecipitated protein complexes were kept in the 1x kinase activity buffer used in the final washing cycle, thus providing the medium for the kinase activity assays that immediately followed. To measure the ability of IKKβ to phosphorylate p65 in the presence and absence of HDAC9, substrate was added in the form of 400 ng recombinant human p65 (Active Motif, USA). The solution was then immediately incubated with 50.72 µg (100 µM) ATP (Sigma-Aldrich, Germany), whereby the vial containing the solution was placed in a water bath (Gesellschaft für Labortechnik, Germany) at a temperature of 34°C. Following 45 minutes of incubation, kinase activity was inhibited with the addition of 10 µl 4x Laemmli protein sample buffer (Bio-Rad, USA). Samples were then boiled for 20 minutes at 95°C in a block heater (Stuart Scientific, United Kingdom), after which a magnetic stand (Invitrogen, USA) was used to separate the magnetic beads (Invitrogen, USA) previously used for immunoprecipitation, thus enabling the transfer of the reagents for electrophoresis.

5.2.2.4. *Electrophoresis*

SDS-PAGE upper and lower gels with a thickness of 1 mm were prepared following the respective recipes. Pouring stands were prepared using glass plates, glass plate holders and sponges (Bio-Rad, USA) to accommodate the preparation of 7.5% sodium dodecyl sulphate (SDS) that was used to separate proteins. The lower gel

solution, described above, was added to amount for the lower 70% of the volume between the glass plates. To allow for the development of a smooth upper surface during gel polymerisation, isopropanol (Sigma-Aldrich, Germany) was added above the lower gel solution and removed again after 30 minutes post-polymerisation, after which the lower gel's upper surface was rinsed with ddH_2O (Merck, Germany). The upper gel solution, described above, was added to the upper 30% of the volume between the glass plates and underwent polymerisation for 30 minutes with a 10-well comb inserted.

Samples with equivalent total protein weight were filled into each well and 10 µl of a pre-stained protein standard marker (Bio-Rad, USA) was added to enable the approximation of molecular weight. SDS-Page electrophoresis was conducted at between 100 V to 150 V over 60 to 90 minutes in an electrophoresis cell (Bio-Rad, USA) containing 1x running buffer, described above. Smaller, negatively charged proteins migrated towards the cathode at higher speed and electrophoresis was ended when those proteins had travelled the entire distance of the gel, as demarcated by the protein marker.

5.2.2.5. Western Blot

PVDF membrane (Bio-Rad, USA) was used for protein transfer. In preparation, the membrane was activated in methanol (Roth, Germany) for 10 seconds before being deposited in 1x blotting buffer, described above, for 10 minutes on a rocking shaker (Ingenieurbüro CAT, Germany). Thick blot filter paper (Bio-Rad, USA) was submerged in 1x blotting buffer before the transfer module (Bio-Rad, USA) was arranged in the following order: anode – mesh – blot filter paper – PVDF membrane – gel – blot filter paper – cathode. The module was then placed into the electrophoresis cell with 1x blotting buffer. To maintain temperature conditions, via prevention of the blotting buffer overheating in the electrophoresis cell, a cold pack was added and the module placed on a magnetic stirrer (IKA-Werke, Germany). Protein transfer was conducted over 60 minutes at 100 V, 250 mA and 50 W, the

quality of which was verified through the existence of the standard marker's coloured bands on the PVDF membrane demarcating the range of molecular weights.

Following completion of the protein transfer, the PVDF membrane was submerged in 5 ml 5% blocking buffer, described above, for 60 minutes on a rocking shaker (Ingenieurbüro CAT, Germany), at 20°C. It was then incubated with a primary antibody on the rocking shaker at 4°C overnight, whereby 5 to 10 ml of the primary antibody was dissolved in 5 ml of either 1% or 5% BSA solution (Sigma-Aldrich, Germany). The PVDF membrane was then rinsed with TBS-T, described above, in 3 to 5 cycles of between 5 to 15 minutes. Depending on the host species of the primary antibody, a secondary HRP-conjugated anti-mouse (Agilent Dako, USA) or anti-rabbit antibody (Agilent Dako, USA) was dissolved 1:10.000 in 10 ml 1% BSA solution and the PVDF membrane left to incubate with the secondary antibody on a rocking shaker for 120 minutes. After incubation, the washing process was repeated again. Following application of 600 µl of chemiluminescent HRP substrate (Merck Millipore, USA), the protein bands were visualised using Fusion Fx7 (Vilber, France) and stored for later reuse in a refrigerator at -20°C (Siemens, Germany). Where necessary, protein band areas and intensity were quantified by densitometry using the Image J 1.47v software (Wayne Rasband, USA).

5.2.2.6. ELISA

Murine BMDMs' secretion of cytokines and chemokines was quantified via ELISA for various conditions. Here, the effect of the absence of *Hdac9* and inhibition of the NF-κB pathway and the interplay between the two were assessed. BMDMs from *Hdac9*$^{+/+}$ *Apoe*$^{-/-}$ and *Hdac9*$^{-/-}$ *Apoe*$^{-/-}$ mice were used. Following BMDM-isolation from their femurs and tibiae, the cells were cultivated in BMDM growth medium with LCM, both described above. 1 million cells were seeded for 24 hours in LCM-free BMDM growth medium, allowing them to adhere to the surface of a 6-well plate (Thermo Fisher Scientific, USA). They were left untreated (14.1 µM DMSO as vehicle control) or pretreated for 60 minutes with either 100 nM or 250 nM TPCA-1 (Abcam, United Kingdom), a selective IKKβ-inhibitor. After pre-treatment, all samples

were stimulated for 24 hours with 2.87 µM mouse TNFα (Thermo Fisher Scientific, USA), keeping the cells incubated at 37°C. The supernatant was collected and centrifuged for 10 minutes at 500 g (Thermo Fisher Scientific, USA). Using commercially available ELISA kits, BMDM-secretion of Ccl2, Cxcl1 and TNFα (all R&D systems, USA) was quantified adhering to the supplier's protocols. To ensure cytokine and chemokine levels fell within the kits' detection ranges, samples were diluted as appropriate (Ccl2 and TNFα: 1:400, Cxcl1: 1:100). 100 µl of each diluted sample or standard was incubated for 2 hours at room temperature in a 96-well plate (Sigma-Aldrich, Germany) pre-treated with kit-enclosed capture antibody. Following aspiration and three washing cycles with wash buffer, the samples were incubated for 2 hours at room temperature with 100 µl kit-enclosed detection antibody, after which aspiration and washing was repeated. Samples were then incubated for 20 minutes with 100 µl kit-enclosed Strepdavidin-HRP. Following aspiration and the addition of 100 µl substrate solution and 50 µl stop solution, colorimetry was performed using a microplate absorbance reader (Bio-Rad, USA) and Microplate Manager Software 6 (Bio-Rad, USA). Absorbance was measured at 595 nm and 450 nm, whereby the first reading was subtracted from the latter and the result was plotted against a standard curve.

5.3. Statistical analysis

Western Blot readouts on acetylation and phosphorylation status were quantified via densitometry using Image J 1.47v (Wayne Rasband, USA). Both densitometry and ELISA results underwent statistical analysis with Graphpad Prism 7.0 (Graphpad Software Inc., USA), whereby data was represented as means ± SEM and the sample size ranged from 3 to 6. Data was tested for normality using the Shapiro-Wilk test next to visual inspection of the quantile-quantile plots. There were two scenarios: first, a comparison of two groups, whereby a two-sided non-parametric Mann-Whitney U test was applied. Second, experiments with two variants and at least three groups, where Two-Way Analysis of Variance (ANOVA) was conducted, followed by Bonferroni's or Dunnett's multiple comparisons tests. A result was considered statistically significant at $p<0.05$.

6. Results

6.1. HDAC9 interacts with IKKα and IKKβ of IκB kinase enzyme complex

The primary aim of this study was to identify HDAC9's role in atherogenesis by screening for potential interaction partners within the NF-κB signalling pathway. For proof of concept, interactions were detected or ruled out in HEK293 cells: a cell line chosen for its simple maintenance, high growth rate and excellent transfection efficiency[173,174]. To render a positive overall screening result, candidates required independent positive results in both directions – via pull down of HDAC9 and the investigated interaction partner, respectively. Identified interactions were then reproduced in atherosclerosis-relevant primary cells. Investigation of specific interaction partners was prioritised systematically, based on existing literature and previous findings within our research group.

6.1.1. HDAC9 interacts with IKKα and IKKβ, but not with IKKγ in HEK293 cells

Earlier TNFα-stimulation experiments in our research group identified HDAC9 to promote the phosphorylation of p65's serine residues 468 and 536 in three different atherosclerosis-relevant cell types. Thus, we hypothesized an interaction between HDAC9 and at least one NF-κB-relevant protein kinase[1].

A systematic screening of potential interaction partners for HDAC9 was employed via protein complex immunoprecipitation experiments in HEK293 cells. Exploration of candidate interactions was based on, (A) kinase activity relevant to phosphorylating p65's serine residues 468 and 536 and, (B) relevance to canonical NF-κB-signalling, whereby candidates meeting both (A) and (B) were prioritised. *FLAG*-tagged *HDAC9* or *FLAG* alone control were transiently co-transfected in HEK293 cells with one of the potential *HA*- or *T7*-tagged interaction partners, as described above.

Based on their association with the phosphorylation of p65's ser536 and ser468-residues, IKKα, IKKβ, IKKε, RSK1 and GSK3β underwent screening[117,138,150–

[152,164,175,176]. IκBα and the kinase IKKγ/NEMO were employed as controls due to their relevance in canonical NF-κB-signalling – though neither demonstrate kinase activity[116,124,125,131,135,140,142]. TBK1 was not screened for, because it was previously already identified to interact with and undergo deacetylation by HDAC9[100].

Meeting both (A) and (B), IKKα and IKKβ were hypothesised as key candidates for HDAC9-interaction[138,150,164,175,176]. Though IKKα is not typically defined as canonical, literature indicates a major, even dominant role in canonical NF-κB-signalling[138,144].

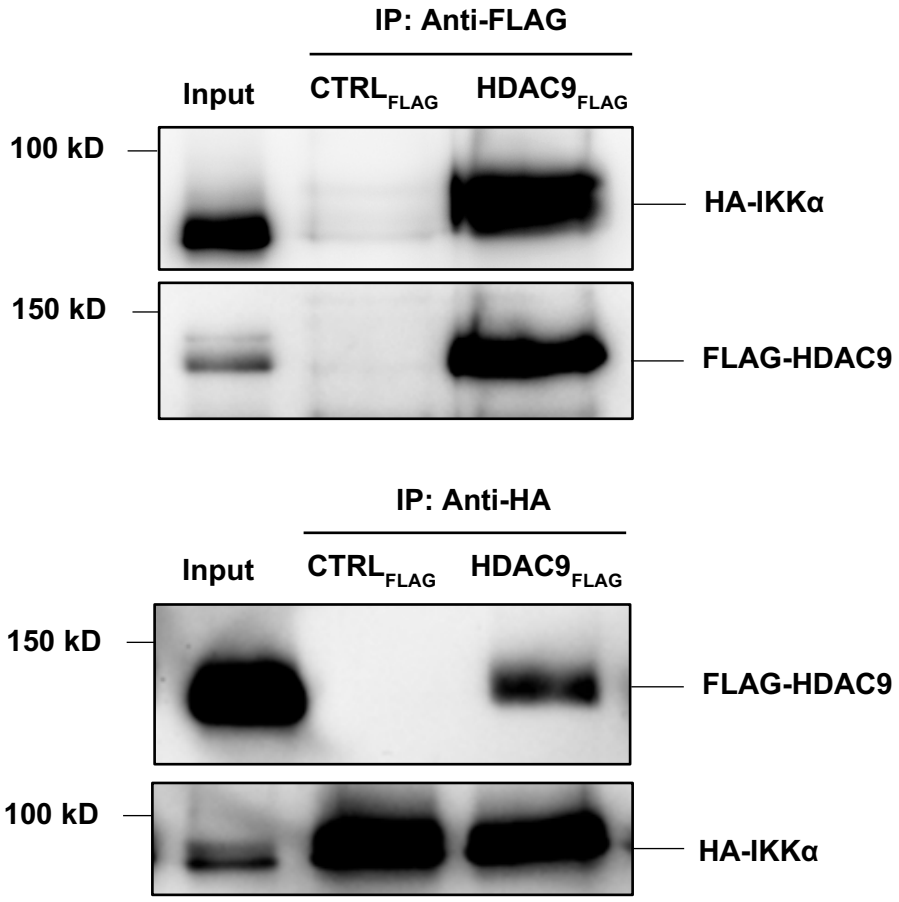

Figure 12: HDAC9 interacts with IKKα in HEK293 cells

Representative immunoblot images depicting the interaction between HDAC9 and IKKα following protein complex immunoprecipitation of whole cell lysate from HEK293 cells previously transfected with *FLAG-HDAC9* or *FLAG*-tagged control (CTRL) and *HA-IKKα*. **Top:** Anti-FLAG was used to pull down HDAC9 and its interaction partner, IKKα. IKKα was visualised via immunoblot with anti-HA and the pulldown of HDAC9 confirmed via anti-FLAG. **Bottom:** To validate the finding, the same sample and experimental setup was used to pull down IKKα and its interaction partner, HDAC9, using anti-HA. HDAC9 was visualised via immunoblot with anti-FLAG and the pulldown of IKKα confirmed via anti-HA. Shown on the left are molecular weights in kilodaltons (kDa), as determined by the protein standard marker. n=4. Results previously published in Asare et al. (2020)[1].

Indeed, screening confirmed the hypothesis and identified interactions between HDAC9 and both IKKα and IKKβ. The interactions were replicated in 4 independent samples respectively. For each sample, the interaction was first identified via pull down of HDAC9's FLAG-tag, with detection of either IKKα or IKKβ via immunoblotting of the HA-tag. The findings were validated in a second experiment using the same sample via pull down of the HA-tagged kinase and detection of HDAC9 via the FLAG-tag. Representative images are shown in Figures 12 and 13.

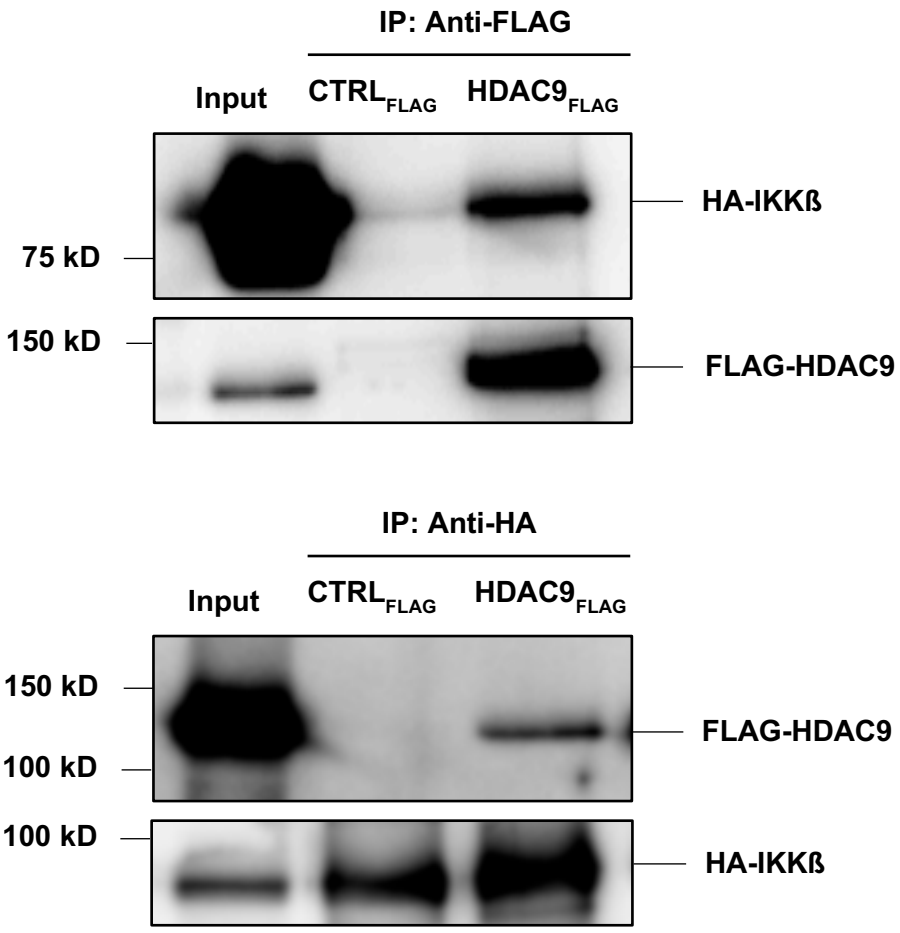

Figure 13: HDAC9 interacts with IKKβ in HEK293 cells

Representative immunoblot images depicting the interaction between HDAC9 and IKKβ following protein complex immunoprecipitation of whole cell lysate from HEK293 cells previously transfected with *FLAG-HDAC9* or *FLAG*-tagged control (CTRL) and *HA-IKKβ*. **Top:** Anti-FLAG was used to pull down HDAC9 and its interaction partner, IKKβ. IKKβ was visualised via immunoblot with anti-HA and the pulldown of HDAC9 confirmed via anti-FLAG. **Bottom:** To validate the finding, the same sample and experimental setup was used to pull down IKKβ and its interaction partner, HDAC9, using anti-HA. HDAC9 was visualised via immunoblot with anti-FLAG and the pulldown of IKKβ confirmed via anti-HA. Shown on the left are molecular weights in kilodaltons (kDa), as determined by the protein standard marker. n=4. Results previously published in Asare et al. (2020)[1].

Inputs of between 0.25% and 0.5% of total protein weight were used and refer to the entirety of protein content prior to protein complex immunoprecipitation, thus providing a reference for the evaluation of protein levels within the sample. This was maintained for all following protein complex immunoprecipitation experiments.

IKKα and IKKβ represent two of the three subunits of the IKK-complex. Both are catalytic, phosphorylating downstream targets. The third, IKKγ/NEMO, maintains a regulatory function and – notwithstanding its status as a kinase – is not typically involved in the phosphorylation of other proteins[177]. Thus, specificity for HDAC9's interaction with IKKα and IKKβ was hypothesised, whereby – in line with (A) and (B) – IKKγ/NEMO was postulated not to interact with HDAC9 and thus employed as a screening control.

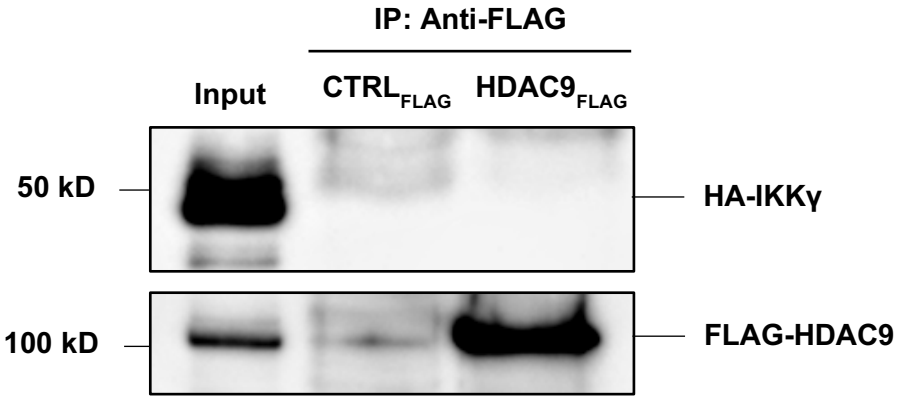

Figure 14: HDAC9 and IKKγ/NEMO do not interact

Representative immunoblot image depicting no interaction between HDAC9 and IKKγ/NEMO following protein complex immunoprecipitation of whole cell lysate from HEK293 cells previously transfected with *FLAG-HDAC9* or *FLAG*-tagged control (CTRL) and *HA-IKKγ/NEMO*. Anti-FLAG was used to pull down HDAC9 and its hypothesized interaction partner, IKKγ/NEMO. IKKγ/NEMO was visualized via immunoblot with anti-HA and the pulldown of HDAC9 confirmed via anti-FLAG. Shown on the left are molecular weights in kilodaltons (kDa), as determined by the protein standard marker. n=2. Results previously published in Asare et al. (2020)[1].

Indeed, the absence of an interaction between HDAC9 and IKKγ/NEMO both supported the hypothesis of specificity and validated the experimental setup. Because pulldown via HDAC9 was negative and bidirectional positive results were necessary for a screening result to be deemed positive, validation via HA-pulldown was rendered unnecessary. A representative image is shown in Figure 14.

6.1.2. HDAC9 interacts with IKKα and IKKβ in HUVECs

While HEK293 cells' high growth rate and transfection efficiency provide practical conditions for proof of concept, key findings concerning atherogenesis are ideally validated in atherosclerosis-relevant primary cells. Thus, following initial screening in HEK293 cells, HUVECs were used to replicate findings. The experimental design was adapted to accommodate for differences in cell cultivation and transfection.

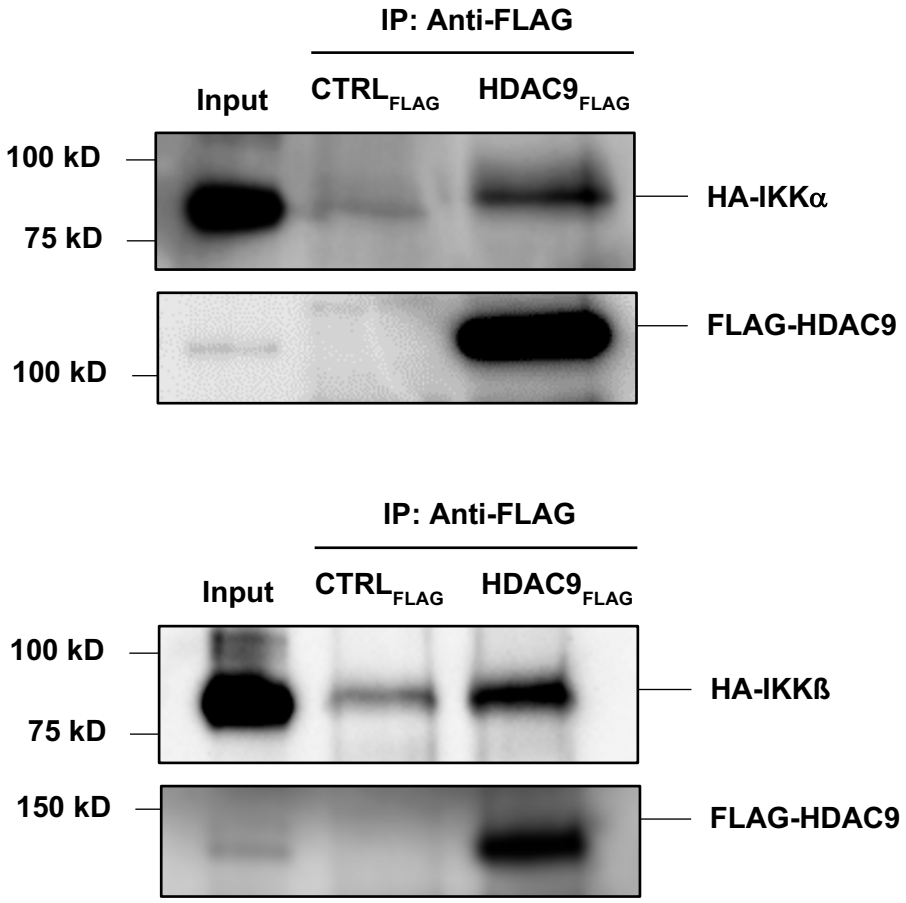

Figure 15: HDAC9 interacts with IKKα and IKKβ in HUVECs

Representative immunoblot images depicting the interactions of HDAC9 with IKKα and IKKβ, following protein complex immunoprecipitation of whole cell lysate from HUVECs previously transfected with *FLAG-HDAC9* or *FLAG*-tagged control (CTRL) and either *HA-IKKα* or HA-IKKβ. Anti-FLAG was used to pull down HDAC9 and the interacting kinase. **Top:** Anti-HA was used to visualise IKKα via immunoblot, after which the pulldown of HDAC9 was confirmed via anti-FLAG. n=3. **Bottom:** Anti-HA was used to visualise IKKβ via immunoblot and HDAC9-pulldown again confirmed via anti-FLAG. n=3. Shown on the left are molecular weights in kilodaltons (kDa), as determined by the protein standard marker. Results previously published in Asare et al. (2020)[1].

Indeed, protein complex immunoprecipitation in HUVECs validated both previous findings: interaction between HDAC9 and IKKα and IKKβ was replicated in three independent experiments respectively, in which the complex underwent pulldown via FLAG-tag and immunoblotting via the HA-tag. Representative images are shown in Figure 15. Confirmation of the protein interactions in this atherosclerosis-relevant cell type substantiated the concept of a significant role for HDAC9-mediated alterations to NF-κB-signalling in atherogenic inflammation. The findings led to two pressing questions: are IKKα and IKKβ the only NF-κB-relevant proteins to interact with HDAC9 and how do these interactions modify NF-κB-signalling?

6.1.3. HDAC9 does not interact with RSK1, GSK3β, IKKε or IκBα

Screening involved further protein complex immunoprecipitation experiments investigating interactions between HDAC9 and the remaining shortlisted proteins. Based on their ability to phosphorylate p65 at ser468 and ser536, three additional non-canonical kinases and, for control, a downstream target of IKKα and IKKβ within the NF-κB signalling pathway – IκBα – were investigated.

RSK1 was of interest, because it is a serine/threonine-kinase and a downstream effector of the MAPK/ERK-pathway. Its biological functions include activating transcription and translation as well as cell cycle regulation[178]. Critically to NF-κB-signalling, RSK1 activates NF-κB directly, via phosphorylation at ser536, and indirectly, via phosphorylation of IκBα, thus inducing its degradation[150,178–180].

Using whole cell lysates from HEK293 cells previously transfected with *FLAG-HDAC9* or *FLAG* alone control and *HA-RSK1*, pulldown was conducted via FLAG and immunoblotting via HA. However, three independent protein complex immunoprecipitation experiments confirmed no interaction between HDAC9 and RSK1. A representative image depicting no interaction is shown in Figure 16.

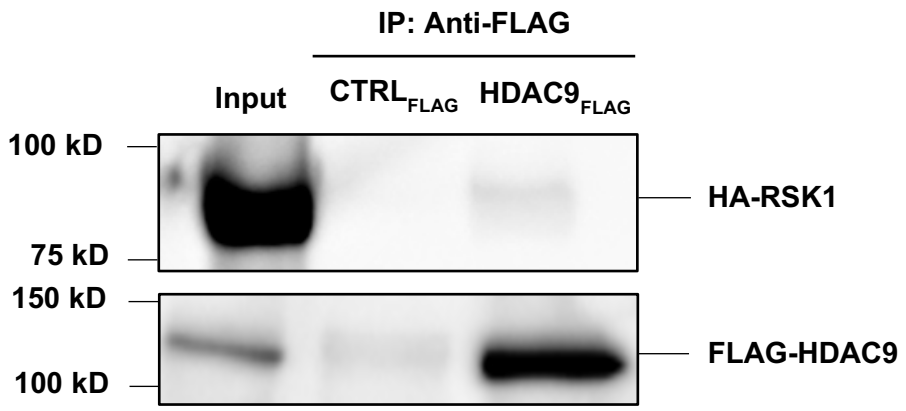

Figure 16: HDAC9 and RSK1 do not interact

Representative immunoblot image depicting no interaction between HDAC9 and RSK1 following protein complex immunoprecipitation of whole cell lysate from HEK293 cells previously transfected with *FLAG-HDAC9* or *FLAG*-tagged control (CTRL) and *HA-RSK1*. Anti-FLAG was used to pull down HDAC9 and its hypothesized interaction partner, RSK1. RSK1 was visualized via immunoblot with anti-HA and the pulldown of HDAC9 confirmed via anti-FLAG. Shown on the left are molecular weights in kilodaltons (kDa), as determined by the protein standard marker. n=3. Results previously published in Asare et al. (2020)[1].

Described as "the busiest kinase", with involvement in a range of biological functions and over 100 substrates, GSK3β was of natural interest for this study[181]. This non-canonical serine/threonine-kinase regulates various cellular processes from glycogen metabolism to cell cycle progression. Notably, it phosphorylates p65 at ser468 with an inhibitory effect, thereby reducing basal NF-κB-activty[151,181].

As above, whole cell lysates derived from HEK293 cells were transfected with *HA*-tagged *GSK3β* and *FLAG*-tagged *HDAC9* or *FLAG* alone control. Pulldown via FLAG with HA-immunoblotting was negative. The interaction between HDAC9 and GSK3β was ruled out in three independent samples. A representative image depicting no interaction is shown in Figure 17.

IKKε, a non-canonical serine/threonine-kinase shown to phosphorylate ser536 basally and ser468, was the final screening candidate[150,152]. Notwithstanding its name, it plays a secondary role in NF-κB-activation and does not associate with other IκB kinases – forming distinct complexes separate to those of IKKα, IKKβ and IKKγ/NEMO[153,154]. Thus, following positive screening for IKKα and IKKβ, an

interaction between HDAC9 and IKKε may have been indicative of multiple communication pathways with the NF-κB pathway.

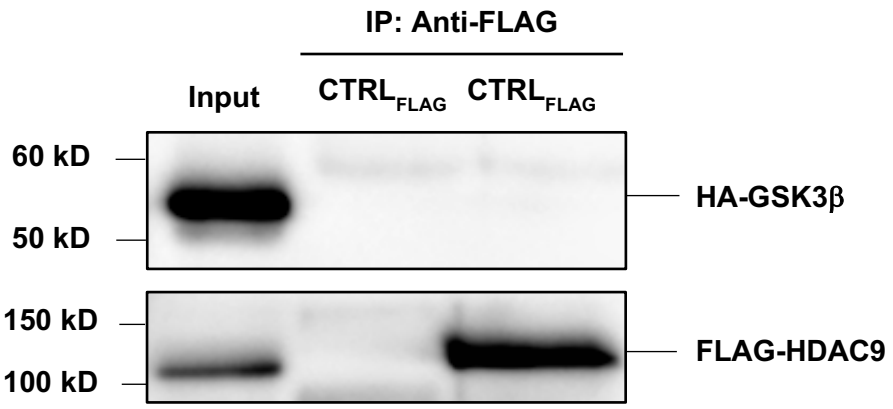

Figure 17: HDAC9 and GSK3β do not interact

Representative immunoblot image depicting no interaction between HDAC9 and GSK3β following protein complex immunoprecipitation of whole cell lysate from HEK293 cells previously transfected with *FLAG-HDAC9* or *FLAG*-tagged control (CTRL) and *HA-GSK3β*. Anti-FLAG was used to pull down HDAC9 and its hypothesized interaction partner, GSK3β. GSK3β was visualized via immunoblot with anti-HA and the pulldown of HDAC9 confirmed via anti-FLAG. Shown on the left are molecular weights in kilodaltons (kDa), as determined by the protein standard marker. n=3. Results previously published in Asare et al. (2020)[1].

Here, whole cell lysates derived from HEK293 cells previously transfected with *FLAG-HDAC9* or *FLAG* alone control and *T7*-tagged IKKε were employed. Three independent samples were prepared for protein complex immunoprecipitation. Initial pulldown was conducted via FLAG and immunoblotting via T7. While one experiment rendered a negative screening result, two remained inconclusive, showing only minimal band visibility versus the 0.25% input. To rule out an interaction, reciprocal experiments were performed pulling down via T7 and immunoblotting via FLAG. Here, all three experiments rendered a negative result and thus confirmed no communication between HDAC9 and IKKε. Representative images of the pulldown in both directions are depicted in Figure 18.

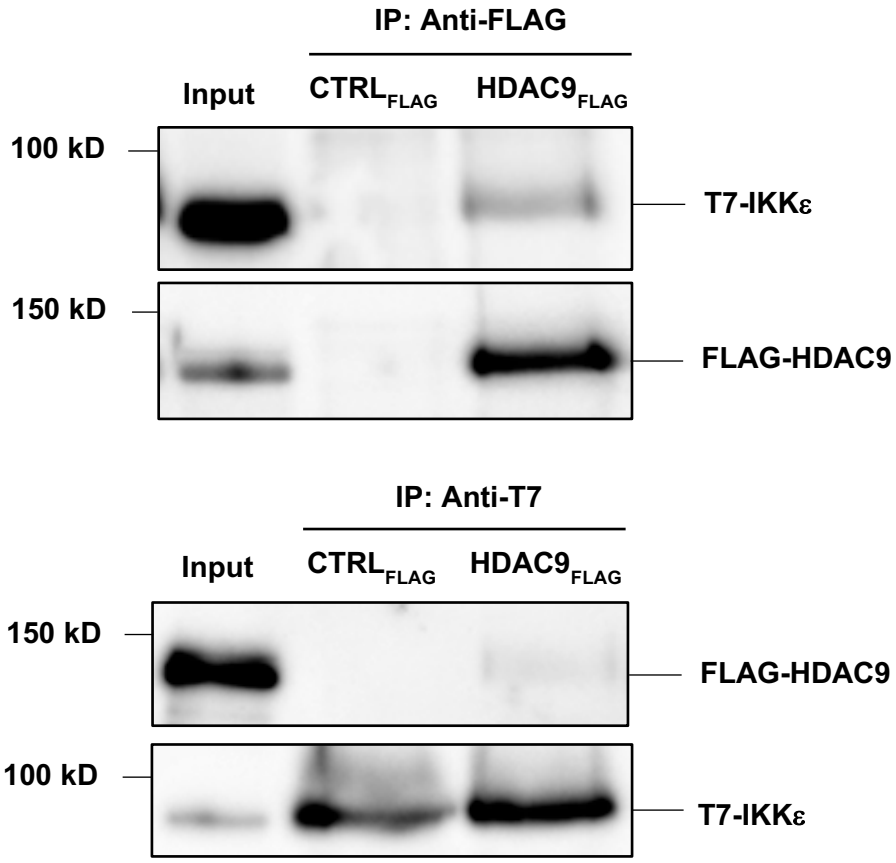

Figure 18: HDAC9 and IKKε do not interact

Representative immunoblot images depicting no interaction between HDAC9 and IKKε following protein complex immunoprecipitation of whole cell lysate from HEK293 cells previously transfected with *FLAG-HDAC9* or *FLAG*-tagged control (CTRL) and *T7-IKKε*. **Top:** Anti-FLAG was used to pull down HDAC9 and its hypothesized interaction partner, IKKε. Immunoblotting of IKKε via anti-T7 gave one negative and two inconclusive results out of three experiments. Pulldown of HDAC9 was confirmed for each experiment via anti-FLAG. **Bottom:** To rule out an interaction, the same sample and experimental setup was used to pull down IKKε and its interaction partner, HDAC9, using anti-T7. HDAC9 could not be visualised via immunoblot with anti-FLAG while the pulldown of IKKε was confirmed via anti-T7. Shown on the left are molecular weights in kilodaltons (kDa), as determined by the protein standard marker. n=3.

The final protein under investigation was IκBα, the most abundant IκB-isomer. A key regulator of NF-κB-signalling, IκB is the most significant downstream target for IKKα and IKKβ. IκB-degradation is an intermediary milestone in canonical NF-κB-signalling and hinges on its phosphorylation by activated IKKβ. Its degradation paves the way for NF-κB's nuclear translocation[116,140–143]. It was therefore of interest to assess its potential for involvement in a protein super-complex next to HDAC9 and the two previously identified kinases.

Maintaining the same experimental setup, HEK293 whole cell lysates previously transfected with *FLAG-HDAC9* or *FLAG* alone control and *HA-IκBα* were used. Pulldown was conducted via FLAG and immunoblotting attempted via HA. Two independent protein complex immunoprecipitation experiments confirmed no interaction between HDAC9 and IκBα. Figure 19 depicts a representative image.

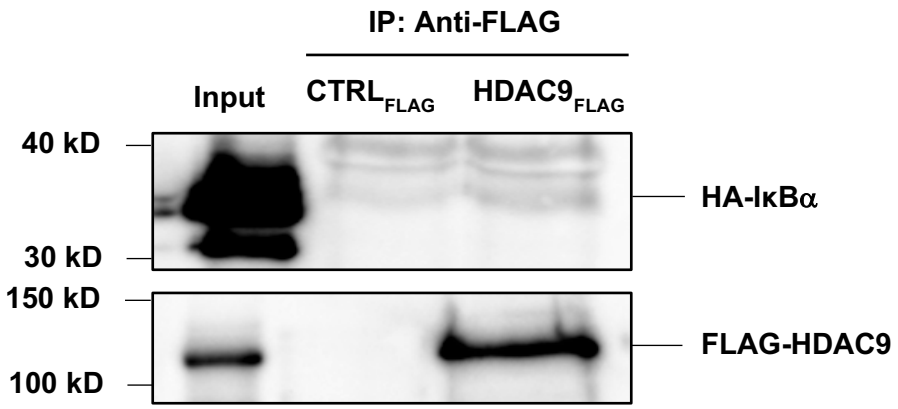

Figure 19: HDAC9 and IκBα do not interact

Representative immunoblot image depicting no interaction between HDAC9 and IκBα following protein complex immunoprecipitation of whole cell lysate from HEK293 cells previously transfected with *FLAG-HDAC9* or *FLAG*-tagged control (CTRL) and *HA-IκBα*. Anti-FLAG was used to pull down HDAC9 and its hypothesized interaction partner, IκBα. IκBα was visualized via immunoblot with anti-HA and the pulldown of HDAC9 confirmed via anti-FLAG. Shown on the left are molecular weights in kilodaltons (kDa), as determined by the protein standard marker. n=2. Results previously published in Asare et al. (2020)[1].

These negative screening results, which rule out interactions between HDAC9 and three significant non-canonical kinases as well as IKKβ's primary canonical downstream target, are noteworthy. The lack of interactions with RSK1, GSK3β and IKKε underline the above-described overlap between HDAC9's gene expression in inflammation and NF-κB-dependent canonical transcriptional responses. Said overlap had substantiated the hypothesis of HDAC9's pro-atherogenic downstream effects being mediated by canonical NF-κB-signalling. These findings further confirm the specificity of HDAC9's interaction with IKKα and IKKβ, rendering the involvement of RSK1, GSK3β and IKKε – all previously described to phosphorylate p65 at ser468 and/or ser536 – unlikely. Further, the lack of interaction between HDAC9 and IκBα reduces the likelihood of the involvement of a protein super-complex. This is

significant, because it minimises risk of off-target effects by other unknown proteins to mediate HDAC9's atherosclerotic downstream manifestations.

Though IκBα has been described to interact with other non-canonical kinases, the absence of interaction with HDAC9 – and the lack of communication between HDAC9 and RSK1, GSK3β or IKKε – reduced the likelihood of non-canonical involvement in mediating HDAC9's downstream effects[182,183]. Thus, screening of further potential interactions between HDAC9 and other non-canonical kinases was deprioritised to facilitate exploration of the mechanistic role of its interaction with IKKα and IKKβ.

6.2. HDAC9-mediated deacetylation of IKKα and IKKβ leads to activation of IKKβ

Following identification of HDAC9's interaction partners within NF-κB signalling, the second aim of this study was to explore the mechanistic role of interactions. Due to HDAC9's previously described class-atypical enzymatic activity – enabling the deacetylation of both histones and non-histone proteins, such as the non-canonical kinase TBK1 – potential deacetylation of interaction partners was investigated[75,96,100]. As with the former experiments to identify protein interactions, protein complex immunoprecipitation was employed to evaluate HDAC9-mediated deacetylation of IKKα and IKKβ. Proof of concept was conducted in HEK293 cells. To validate positive results in atherosclerosis-relevant primary cells, findings would be replicated in HUVECs. HDAC9 was hypothesised to mediate the deacetylation of both IKKα and IKKβ.

6.2.1. HDAC9 mediates deacetylation of IKKα and IKKβ in HEK293 cells

To assess IKKα and IKKβ's HDAC9-dependent pan-acetylation status in HEK293 cells, the previously prepared samples containing transiently co-transfected FLAG-tagged HDAC9 or FLAG alone control with one of the HA-tagged interaction partners

were either reused or prepared afresh. Protein complex immunoprecipitation was employed using the above-described experimental setup. In each sample, pull down was conducted via the kinase's HA-tag. IKKα and IKKβ's respective pan-acetylation levels, in the presence and absence of HDAC9, were detected via immunoblotting of acetylated lysine-residues using acetyl lysine-antibody. Acetylation of IKKα and IKKβ was quantified and normalised to total IKKα or IKKβ protein levels, in five and six independent experiments respectively. Total amounts of kinase in each sample were quantified via immunoblotting of pulled down HA-tag. A two-sided non-parametric Mann-Whitney U test compared HDAC9-samples to control.

Both IKKα and IKKβ rendered positive results, showing significantly reduced levels of pan-acetylation in the presence of HDAC9. This confirmed the hypothesis. Compared to the FLAG alone control, IKKα's relative acetylation in the presence of FLAG-HDAC9 was 0.71 ($p=0.008$), suggesting a 29% reduction in pan-acetylation mediated by HDAC9. Similarly, for IKKβ, relative acetylation in the presence of FLAG-HDAC9 was 0.74 ($p=0.004$) compared to control. Here, HDAC9 mediated a 26% reduction of IKKβ's levels of pan-acetylation. Representative images, as well as a graphical quantification of IKKα and IKKβ's relative acetylation levels in HEK293 cells, are depicted in Figure 20.

6.2.2. HDAC9 mediates deacetylation of IKKβ in HUVECs

The finding concerning HDAC9's role in mediating the deacetylation of kinases in HEK293 cells warranted validation in atherosclerosis-relevant primary cells. Thus, replication of the results was attempted in HUVECs. Here, IKKβ was prioritised due to its greater significance for canonical NF-κB-signalling. The experimental setup was adapted to accommodate for differences in cell cultivation and transfection, as described above.

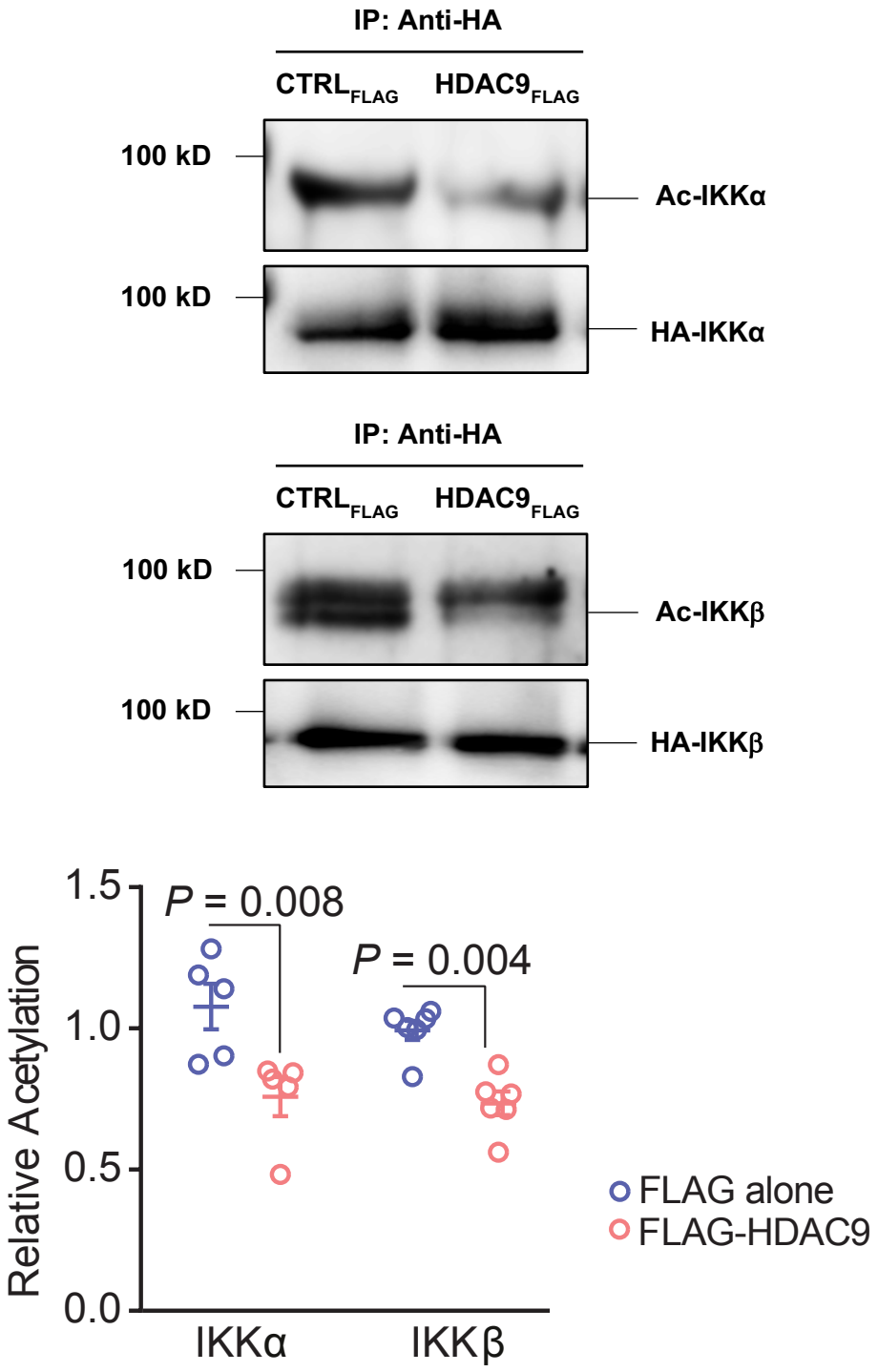

Figure 20: IKKα and IKKβ undergo HDAC9-mediated deacetylation in HEK293 cells

Representative immunoblot images depicting the HDA9-mediated reduction in pan-acetylation of IKKα **(Top)** and IKKβ **(Middle)**. Protein complex immunoprecipitation was conducted with whole cell lysate from HEK293 cells previously transfected with *FLAG-HDAC9* or *FLAG*-tagged control (CTRL) and *HA-IKKα* or *HA-IKKβ*. Anti-HA was used to pull down each kinase with the interaction partner, HDAC9. Acetylation was visualized via immunoblot with anti-acetyl lysine. Kinase pulldown was confirmed and total kinase amounts quantified via immunoblot with anti-HA. Shown on the left are molecular weights in kilodaltons (kDa), as determined by the protein standard marker. **Bottom:** Relative acetylation of IKKα (n=5) and IKKβ (n=6) in the presence of FLAG-HDAC9 versus FLAG alone. Both were reduced in the presence of HDAC9. Relative acetylation of IKKα: 0.71 (p=0.008). Relative acetylation of IKKβ: 0.74 (p=0.004). Error bars indicate SEM. Results previously published in Asare et al. (2020)[1].

Four independent experiments reproduced the same positive results for IKKβ. A significant reduction in levels of pan-acetylation was identified in the presence of HDAC9 versus control, thus validating the earlier findings in HEK293 cells. Compared to the FLAG alone control, IKKβ's relative acetylation in the presence of FLAG-HDAC9 was 0.47 (p=0.002), representing a 53% reduction of pan-acetylation in the presence of HDAC9. A representative image, as well as a graphical quantification of HDAC9-mediated relative acetylation levels for IKKβ in HUVECs, are depicted in Figure 21.

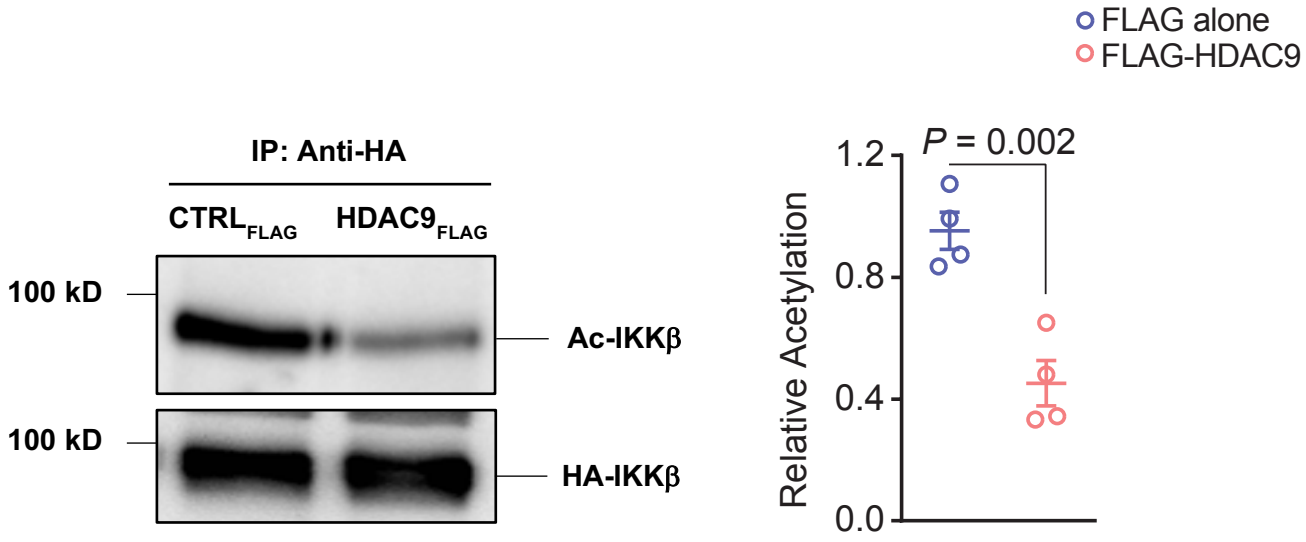

Figure 21: IKKβ undergoes HDAC9-mediated deacetylation in HUVECs

Left: Representative immunoblot image depicting the reduction in pan-acetylation of IKKβ in the presence of FLAG-HDAC9 versus control. Protein complex immunoprecipitation was conducted with whole cell lysate from HUVECs previously transfected with *FLAG-HDAC9* or *FLAG*-tagged control (CTRL) and *HA-IKKβ*. Anti-HA was used to pull down IKKβ with its interaction partner, HDAC9. Acetylation was visualized via immunoblot with anti-acetyl lysine. IKKβ-pulldown was confirmed and total IKKβ quantified via immunoblot with anti-HA. Shown on the left are molecular weights in kilodaltons (kDa), as determined by the protein standard marker. **Right:** Quantification of IKKβ's relative acetylation in the presence of FLAG-HDAC9 versus FLAG alone. Relative acetylation of IKKβ was significantly reduced in the presence of HDAC9 compared to control (0.47, p=0.002). n=4. Error bars indicate SEM. Results previously published in Asare et al. (2020)[1].

6.2.3. HDAC9 mediates increase in IKKβ kinase activity

Previous research has found acetylation of IKKα and IKKβ's catalytic domains to have an inhibitory effect on their kinase activity, thus preventing kinase activation and phosphorylation of IκBα in response to pro-inflammatory stimuli[122]. Downstream,

IKKα and IKKβ also phosphorylate p65 at ser536, which stimulates NF-κB's transcriptional activity by facilitating p65 to bind DNA[150]. However, the exact link between IKK's acetylation status and p65's phosphorylation levels at ser536 remained unclear.

Hence, the effect of HDAC9-mediated IKKβ-deacetylation on IKKβ's kinase activity was explored via quantification of p65's phosphorylation levels at ser536. The findings introduced between 6.1 and 6.2.2. presented the concept of HDAC9-mediated IKK-deacetylation while our research group's previous work linked HDAC9 to ser536-phosphorylation. Taken together, these findings suggested a potential mechanistic role for HDAC9's interaction with IKKβ. It was thus hypothesised that the HDAC9-mediated deacetylation of IKKβ enhances IKKβ's kinase activity, leading to the phosphorylation of ser536 and stimulation of NF-κB's transcriptional activity.

To investigate this hypothesis, kinase activity assays were conducted. For proof of concept, whole cell lysates were derived from HEK293 cells previously co-transfected with *HA-IKKβ* and *FLAG-HDAC9* or *FLAG* alone control. Using the above-described experimental design, protein complex immunoprecipitation samples that had previously undergone pulldown via FLAG or HA (n=2 respectively) were exposed to recombinant human p65-substrate. Kinase activity was visualised via immunoblotting with anti-p-p65 (ser536).

All four independent experiments displayed increased phosphorylation of ser536 in the presence of HDAC9 versus control, thus confirming the hypothesis of an HDAC9-mediated stimulation of IKKβ kinase activity. Representative images depicting results of these kinase activity assays conducted in HEK293 cells are shown in Figure 22.

To replicate the findings of heightened, HDAC9-mediated kinase activity in atherosclerosis-relevant primary cells, two independent validation experiments with a cell-adapted setup were repeated in HUVECs. Due to the significant quantity of cellular material required for each sample, pulldown was conducted one-way via FLAG.

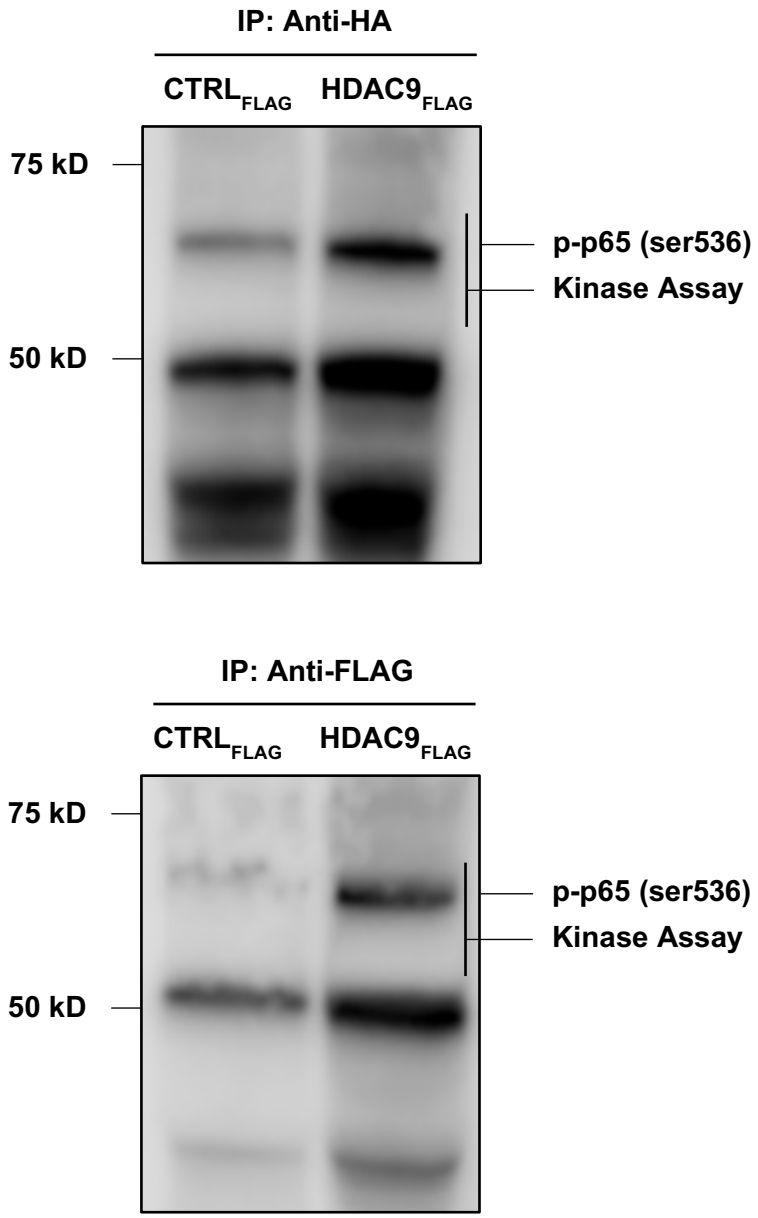

Figure 22: HDAC9 stimulates ser536-phosphorylation by IKKβ in HEK293 cells

Representative immunoblot images depicting increased HDAC9-mediated phosphorylation of p65 at ser536 following protein complex immunoprecipitation of whole cell lysate from HEK293 cells previously transfected with *FLAG-HDAC9* or *FLAG*-tagged control (CTRL) and *HA-IKKβ*. **Top:** Anti-HA was used to pull down IKKβ and its interaction partner, HDAC9, before IKKβ's substrate, recombinant p65, was added to initiate the kinase activity assay. Phosphorylation of p65 at ser536 was visualized via immunoblot with anti-p-p65 (ser536). n=2. **Bottom:** The finding was validated by pulldown of HDAC9 and its interaction partner, IKKβ, via anti-FLAG. The subsequent kinase activity assay and immunoblotting followed the same process described above. n=2. Shown on the left are molecular weights in kilodaltons (kDa), as determined by the protein standard marker. Results previously published in Asare et al. (2020)[1].

Confirming the previous findings, both HUVEC-based experiments rendered an identical result, displaying an increase in phosphorylation levels at ser536 in the presence of HDAC9 versus control. A representative image is depicted in Figure 23.

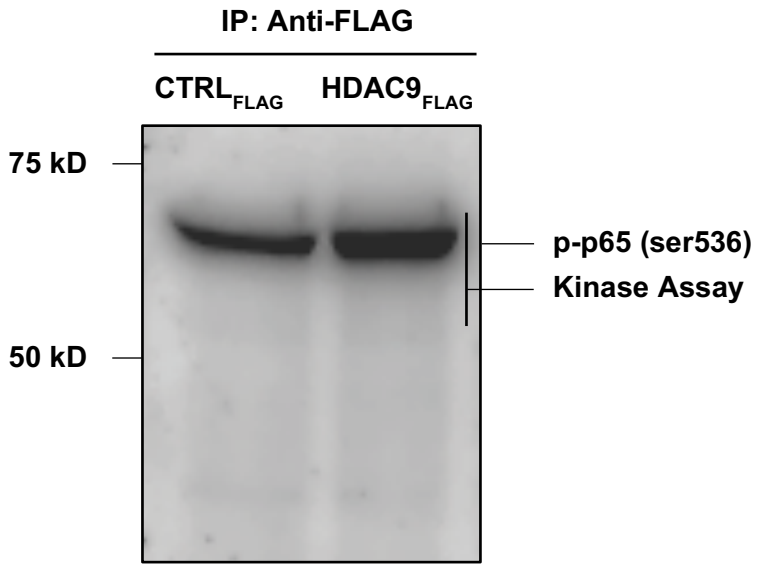

Figure 23: HDAC9 stimulates ser536-phosphorylation by IKKβ in HUVECs

Representative immunoblot image depicting increased HDAC9-mediated phosphorylation of p65 at ser536 following protein complex immunoprecipitation of whole cell lysate from HUVECs previously transfected with *FLAG-HDAC9* or *FLAG-tagged control (CTRL) and HA-IKKβ*. Anti-FLAG was used to pull down HDAC9 and its interaction partner, IKKβ, before IKKβ's substrate, recombinant p65, was added to initiate the kinase activity assay. Phosphorylation of p65 at ser536 was visualized via immunoblot with anti-p-p65 (ser536). n=2. Shown on the left are molecular weights in kilodaltons (kDa), as determined by the protein standard marker. Results previously published in Asare et al. (2020)[1].

6.3. Further findings

6.3.1. p65-phosphorylation at ser276 unaffected by *HDAC9*-knockdown

Earlier TNFα-stimulation experiments in our research group identified HDAC9 to promote the phosphorylation of p65 at residues ser468 and ser536 in three different atherosclerosis-relevant cell types[1]. To explore the specificity of the identified effect of *HDAC9*-knockdown on phosphorylation levels at these residues, the previous experimental setup with HUVECs was maintained. Here, p65's phosphorylation levels at another site, ser276, were assessed in three independent HUVEC-based TNFα-stimulation experiments.

ser276, located in p65's RHD, is also involved in transcriptional co-activation, though phosphorylation is conferred by other kinases[117,160–162]. Hence, absence of changes to phosphorylation levels at ser276 would serve as further confirmation of the specificity of HDAC9's interaction with IKKα and IKKβ, since their mediation of downstream effects do not involve phosphorylation of ser276. Thus, no significant HDAC9-dependent change in its phosphorylation levels was hypothesised.

This hypothesis was confirmed in three independent TNFα-stimulation experiments, with no significant difference in phosphorylation, irrespective of duration of stimulation. Quantification of p65-phosphorylation at ser276 normalised to total p65 showed comparable results for HUVECs that had undergone siRNA-mediated *HDAC9*-depletion and those treated with *SCR* RNA. A representative image, as well as a graphical quantification of results, are depicted in Figure 24.

6.3.2. *Hdac9*-knockout reduces effect of IKKβ-inhibition on CCL2-secretion in murine BMDMs

Notwithstanding identification of HDAC9's interaction partners in NF-κB-signalling, along with evidence of HDAC9's mechanistic role, downstream effects of the interaction remained to be explored. The findings gave rise to the question of whether HDAC9's pro-inflammatory effect is mediated exclusively via IKK.

Earlier ELISA results in our research group identified *Hdac9*-knockout in murine BMDMs to reduce secretion of key pro-inflammatory cytokines and chemokines, including Ccl2, Cxcl1 and Tnfα[1]. To determine the exclusivity of IKKβ as a mediator of HDAC9-associated pro-inflammation, the effect of IKKβ-inhibition on protein secretion levels was investigated in HDAC9-depleted cells versus control. IKKβ was hypothesised to mediate at least part of HDAC9's pro-inflammatory target gene expression. Maintaining our group's previous experimental design, secreted levels of Ccl2, Cxcl1 and Tnfα were compared between *Hdac9*-depleted murine BMDMs and wild type controls in three independent experiments. Here, BMDMs were stimulated with TNFα and either left untreated or underwent IKKβ-inhibition with 100 nM or 250

nM TPCA-1. Protein levels were measured via ELISA of the collected supernatant, after which multiple comparison statistical analysis followed.

Levels of Ccl2 were reduced in untreated *Hdac9*-knockout BMDMs compared to wild type controls, replicating our group's earlier findings. The same effect was seen in groups treated with 100 nM and 250 nM TPCA-1, where *Hdac9*-deficiency attenuated Ccl2-secretion compared to wild type controls.

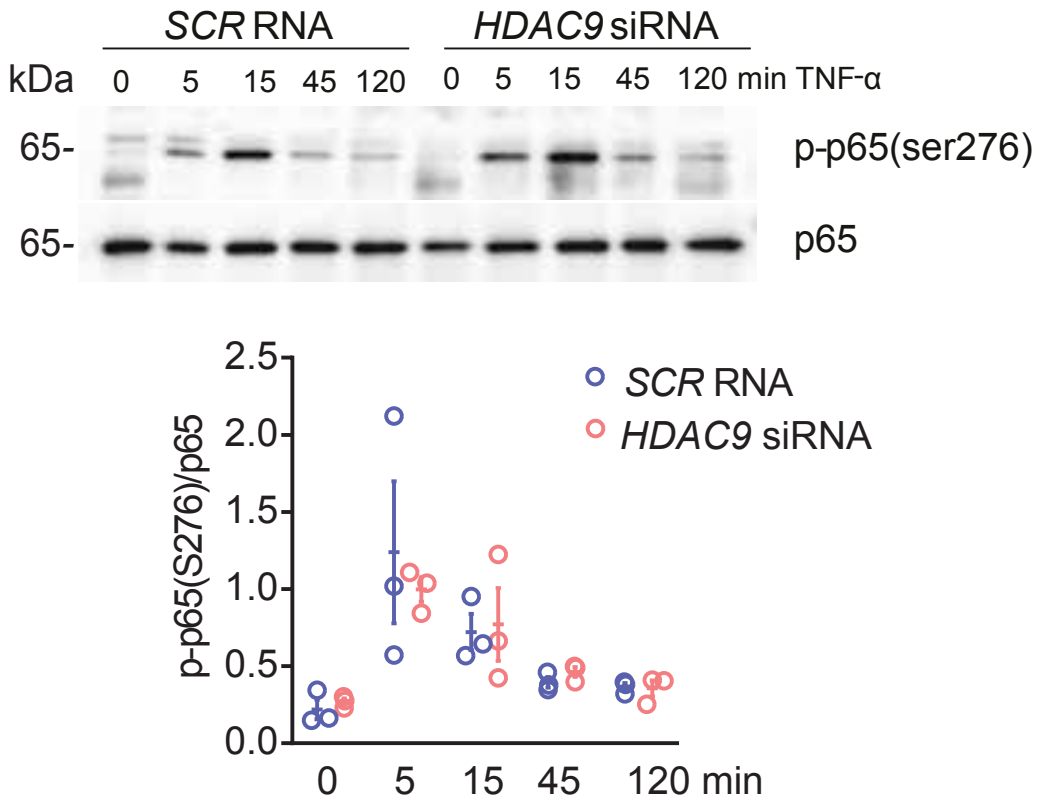

Figure 24: HDAC9-depletion does not affect p65-phosphorylation at ser276

Top: Representative immunoblot image depicting p65-phosphorylation levels at ser276 and total p65 in HUVECs following co-transfection with *HDAC9* siRNA or *SCR* siRNA control and TNFα-stimulation at various durations. Total p65 and levels of site-specific phosphorylation were visualized via immunoblotting with anti-p65 and anti-p-p65 (ser276). **Bottom:** Quantification of relative phosphorylation at ser276 in HDAC9-depleted samples normalized to total p65 versus non-HDAC9-depleted control. Absence of HDAC9 had no effect on p65-phosphorylation at ser276. n=3. Shown on the left are molecular weights in kilodaltons (kDa), as determined by the protein standard marker. Error bars indicate SEM. Results previously published in Asare et al. (2020)[1].

Interestingly, IKKβ-inhibition-dependent Ccl2-secretion in *Hdac9*-knockout BMDMs contrasted that in wild type BMDMs. IKKβ-inhibition significantly reduced Ccl2-secretion in wild type BMDMs compared to non-inhibited controls. However, in *Hdac9*-knockout BMDMs, the reduction in Ccl2-secretion was not significant in IKKβ-inhibited samples compared to the untreated *Hdac9*-knockout control. The results suggest TPCA-1's effect to have been, in part, pre-empted by *Hdac9*-depletion. Two-way analysis of variance (ANOVA) further identified *Hdac9* as the main source of variation in Ccl2-levels (p=0.0004). Combined, these results introduce early evidence supporting the hypothesis of a non-additive mechanistic overlap between HDAC9 and IKKβ in regulating Ccl2-secretion. This was not the case for Cxcl1 and Tnfα.

A schematic representation of the experimental setup, as well as a graphical description of the multiple comparison statistical analysis, are depicted in Figure 25.

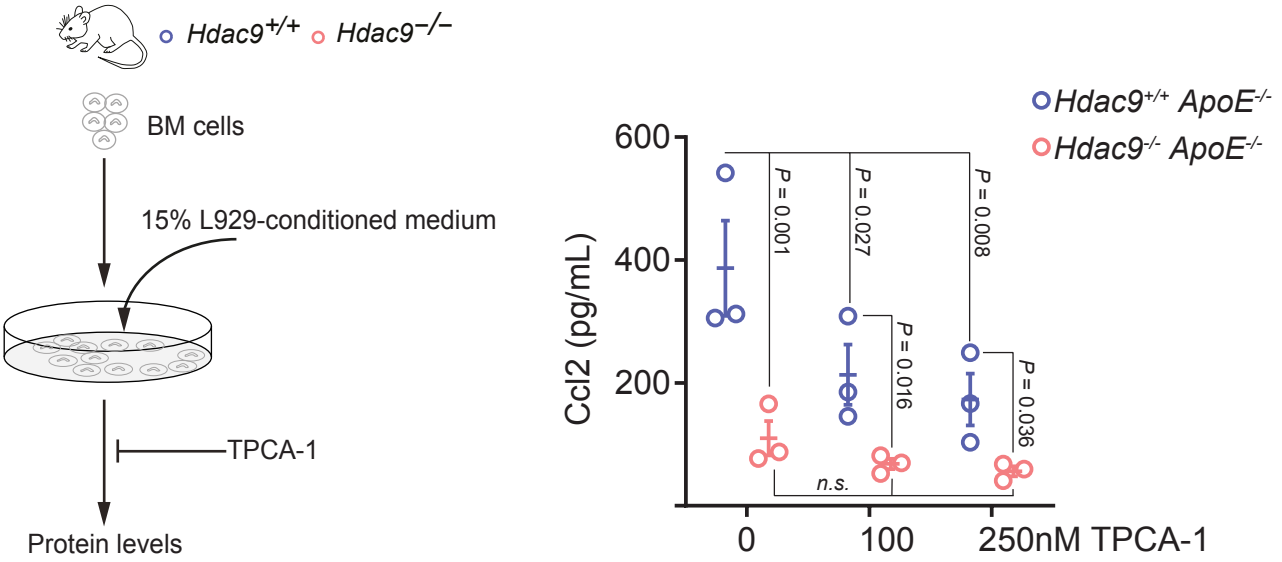

Figure 25: IKKβ-inhibition does not reduce Ccl2-secretion in *Hdac9*-depleted BMDMs

Left: BMDMs isolated from *Hdac9*$^{-/-}$*Apoe*$^{-/-}$ and *Hdac9*$^{+/+}$*Apoe*$^{-/-}$ mice were cultivated in BMDM growth medium with 15% LCM. Following seeding, they were treated for 60 minutes with either DMSO (untreated control), 100 nM or 250 nM TPCA-1 before undergoing TNFα-stimulation for 24 hours. Protein levels were measured via ELISA. Figure adapted from Asare et al. (2020)[1]. **Right:** Secretion levels of Ccl2 (pg/mL) in *Hdac9*$^{-/-}$ compared to *Hdac9*$^{+/+}$ BMDMs. Ccl2-secretion was significantly reduced in *Hdac9*$^{-/-}$ compared to *Hdac9*$^{+/+}$ BMDMs, across all TPCA-1-treatment conditions. IKKβ-inhibition significantly decreased Ccl2-secretion in *Hdac9*$^{+/+}$ BMDMs, while it had no significant effect on *Hdac9*$^{-/-}$ BMDMs. n=3. Error bars indicate SEM.

7. Discussion

7.1. Summary of results and relevance

LAS represents a fifth of ischaemic stroke cases worldwide, attributed to the rupture of atherosclerotic plaques located in vessels supplying the brain[8,9]. Various GWAS have associated *HDAC9* with LAS and other catastrophic atherosclerotic complications[16,18,19,22–27]. rs2107595, an *HDAC9*-variant, was linked to elevated *HDAC9*-expression in two atherosclerosis-relevant cells – macrophages and human peripheral blood mononuclear cells – before upregulated *HDAC9*-expression was shown to result in increased atherosclerotic plaque size and formation[20,21,23]. HDAC9 was then found to increase atherosclerotic plaque vulnerability and promote pro-inflammatory responses via secretion of various pro-atherogenic cytokines and chemokines. The findings led to the exploration of NF-κB-involvement in HDAC9's pro-atherogenicity, whereby TNFα-stimulation experiments showed elevated phosphorylation of p65 at ser468 and ser536[1].

With NF-κB-signalling hypothesised to mediate HDAC9's pro-atherogenic downstream effects via interaction, the aims of this study were **1)** to clarify HDAC9's role in atherogenesis via screening for and identification of its potential interaction partners within the NF-κB signalling pathway, **2)** to explore the mechanistic role of HDAC9's interaction with NF-κB-signalling and **3)** to investigate downstream effects of HDAC9 in the NF-κB signalling pathway.

Among others, these aims were addressed via protein complex immunoprecipitation, kinase activity assays and TNFα-stimulation experiments. The results of this study reveal crosstalk between HDAC9 and NF-κB-signalling. The findings can be summarised as **1)** HDAC9 interacts with NF-κB-signalling via IKKα and IKKβ, **2)** IKKα and IKKβ are deacetylated in the presence of HDAC9 and **3)** HDAC9 increases IKKβ kinase activity, stimulating downstream NF-κB-signalling alterations.

7.1.1. HDAC9 interacts with NF-κB-signalling via IKKα and IKKβ

The central finding in this study – providing a basis for subsequent results – was the discovery of a key link between HDAC9 and pro-atherogenic inflammation: the interaction between HDAC9 and two components crucial to canonical NF-κB-signalling. Screening of HDAC9's potential interaction partners was prioritised based on (A) kinase activity relevant to phosphorylating p65's serine residues 468 and 536 – for which our group had previously demonstrated an HDAC9-dependency – and (B) relevance to canonical NF-κB-signalling[1]. Our approach was supported by the *barcode hypothesis*, which associates specific phosphorylation sites of p65 with distinctive transcriptional responses[112,184]. The catalytic subunits of the IKK-complex, IKKα and IKKβ, were defined as key candidates for interaction with HDAC9 as they met both criteria (A) and (B)[138,150,164,175,176]. Though IKKα is not typically defined as a canonical kinase, earlier findings indicate a major, sometimes dominant role in canonical signalling[138,144]. Protein complex immunoprecipitation experiments were initially conducted in HEK293 cells for proof of concept. These confirmed the hypothesis, finding HDAC9 to interact with both IKKα and IKKβ. By contrast, interactions with the canonical and non-canonical entities IKKγ/NEMO, IκBα, RSK1, GSK3β and IKKε were eliminated via negative protein complex immunoprecipitation results. Critically, these findings indicate specificity for HDAC9's interaction with IKKα and IKKβ by ruling out interaction partners previously described to phosphorylate p65. They also minimise the risk of off-target effects by other unknown proteins to mediate HDAC9's atherosclerotic downstream manifestations. Findings were then validated for applicability to atherosclerosis via reproduction of the results in HUVECs, an atherosclerosis-relevant primary cell type.

The relevance of these findings goes beyond corroborating HDAC9-involvement in atherosclerotic inflammation. The immunoblot readouts are the first documented evidence of crosstalk between HDAC9 and the NF-κB signalling cascade – a critical immunological pathway – and provide a mechanistic link informing the overlap between HDAC9's pro-inflammatory gene expression and NF-κB-dependent canonical transcriptional responses, including *VCAM-1*, *ICAM-1* and *CCL2*[1,113]. Due to NF-κB's central role in inflammation, the finding may provide spill over-effects to

other inflammatory diseases involving HDAC9. Researchers in oncology will monitor these results with particular interest as they examine therapeutic targets for various tumour entities[83–87].

Beyond the unspecific inhibition of HDAC9 with TMP195, the identification of HDAC9's interaction with IKKα and IKKβ delivers a new therapeutic target and thus potential for advances in drug discovery. With both kinases functioning as significant regulators of target gene-specific NF-κB-transactivation, research into the inhibition of these newly identified PPIs may deliver therapeutic innovation in atherosclerosis and beyond[118–120]. Small molecule drugs (SMDs), monoclonal antibodies (mAbs) and interfering peptide therapeutics could provide viable mechanisms to disrupt PPIs and may thus represent key opportunities as candidates for specific inhibition of HDAC9's interaction with IKKα and IKKβ[185–193].

While light has been shed on the interplay between HDAC9 and canonical NF-κB signalling, IKKα also plays a prominent non-canonical role, processing p100 to p52 in conjunction with NIK and subsequently activating p52/RelB-dimers[116,144,149]. Thus, further exploration of non-canonical involvement may be informative. Protein complex immunoprecipitation of HDAC9 with NIK, p100 or RelB could provide further valuable insights into the specificity of canonical components in conferring HDAC9's pro-atherogenic effects.

7.1.2. IKKα and IKKβ are deacetylated in the presence of HDAC9

Perhaps the most interesting finding – not least due to considerable novelty factor – was the identification of HDAC9's mechanistic role in its interaction with IKKα and IKKβ: HDAC9-mediated deacetylation of both interaction partners was demonstrated in two cell types. First, proof of concept was attained in HEK293 cells before reproduction of the results in HUVECs indicated vascular relevance.

Solidifying the suspicion of HDAC9's uncharacteristic mechanistic ability to deacetylate non-histone proteins, this finding has far-reaching scientific potential –

particularly in light of HDAC9's involvement in various regulatory cellular processes and diseases. Class IIa HDACs generally exhibit lower enzymatic activity compared to their class I counterparts. However, IKKα and IKKβ's HDAC9-mediated deacetylation underlines the case of potential exceptions[75,96,100].

Previously, HDAC9 had been found to interact endogenously with TBK1, leading to its deacetylation and heightened kinase activity[100]. Acetylation of IKKα and IKKβ's catalytic domains has been shown to confer an inhibitory effect on NF-κB-activity, mediated via delayed phosphorylation within their activation loops and subsequent kinase inactivation[122,159]. Our research group's discoveries, indicating enhanced NF-κB-activity in the presence of HDAC9, are coherent with these earlier findings, as deacetylation of IKKα and IKKβ could be expected to augment NF-κB-activity.

The protein complex immunoprecipitation-protocol was adapted for both cell types to detect IKKα and IKKβ's acetylation levels via immunoblotting of acetylated lysine-residues. Thus, pan-acetylation in the presence of HDAC9 was assessed, whereby the interaction partner's cumulative acetylation of all lysine residues was normalised to the total amount of protein. Acetylation at specific residues was not quantified.

Specific acetylation sites in the acetylation domain have already been associated with kinase activation for both IKKα and IKKβ: thr179 for IKKα and thr180 for IKKβ[122]. However, commonly available antibodies, as used in this study, currently only assess for pan-acetylation of lysine residues. The results thus propose significant potential for the identification of new candidate residues with relevance to kinase activity. Mass spectrometry is required for the definition of these novel acetylation sites.

Changes in a protein's acetylation-state are associated with alterations in function and conformation. This may explain subsequent evidence, described in detail below, showing heightened kinase activity for IKKβ[59,100,194]. Again, mass spectrometry may be appropriate to further the understanding of acetylation-dependent conformational changes to IKKα and IKKβ and their effect on enzymatic activity.

Since publication of these results, evidence on HDAC9's enzymatic ability to deacetylate non-histone proteins has undergone further substantiation, finding it to induce neuronal death via interaction with and deacetylation of Hypoxia-inducible Factor 1 (HIF-1) and Transcription factor Sp1[195]. With this novel understanding of HDAC9-involvement in the deacetylation of non-histone proteins, re-evaluation of its mechanistic role in other PPIs and signalling pathways may be warranted to expand understanding of HDAC9's broader biological impact. More specific inhibition – perhaps with affinity for HDAC9's catalytic domain – may provide a promising therapeutic strategy, heightening selectivity and reducing off-target effects.

7.1.3. HDAC9 increases IKKβ kinase activity, stimulating downstream NF-κB-signalling alterations

Further results triangulate evidence for downstream effects of HDAC9's interaction with IKKα and IKKβ. Findings from kinase activity assays, TNFα-stimulation experiments and ELISAs indicate a significant mechanistic role for HDAC9 in altering pro-atherogenic NF-κB-signalling.

To assess the effect of HDAC9-presence on kinase activity, kinase activity assays were conducted using protein complex immunoprecipitation samples obtained from HEK293 cell and HUVEC-derived whole cell lysates. IKKβ was prioritised due to its greater relevance to NF-κB-activation in canonical signalling. In both cell types, presence of HDAC9 stimulated kinase activity for IKKβ, conferring increased phosphorylation of p65 at ser536. The finding mimics earlier results described for TBK1, which displayed heightened kinase activity following deacetylation by HDAC9[100]. The result is logically consistent with the documented inhibitory effect for acetylation of IKKα and IKKβ's catalytic domains on respective kinase activity[122].

One hypothesis to explain IKKβ's heightened catalytic activity could be conformational change of its structure following a deacetylation-induced change in charge state[100]. Lysine deacetylation of IKKβ may also induce allosteric regulation of its kinase domain to promote the recruitment of p65[196]. Deacetylation-induced

changes in its cellular localisation are also possible, but less likely in the context of NF-κB-signalling due to IKKβ's localisation in the cytoplasm and p65's shuttling into the nucleus hinging on IκB-degradation[197].

Leading to the hypothesis of IKKα and IKKβ-involvement, earlier TNFα-stimulation experiments in our research group had identified HDAC9 to promote p65-phosphorylation at ser468 and ser536[1]. Whether the effect of *HDAC9*-knockdown was specific to phosphorylation levels at these phosphorylation sites remained to be explored. ser276's phosphorylation, which also promotes transcriptional co-activation, is not conferred by IKKα or IKKβ[117,160–162]. Indeed, TNFα-stimulation experiments conducted for this study concluded no relationship between HDAC9 and ser276-phosphorylation. Taken together, the downstream effects revealed by the kinase activity assays and TNFα-stimulation indicate a high specificity for HDAC9 in its role of activating IKKβ and potentially IKKα. Interestingly, early findings suggested phosphorylation at ser276 to play a significant role in p65-transactivation[198,199]. The *barcode hypothesis* is a likely explanation, as site-differential p65-phosphorylation regulates selective target gene-expression and downstream effects[119,200]. Further, the question of whether IKKβ's activation is conferred directly via HDAC9 or another co-activating HDAC with deacetylase activity, remains to be explored[72,156].

Finally, to assess the mechanistic link between HDAC9's interaction with IKKβ and downstream NF-κB-dependent chemokine-secretion, ELISA experiments were conducted in *Hdac9*-knockout and *Hdac9*-wild type BMDMs. Replicating our group's earlier findings, levels of Ccl2 were reduced in *Hdac9*-knockout BMDMs compared to wild type controls. IKKβ-inhibition with TPCA-1 also reduced Ccl2-secretion in wild type BMDMs, confirming earlier evidence on the inhibitor's downstream effects[201]. Interestingly, however, IKKβ-inhibition did not significantly reduce Ccl2-secretion in *Hdac9*-knockout cells compared to untreated controls, suggesting that *Hdac9*-depletion had largely pre-empted TPCA-1's effect. Statistical analysis further identified *Hdac9* as the main source of variation in Ccl2-levels. The results suggest a non-additive mechanistic overlap between HDAC9 and IKKβ in regulating Ccl2-secretion, whereby HDAC9's effect is mediated via modulation of IKKβ-activity. The observation is congruent with preceding findings introduced in this study, whereby

the likely non-additivity of HDAC9 and IKKβ in regulating Ccl2-secretion underlines the central role of their interaction to promote pro-atherogenic inflammation.

In summary, these novel results represent a paradigm shift in our understanding of pro-atherogenic NF-κB-signalling. HDAC9 has been elucidated as a key player in mediating atherogenic inflammation, interacting with two central components of the NF-κB pathway. Notwithstanding earlier evidence to the contrary, the above-described results – and those presented in response by other researchers – corroborate evidence indicative of deacetylase properties in class IIa HDACs. Both IKKα and IKKβ undergo HDAC9-mediated deacetylation, resulting in IKKβ-activation and, subsequently, enhanced p65-phosphorylation at ser468 and ser536, but not ser276. HDAC9 thus confers pro-atherogenic inflammation via its interaction with IKKα and IKKβ. Subsequent research already suggests this finding's significance to stretch beyond atherosclerosis.

7.2. Limitations

7.2.1. Protein overexpression system

To date, the search for HDAC9's endogenous interaction partners continues, whereby candidate substrates have typically been explored in over-expression systems[109]. This study is no different, with both HDAC9 and the interaction partners undergoing investigation via overexpression by plasmid DNA transfection. Though appropriate for proof of concept, the biological relevance of findings discovered via protein overexpression may be limited, as elevated protein levels could stimulate cellular processes unlikely to occur endogenously[202]. These non-ideal, potentially cytotoxic conditions may be mediated by resource overload of biological pathways, misfolding and aggregation[202–205]. Notably for HDAC9 and this study, protein overexpression may also cause stoichiometric imbalance of protein complexes and promiscuous off-target mis-interactions[202,204,206,207]. Experiments involving plasmids to overexpress glycolytic enzymes estimate the maximum protein burden limit of some non-harmful proteins – as a percentage of a cell's total protein levels – at 15%, with others significantly lower. This protein burden limit represents the protein

expression level at which cells exhibit growth defects due to an overload of protein synthesis resources[204]. However, cellular functions may in fact already be altered at lower levels of protein overexpression, thus potentially reducing the internal and external validity of experimental overexpression setups. In this study, the success of plasmid DNA transfection was verified qualitatively via microscopic control of co-transfected GFP's green fluorescence. Notwithstanding quantification of total protein concentrations, neither the protein levels of HDAC9 nor those of its interaction partners were quantified, though the value of such quantification remains debatable due to the lack of experimental setup alternatives. It is assumed that the identified PPIs would also occur at endogenous concentrations. While protein overexpression systems – though common and well-established – may not fully replicate physiological conditions, the findings of this study are supported by a series of diverse experiments collectively contributing to a cohesive and consistent overall narrative, thus providing a comprehensive understanding of the underlying mechanisms. However, confirmation of our findings at endogenous protein levels and potentially mass spectrometry may contribute to our understanding of the field.

7.2.2. Role of a potential super-complex in the deacetylation of IKKα and IKKβ

While other class IIa HDAC-family members exhibit reduced deacetylase activity, HDAC9 has been shown to deacetylate both histone and non-histone proteins[75,96,100,195]. Previously, HDAC9's endogenous deacetylation of TBK1 was shown to heighten kinase activity, leading to an enhanced antiviral innate immune response[100]. Since publication of this study's results, HDAC9 was further found to induce neuronal death via deacetylation of HIF-1 and Transcription factor Sp1[195]. Nonetheless, the exact mechanism underlying IKKα and IKKβ's deacetylation in the presence of HDAC9 requires further exploration. Though the setup for the protein complex immunoprecipitation experiments attempts to limit off-target effects introduced by unknown interaction partners, the formation of larger multiprotein complexes – potentially involving further unidentified proteins next to overexpressed HDAC9 and kinases – is not unfeasible. Oligomerisation is a shared theme for NF-κB signalling components and is well-documented for TRAF and RIP-proteins, as

well as IKKγ/NEMO[116]. Similarly, HDACs are described to establish large multiprotein complexes that may include further HDACs[64]. In particular, class IIa HDACs have been found to involve HDAC3 – a class I HDAC – to confer deacetylation activity[72]. HDAC3 has also been identified to co-activate pro-inflammatory NF-κB-signalling by deacetylating p65 at various lysine residues to reduce inhibitory effects on p65-activity[156]. Likewise, HDAC5 deacetylates PP2A to positively regulate NF-κB-signalling via the phosphorylation of IKKβ and p65 at ser536[208]. Here, the controlled environment – facilitated by protein overexpression, tag-based purification for selective complex isolation and negative controls – reduces the risk of mediation of IKKα and IKKβ's deacetylation by an unidentified member of a multiprotein complex. Replication of the above-described experiments, leveraging plasmid DNA for deacetylase-dead HDAC9 via point mutations in its catalytic domain, may offer a robust strategy – alongside mass spectrometry – to rule out such off-target effects.

7.3. Outlook

The results introduced herein represent a paradigm shift in our understanding of pro-atherogenic NF-κB-signalling. Scientific interest in the findings has been significant.

Since publication of these results, HDAC9's enzymatic ability to deacetylate non-histone proteins has enjoyed further substantiation: its interaction with and deacetylation of HIF-1 and Transcription factor Sp1 has been found to induce neuronal death[195]. More generally, class IIa HDAC-mediated deacetylation of IKKα and IKKβ has also been replicated. In a similar experimental setup to the one described above, HDAC7 was shown to interact and deacetylate both IKKα and IKKβ. In contrast to HDAC9, HDAC7 also interacted with IKKγ/NEMO without affecting its acetylation, indicating specificity for the deacetylation of interaction partners. Equally, HDAC7-overexpression enhanced IKKβ-activity, mediated by increased phosphorylation of p65 at both ser468 and ser536[209]. Demonstrated in a mouse model of astrocyte-mediated inflammation, these findings propose relevance for HDAC9's interaction with IKKα and IKKβ beyond atherosclerosis in other non-atherogenic inflammatory diseases. Moreover, the findings surrounding HDAC7

represent the latest chapter in a recent row of developments that are shifting understanding of class IIa HDACs. The tide seems to be turning on the assumption of low deacetylase activity, with recent evidence to the contrary now in circulation for HDAC5 and HDAC7, next to the findings presented for HDAC9[100,195,208,209]. This may open the field to a promising new therapeutic target: specific inhibition of class IIa HDACs' enzymatic activity, potentially via their catalytic domains.

Interest in HDAC-inhibition continues to gain traction. Notably, TMP195 – a first-in-class selective competitive inhibitor of the class IIa HDAC-family – stands out. Earlier *in vivo* evidence confirms a reduction of tumour burden and metastasis via macrophage modulation in various cancers[109–111].

Critically, our research group was able to demonstrate TMP195 to confer atheroprotection and reverse many of the findings presented in this study: in mice, TMP195 attenuates early lesion formation and mitigates the initiation of atherosclerosis by limiting leucocyte recruitment. It decreases atheroprogression by conferring plaque stability via reduced necrotic core formation and increased fibrous cap thickness. Importantly for this study, TMP195 limits pro-inflammatory responses consistent with attenuated IKKβ-activity. While IKKβ's pan-acetylation levels in BMDMs are increased, kinase activity is reduced in HEK293 cells and TNFα-induced p65-phosphorylation at ser536 is also limited. NF-κB target gene-expression is reduced both in mice and humans[1]. Thus, more so than its broad-spectrum counterparts – some of which exacerbate atherosclerotic lesion size – TMP195 qualifies as a promising new therapeutic strategy in the treatment of atherosclerosis[210]. Further, TMP195-mediated HDAC-inhibition has since shown early evidence of efficacy in treating neuroinflammatory psychiatric disorders, via inhibition of NF-κB-activation[209]. It shows similar effects in the treatment of acute kidney injury and – using nanoparticle drug delivery – in enhanced fracture recovery[211,212].

However, reflecting the fast pace of the field, the results presented in this study – identifying various potential therapeutic targets – may already warrant the exploration of new treatment strategies. HDAC9 is now understood to interact with

IKKα and IKKβ, whereby each kinase functions as a regulator of target gene-specific NF-κB-transactivation[118–120]. SMDs, mAbs and interfering peptide therapeutics may thus provide effective and more selective inhibition of these newly discovered PPIs[185–193]. Further, with mounting evidence for class IIa HDACs' deacetylase activity, inhibition of HDAC9's catalytic domain may offer explorative potential. For example, selective inhibition of HDAC9's catalytic domain or PPIs may reduce adverse events induced by genetic deletion and other less targeted approaches, including cardiac hypertrophy and other cardio-anatomical abnormalities[63,64,70].

Several further research priorities emerge from this study. To gain deeper insights into the mechanisms underlying IKKα and IKKβ-activation, the identification of specific acetylation sites for both proteins remains essential. Mass spectrometry experiments are recommended, also to explore the role of deacetylation-induced conformational changes in stimulating IKKβ kinase activity. Positive findings would bear significant potential for the definition of new therapeutic targets for atherosclerosis and other HDAC9-associated diseases.

Appropriate strategies to evaluate the direct deacetylation of IKKα and IKKβ by HDAC9 could include mass spectrometry or replication of the above-described experiments, leveraging plasmid DNA for HDAC9 with point mutations in its catalytic domain. Ruling out the presence of other HDACs with deacetylase activity in a potential multiprotein complex renders off-target IKKβ-activation less likely. Further, IKKα's prominent role in non-canonical NF-κB-signalling prompts the exploration of non-canonical components in mediating HDAC9's atherogenic downstream effects.

The relevance of these findings goes beyond corroborating HDAC9-involvement in atherosclerotic inflammation. Rather, these novel insights associate HDAC9 with the deacetylation of non-histone proteins. Thus, re-evaluation of HDAC9's mechanistic role in other PPIs and signalling pathways may be warranted to support understanding of its broader biological impact.

8. Conclusion

HDAC9 boasts a prominent role as a driver of pro-atherogenic vascular inflammation, atheroprogression and plaque vulnerability. Our research group previously confirmed HDAC9-dependent phosphorylation of p65 at ser468 and ser536, associating HDAC9 with the activation of NF-κB-signalling. However, the exact link between HDAC9 and NF-κB, the underlying mechanisms, as well as their potential for therapeutic targeting required further investigation.

To shed light on these evidence gaps and identify viable therapeutic strategies, this study screened for and explored interactions between HDAC9 and NF-κB-signalling and, further, investigated HDAC9's mechanistic role and downstream effects on NF-κB. Samples generated from murine BMDMs, HEK293 cells and HUVECs – co-transfected with HDAC9 and key NF-κB components – were employed for protein complex immunoprecipitation, kinase activity assays, TNFα-stimulation and ELISAs.

The findings represent a paradigm shift in our understanding of HDAC9 and pro-atherogenic NF-κB-signalling. Interactions for HDAC9 with IKKα and IKKβ were identified in two cell types, establishing a crucial link to pro-atherogenic inflammation. Further, IKKα and IKKβ were discovered to undergo HDAC9-mediated deacetylation, inaugurating a potential reversal of assumptions concerning low enzymatic activity in class IIa HDACs. HDAC9-presence resulted in IKKβ-activation and enhanced p65-phosphorylation at ser536, but not ser276. HDAC9 thus confers pro-atherogenic inflammation via interaction with IKKα and IKKβ, though potential super-complex involvement should be excluded and the results reproduced at endogenous levels.

Several research priorities emerge, not least because recent findings indicate significance beyond atherosclerosis. Mass spectrometry should be employed to identify the specific acetylation sites for IKKα and IKKβ. Further, the results bear significant potential for novel therapeutic strategies: SMDs, mAbs and interfering peptide therapeutics may offer opportunities to inhibit enzymatic HDAC-activity and newly discovered PPIs, heightening selectivity and reducing off-target effects.

9. List of abbreviations

APS	Ammonium persulfate
ATP	Adenosine triphosphate
BMDM	Bone marrow-derived macrophage
BSA	Bovine serum albumin
CAD	Coronary artery disease
CCL2	Chemokine (C-C motif) ligand 2
CVD	Cardiovascular disease
CXCL1	Chemokine (C-X-C motif) ligand 1
DALY	Disability-adjusted life year
ddH_2O	Double-distilled water
DMEM	Dulbecco's modified eagle medium
DMSO	Dimethyl sulfoxide
DNA	Deoxyribonucleic acid
DTT	Dithiothreitol
EDTA	Ethylenediaminetetraacetic acid
ELISA	Enzyme-linked immunosorbent assay
FBS	Fetal bovine serum
FOXP3	Forkhead box P3
GFP	Green fluorescent protein
GSK3β	glycogen synthase kinase-3 beta
GWAS	Genome-wide association study
HAoSMC	Human aortic smooth muscle cell
HAT	Histone acetyltransferase
HDAC	Histone deacetylase
HEK293	Human embryonic kidney cell
HIF-1	Hypoxia-inducible Factor 1
HUVEC	Human umbilical vein endothelial cell
ICAM-1	Intercellular adhesion molecule 1
IκB	Inhibitor of kappa B
IKK	Inhibitor of kappa B kinase
IKKα	Inhibitor of kappa B kinase alpha
IKKβ	Inhibitor of kappa B kinase beta
IKKγ (NEMO)	Inhibitor of kappa B kinase gamma

IKKε	Inhibitor of kappa B kinase epsilon
IL-1β	Interleukin-1 beta
IL12	Interleukin-12
KCl	Potassium chloride
KH_2PO_4	Potassium dihydrogen phosphate
LAS	Large artery stroke
LCM	L929 conditioned medium
LDL	Low density lipoprotein
LPS	Lipopolysaccharide
lys	Lysine residue
mAb	Monoclonal antibody
MEF2	Myocyte enhancer factor-2
MIF	Macrophage migration inhibitory factor
MSK1	Mitogen- and stress-activated protein kinase-1
NaCl	Sodium chloride
Na_2HPO_4	Di-Sodium hydrogen phosphate
NEMO (IKKγ)	NF- κB essential modulator
NIK	NF-κB-inducing kinase
N-CoR	Nuclear receptor co-repressor 1
PAD	Peripheral artery disease
PBS	Phosphate buffer saline
PIM1	Moloney murine leukemia virus-1
PKAc	Protein kinase A (catalytic subunit)
PMSF	Phenylmethylsulfonyl fluoride
PP2A	Protein phosphatase 2A
PPI	Protein-protein interaction
PTM	Post-translational modification
PVDF	Polyvinylidene fluoride
RHD	Rel homology domain
RIP	Receptor-interacting protein
SCR	Scrambled
SDS	Sodium dodecyl sulfate
ser	Serine residue
SEM	Standard error of the mean
siRNA	Small interfering RNA

SMC	Smooth muscle cell
SMD	Small molecule drugs
SMRT	Nuclear receptor co-repressor 2
SNP	Single nucleotide polymorphism
TAD	Transactivation domain
TAK1	Mitogen-activated protein kinase kinase kinase 7
TBK1	TANK-binding kinase 1
TBS-T	Tris-buffered saline and Tween
TEMED	Tetramethylethylenediamine
thr	Threonine residue
TNFα	Tumor necrosis factor α
TNFR1	Tumor necrosis factor receptor 1
TRADD	Tumor necrosis factor receptor type 1-associated death domain protein
TRAF2/5	TNF receptor associated factor 2/5
VCAM-1	Vascular cell adhesion molecule 1

10. Table of figures

11. Acknowledgments

First and foremost, I would like to thank my doctoral advisor, Dr. rer. nat. Yaw Asare, for his support in completing this doctorate – both at the bench and in questions on life throughout our time together. I am extremely grateful to you, Yaw, for introducing me to the stimulating world of science and will never forget the fond memories of joint late-night euphoria decrypting those promising readouts at the Fusion-machine.

I would also like to extend my sincere appreciation to my supervisor, group leader and Institute Director, Prof. Dr. med. Martin Dichgans. Thank you, Martin, for providing me with the opportunity to work on such an important and interesting topic in an environment that is both intellectually and materially state-of-the-art. Thank you also to my colleagues and research group members, for the supportive atmosphere, interesting discussions and assistance throughout our time together.

Most importantly, I would like to distinguish my loved ones, who have supported me tremendously over the years. My family – Mama, Dad and Benny – whom I owe so much for their unconditional love and persevering support throughout my academic journey (and beyond). Thank you, you three, for the odd pinch of patience, when it was necessary, and for providing me with the privilege of an international upbringing with multiple homes, important lessons on life and values and, every now and then, the 4:30AM-chauffeur service to swim training. To my friends, close to home and afar: thank you for your support, reliability, positivity and continuous encouragement. And, of course, for the many wonderful experiences that I cherish so fondly.

These lines bring the most significant chapter in my life so far to a close – a good decade of higher education – and I am filled with happiness and gratitude for the stimulating encounters and opportunities I have had the privilege to experience.

12. Affidavit (Eidesstattliche Versicherung)

Campbell-James, Thomas Alexander

Surname, first name

I hereby declare that the submitted thesis entitled:

HDAC9-related alterations to NF-κB-signalling in atherogenic inflammation

is my own work. I have only used the sources indicated and have not made unauthorised use of services of a third party. Where the work of others has been quoted or reproduced, the source is always given.

I further declare that the dissertation presented here has not been submitted in the same or similar form to any other institution for the purpose of obtaining an academic degree.

Munich, 21st July 2025 — Thomas Campbell-James

Place, Date — Signature doctoral candidate

13. Confirmation of congruency

Campbell-James, Thomas Alexander

Surname, first name

I hereby declare that the electronic version of the submitted thesis, entitled:

HDAC9-related alterations to NF-κB-signalling in atherogenic inflammation

is congruent with the printed version both in content and format.

Munich, 21st July 2025	Thomas Campbell-James
Place, Date	Signature doctoral candidate

14. Curriculum vitae

Suppressed for privacy.

15. References

1. Asare Y, Campbell-James TA, Bokov Y, et al. Histone Deacetylase 9 Activates IKK to Regulate Atherosclerotic Plaque Vulnerability. *Circ Res*. 2020;127(6):811-823. doi:10.1161/CIRCRESAHA.120.316743
2. Feigin VL, Stark BA, Johnson CO, et al. Global, regional, and national burden of stroke and its risk factors, 1990–2019: a systematic analysis for the Global Burden of Disease Study 2019. *Lancet Neurol*. 2021;20(10):795-820. doi:10.1016/S1474-4422(21)00252-0
3. GBD 2016 Lifetime Risk of Stroke Collaborators, Feigin VL, Nguyen G, et al. Global, Regional, and Country-Specific Lifetime Risks of Stroke, 1990 and 2016. *N Engl J Med*. 2018;379(25):2429-2437. doi:10.1056/NEJMoa1804492
4. Sacco RL, Kasner SE, Broderick JP, et al. An Updated Definition of Stroke for the 21st Century. *Stroke*. 2013;44(7):2064-2089. doi:10.1161/STR.0b013e318296aeca
5. Richter D, Weber R, Eyding J, et al. Acute ischemic stroke care in Germany – further progress from 2016 to 2019. *Neurol Res Pract*. 2021;3(1):14. doi:10.1186/s42466-021-00115-2
6. Luengo-Fernandez R, Violato M, Candio P, Leal J. Economic burden of stroke across Europe: A population-based cost analysis. *Eur Stroke J*. 2020;5(1):17-25. doi:10.1177/2396987319883160
7. Campbell BC V., De Silva DA, Macleod MR, et al. Ischaemic stroke. *Nat Rev Dis Primers*. 2019;5(1):70. doi:10.1038/s41572-019-0118-8
8. Rennert RC, Wali AR, Steinberg JA, et al. Epidemiology, Natural History, and Clinical Presentation of Large Vessel Ischemic Stroke. *Neurosurgery*. 2019;85(suppl_1):S4-S8. doi:10.1093/neuros/nyz042
9. Donkor ES. Stroke in the 21st Century: A Snapshot of the Burden, Epidemiology, and Quality of Life. *Stroke Res Treat*. 2018;2018:3238165. doi:10.1155/2018/3238165
10. Adams HP, Bendixen BH, Kappelle LJ, et al. Classification of subtype of acute ischemic stroke. Definitions for use in a multicenter clinical trial. TOAST. Trial of Org 10172 in Acute Stroke Treatment. *Stroke*. 1993;24(1):35-41. doi:10.1161/01.STR.24.1.35
11. Herrington W, Lacey B, Sherliker P, Armitage J, Lewington S. Epidemiology of Atherosclerosis and the Potential to Reduce the Global Burden of Atherothrombotic Disease. *Circ Res*. 2016;118(4):535-546. doi:10.1161/CIRCRESAHA.115.307611
12. Benjamin EJ, Blaha MJ, Chiuve SE, et al. Heart Disease and Stroke Statistics—2017 Update: A Report From the American Heart Association. *Circulation*. 2017;135(10). doi:10.1161/CIR.0000000000000485
13. Lackland DT, Roccella EJ, Deutsch AF, et al. Factors Influencing the Decline in Stroke Mortality. *Stroke*. 2014;45(1):315-353. doi:10.1161/01.str.0000437068.30550.cf
14. Boehme AK, Esenwa C, Elkind MSV. Stroke Risk Factors, Genetics, and Prevention. *Circ Res*. 2017;120(3):472-495. doi:10.1161/CIRCRESAHA.116.308398
15. AMBOSS GmbH. Types of ischemic stroke. Ischemic Stroke. September 21, 2023. Accessed March 11, 2024. https://next.amboss.com/us/article/iJ0JFS?q. Date accessed: 11-03-2024

16. Dichgans M, Pulit SL, Rosand J. Stroke genetics: discovery, biology, and clinical applications. *Lancet Neurol*. 2019;18(6):587-599. doi:10.1016/S1474-4422(19)30043-2
17. Bevan S, Traylor M, Adib-Samii P, et al. Genetic Heritability of Ischemic Stroke and the Contribution of Previously Reported Candidate Gene and Genomewide Associations. *Stroke*. 2012;43(12):3161-3167. doi:10.1161/STROKEAHA.112.665760
18. Bellenguez C, Bevan S, Gschwendtner A, et al. Genome-wide association study identifies a variant in HDAC9 associated with large vessel ischemic stroke. *Nat Genet*. 2012;44(3):328-333. doi:10.1038/ng.1081
19. Malik R, Chauhan G, Traylor M, et al. Multiancestry genome-wide association study of 520,000 subjects identifies 32 loci associated with stroke and stroke subtypes. *Nat Genet*. 2018;50(4):524-537. doi:10.1038/s41588-018-0058-3
20. Azghandi S, Prell C, van der Laan SW, et al. Deficiency of the Stroke Relevant HDAC9 Gene Attenuates Atherosclerosis in Accord With Allele-Specific Effects at 7p21.1. *Stroke*. 2015;46(1):197-202. doi:10.1161/STROKEAHA.114.007213
21. Prestel M, Prell-Schicker C, Webb T, et al. The Atherosclerosis Risk Variant rs2107595 Mediates Allele-Specific Transcriptional Regulation of HDAC9 via E2F3 and Rb1. *Stroke*. 2019;50(10):2651-2660. doi:10.1161/STROKEAHA.119.026112
22. Malhotra R, Mauer AC, Lino Cardenas CL, et al. HDAC9 is implicated in atherosclerotic aortic calcification and affects vascular smooth muscle cell phenotype. *Nat Genet*. 2019;51(11):1580-1587. doi:10.1038/s41588-019-0514-8
23. Markus HS, Mäkelä KM, Bevan S, et al. Evidence HDAC9 Genetic Variant Associated With Ischemic Stroke Increases Risk via Promoting Carotid Atherosclerosis. *Stroke*. 2013;44(5):1220-1225. doi:10.1161/STROKEAHA.111.000217
24. Matsukura M, Ozaki K, Takahashi A, et al. Genome-Wide Association Study of Peripheral Arterial Disease in a Japanese Population. *PLoS One*. 2015;10(10):e0139262. doi:10.1371/journal.pone.0139262
25. Dichgans M, Malik R, König IR, et al. Shared Genetic Susceptibility to Ischemic Stroke and Coronary Artery Disease. *Stroke*. 2014;45(1):24-36. doi:10.1161/STROKEAHA.113.002707
26. Duan L, Wei L, Tian Y, et al. Novel Susceptibility Loci for Moyamoya Disease Revealed by a Genome-Wide Association Study. *Stroke*. 2018;49(1):11-18. doi:10.1161/STROKEAHA.117.017430
27. Deloukas P, Kanoni S, Willenborg C, et al. Large-scale association analysis identifies new risk loci for coronary artery disease. *Nat Genet*. 2013;45(1):25-33. doi:10.1038/ng.2480
28. Weber C, Noels H. Atherosclerosis: current pathogenesis and therapeutic options. *Nat Med*. 2011;17(11):1410-1422. doi:10.1038/nm.2538
29. Libby P, Lichtman AH, Hansson GK. Immune Effector Mechanisms Implicated in Atherosclerosis: From Mice to Humans. *Immunity*. 2013;38(6):1092-1104. doi:10.1016/j.immuni.2013.06.009

30. Vos T, Lim SS, Abbafati C, et al. Global burden of 369 diseases and injuries in 204 countries and territories, 1990–2019: a systematic analysis for the Global Burden of Disease Study 2019. *The Lancet*. 2020;396(10258):1204-1222. doi:10.1016/S0140-6736(20)30925-9
31. Roth GA, Mensah GA, Johnson CO, et al. Global Burden of Cardiovascular Diseases and Risk Factors, 1990–2019. *J Am Coll Cardiol*. 2020;76(25):2982-3021. doi:10.1016/j.jacc.2020.11.010
32. Naghavi M, Abajobir AA, Abbafati C, et al. Global, regional, and national age-sex specific mortality for 264 causes of death, 1980–2016: a systematic analysis for the Global Burden of Disease Study 2016. *The Lancet*. 2017;390(10100):1151-1210. doi:10.1016/S0140-6736(17)32152-9
33. Statistisches Bundesamt (Destatis). Todesursachenstatistik 2019. Genesis. 2022. Accessed March 31, 2023. https://www-genesis.destatis.de/genesis/online?operation=ergebnistabelleQualitaetSeparatAUS&levelindex=3&levelid=1680269294344&downloadname=23211-0001#abreadcrumb
34. Hansson GK, Hermansson A. The immune system in atherosclerosis. *Nat Immunol*. 2011;12(3):204-212. doi:10.1038/ni.2001
35. Moore KJ, Tabas I. Macrophages in the Pathogenesis of Atherosclerosis. *Cell*. 2011;145(3):341-355. doi:10.1016/j.cell.2011.04.005
36. Peiffer V, Sherwin SJ, Weinberg PD. Does low and oscillatory wall shear stress correlate spatially with early atherosclerosis? A systematic review. *Cardiovasc Res*. 2013;99(2):242-250. doi:10.1093/cvr/cvt044
37. Williams KJ, Tabas I. The Response-to-Retention Hypothesis of Early Atherogenesis. *Arterioscler Thromb Vasc Biol*. 1995;15(5):551-561. doi:10.1161/01.ATV.15.5.551
38. Skålén K, Gustafsson M, Rydberg EK, et al. Subendothelial retention of atherogenic lipoproteins in early atherosclerosis. *Nature*. 2002;417(6890):750-754. doi:10.1038/nature00804
39. Glass CK, Witztum JL. Atherosclerosis. *Cell*. 2001;104(4):503-516. doi:10.1016/S0092-8674(01)00238-0
40. Bekkering S, Quintin J, Joosten LAB, van der Meer JWM, Netea MG, Riksen NP. Oxidized Low-Density Lipoprotein Induces Long-Term Proinflammatory Cytokine Production and Foam Cell Formation via Epigenetic Reprogramming of Monocytes. *Arterioscler Thromb Vasc Biol*. 2014;34(8):1731-1738. doi:10.1161/ATVBAHA.114.303887
41. Zernecke A, Weber C. Chemokines in Atherosclerosis. *Arterioscler Thromb Vasc Biol*. 2014;34(4):742-750. doi:10.1161/ATVBAHA.113.301655
42. Libby P. Inflammation in atherosclerosis. *Nature*. 2002;420(6917):868-874. doi:10.1038/nature01323
43. Lusis AJ. Atherosclerosis. *Nature*. 2000;407(6801):233-241. doi:10.1038/35025203
44. Libby P, Buring JE, Badimon L, et al. Atherosclerosis. *Nat Rev Dis Primers*. 2019;5(1):56. doi:10.1038/s41572-019-0106-z

45. Silvestre-Roig C, de Winther MP, Weber C, Daemen MJ, Lutgens E, Soehnlein O. Atherosclerotic Plaque Destabilization. *Circ Res*. 2014;114(1):214-226. doi:10.1161/CIRCRESAHA.114.302355
46. Moore KJ, Sheedy FJ, Fisher EA. Macrophages in atherosclerosis: a dynamic balance. *Nat Rev Immunol*. 2013;13(10):709-721. doi:10.1038/nri3520
47. Falk E, Shah PK, Fuster V. Coronary Plaque Disruption. *Circulation*. 1995;92(3):657-671. doi:10.1161/01.CIR.92.3.657
48. Friedman M, Van den Bovenkamp GJ. The pathogenesis of a coronary thrombus. *Am J Pathol*. 1966;48(1):19-44.
49. Finn A V., Nakano M, Narula J, Kolodgie FD, Virmani R. Concept of Vulnerable/Unstable Plaque. *Arterioscler Thromb Vasc Biol*. 2010;30(7):1282-1292. doi:10.1161/ATVBAHA.108.179739
50. Davies MJ, Bland JM, Hangartner JRW, Angelina A, Thomas AC. Factors influencing the presence or absence of acute coronary artery thrombi in sudden ischaemic death. *Eur Heart J*. 1989;10(3):203-208. doi:10.1093/oxfordjournals.eurheartj.a059467
51. Chen YC, Huang AL, Kyaw TS, Bobik A, Peter K. Atherosclerotic Plaque Rupture. *Arterioscler Thromb Vasc Biol*. 2016;36(8). doi:10.1161/ATVBAHA.116.307993
52. AMBOSS GmbH. Pathogenesis of atherosclerosis. Atherosclerotic cardiovascular disease. 2024. Accessed March 16, 2024. https://next.amboss.com/us/article/9L0N-g. Date accessed: 16-03-2024
53. Olins AL, Olins DE. Spheroid Chromatin Units (v Bodies). *Science (1979)*. 1974;183(4122):330-332. doi:10.1126/science.183.4122.330
54. Strahl BD, Allis CD. The language of covalent histone modifications. *Nature*. 2000;403(6765):41-45. doi:10.1038/47412
55. Allfrey VG, Mirsky AE. Structural Modifications of Histones and their Possible Role in the Regulation of RNA Synthesis. *Science*. 1964;144(3618):559. doi:10.1126/science.144.3618.559
56. Singh BN, Zhang G, Hwa YL, Li J, Dowdy SC, Jiang SW. Nonhistone protein acetylation as cancer therapy targets. *Expert Rev Anticancer Ther*. 2010;10(6):935-954. doi:10.1586/era.10.62
57. Glozak MA, Sengupta N, Zhang X, Seto E. Acetylation and deacetylation of non-histone proteins. *Gene*. 2005;363:15-23. doi:10.1016/j.gene.2005.09.010
58. Choudhary C, Kumar C, Gnad F, et al. Lysine Acetylation Targets Protein Complexes and Co-Regulates Major Cellular Functions. *Science (1979)*. 2009;325(5942):834-840. doi:10.1126/science.1175371
59. Kouzarides T. Acetylation: a regulatory modification to rival phosphorylation? *EMBO J*. 2000;19(6):1176-1179. doi:10.1093/emboj/19.6.1176
60. Shakespear MR, Halili MA, Irvine KM, Fairlie DP, Sweet MJ. Histone deacetylases as regulators of inflammation and immunity. *Trends Immunol*. 2011;32(7):335-343. doi:10.1016/j.it.2011.04.001

61. Falkenberg KJ, Johnstone RW. Histone deacetylases and their inhibitors in cancer, neurological diseases and immune disorders. *Nat Rev Drug Discov*. 2014;13(9):673-691. doi:10.1038/nrd4360
62. Tao R, de Zoeten EF, Özkaynak E, et al. Deacetylase inhibition promotes the generation and function of regulatory T cells. *Nat Med*. 2007;13(11):1299-1307. doi:10.1038/nm1652
63. Zhang CL, McKinsey TA, Chang S, Antos CL, Hill JA, Olson EN. Class II Histone Deacetylases Act as Signal-Responsive Repressors of Cardiac Hypertrophy. *Cell*. 2002;110(4):479-488. doi:10.1016/S0092-8674(02)00861-9
64. Haberland M, Montgomery RL, Olson EN. The many roles of histone deacetylases in development and physiology: implications for disease and therapy. *Nat Rev Genet*. 2009;10(1):32-42. doi:10.1038/nrg2485
65. Lehrman G, Hogue IB, Palmer S, et al. Depletion of latent HIV-1 infection in vivo: a proof-of-concept study. *The Lancet*. 2005;366(9485):549-555. doi:10.1016/S0140-6736(05)67098-5
66. Zhang B, West EJ, Van KC, et al. HDAC inhibitor increases histone H3 acetylation and reduces microglia inflammatory response following traumatic brain injury in rats. *Brain Res*. 2008;1226:181-191. doi:10.1016/j.brainres.2008.05.085
67. Liu KY, Wang LT, Hsu SH. Modification of Epigenetic Histone Acetylation in Hepatocellular Carcinoma. *Cancers (Basel)*. 2018;10(1):8. doi:10.3390/cancers10010008
68. Kazantsev AG, Thompson LM. Therapeutic application of histone deacetylase inhibitors for central nervous system disorders. *Nat Rev Drug Discov*. 2008;7(10):854-868. doi:10.1038/nrd2681
69. Park SY, Kim JS. A short guide to histone deacetylases including recent progress on class II enzymes. *Exp Mol Med*. 2020;52(2):204-212. doi:10.1038/s12276-020-0382-4
70. Backs J, Olson EN. Control of Cardiac Growth by Histone Acetylation/Deacetylation. *Circ Res*. 2006;98(1):15-24. doi:10.1161/01.RES.0000197782.21444.8f
71. Gray SG, Ekström TJ. The Human Histone Deacetylase Family. *Exp Cell Res*. 2001;262(2):75-83. doi:10.1006/excr.2000.5080
72. Fischle W, Dequiedt F, Hendzel MJ, et al. Enzymatic Activity Associated with Class II HDACs Is Dependent on a Multiprotein Complex Containing HDAC3 and SMRT/N-CoR. *Mol Cell*. 2002;9(1):45-57. doi:10.1016/S1097-2765(01)00429-4
73. Uhlén M, Fagerberg L, Hallström BM, et al. Tissue-based map of the human proteome. *Science (1979)*. 2015;347(6220). doi:10.1126/science.1260419
74. Grozinger CM, Hassig CA, Schreiber SL. Three proteins define a class of human histone deacetylases related to yeast Hda1p. *Proceedings of the National Academy of Sciences*. 1999;96(9):4868-4873. doi:10.1073/pnas.96.9.4868
75. Petrie K, Guidez F, Howell L, et al. The Histone Deacetylase 9 Gene Encodes Multiple Protein Isoforms. *Journal of Biological Chemistry*. 2003;278(18):16059-16072. doi:10.1074/jbc.M212935200
76. Wang AH, Kruhlak MJ, Wu J, et al. Regulation of histone deacetylase 4 by binding of 14-3-3 proteins. *Mol Cell Biol*. 2000;20(18):6904-6912. doi:10.1128/MCB.20.18.6904-6912.2000

77. Grozinger CM, Schreiber SL. Regulation of histone deacetylase 4 and 5 and transcriptional activity by 14-3- 3-dependent cellular localization. *Proceedings of the National Academy of Sciences*. 2000;97(14):7835-7840. doi:10.1073/pnas.140199597
78. Muslin AJ, Xing H. 14-3-3 proteins: regulation of subcellular localization by molecular interference. *Cell Signal*. 2000;12(11-12):703-709. doi:10.1016/s0898-6568(00)00131-5
79. Kato H, Tamamizu-Kato S, Shibasaki F. Histone Deacetylase 7 Associates with Hypoxia-inducible Factor 1α and Increases Transcriptional Activity. *Journal of Biological Chemistry*. 2004;279(40):41966-41974. doi:10.1074/jbc.M406320200
80. Seo HW, Kim EJ, Na H, Lee MO. Transcriptional activation of hypoxia-inducible factor-1α by HDAC4 and HDAC5 involves differential recruitment of p300 and FIH-1. *FEBS Lett*. 2009;583(1):55-60. doi:10.1016/j.febslet.2008.11.044
81. Mihaylova MM, Vasquez DS, Ravnskjaer K, et al. Class IIa Histone Deacetylases Are Hormone-Activated Regulators of FOXO and Mammalian Glucose Homeostasis. *Cell*. 2011;145(4):607-621. doi:10.1016/j.cell.2011.03.043
82. Cai Y, Huang D, Ma W, et al. Histone deacetylase 9 inhibition upregulates microRNA-92a to repress the progression of intracranial aneurysm via silencing Bcl-2-like protein 11. *J Drug Target*. 2021;29(7):761-770. doi:10.1080/1061186X.2021.1878365
83. Xiong K, Zhang H, Du Y, Tian J, Ding S. Identification of HDAC9 as a viable therapeutic target for the treatment of gastric cancer. *Exp Mol Med*. 2019;51(8):1-15. doi:10.1038/s12276-019-0301-8
84. Hu Y, Sun L, Tao S, et al. Clinical significance of HDAC9 in hepatocellular carcinoma. *Cell Mol Biol*. 2019;65(4):23-28. doi:10.14715/10.14715/cmb/2019.65.4.4
85. Yang R, Wu Y, Wang M, et al. HDAC9 promotes glioblastoma growth via TAZ-mediated EGFR pathway activation. *Oncotarget*. 2015;6(10):7644-7656. doi:10.18632/oncotarget.3223
86. Milde T, Oehme I, Korshunov A, et al. HDAC5 and HDAC9 in Medulloblastoma: Novel Markers for Risk Stratification and Role in Tumor Cell Growth. *Clinical Cancer Research*. 2010;16(12):3240-3252. doi:10.1158/1078-0432.CCR-10-0395
87. Yang C, Croteau S, Hardy P. Histone deacetylase (HDAC) 9: versatile biological functions and emerging roles in human cancer. *Cellular Oncology*. 2021;44(5):997-1017. doi:10.1007/s13402-021-00626-9
88. Kaluza D, Kroll J, Gesierich S, et al. Histone Deacetylase 9 Promotes Angiogenesis by Targeting the Antiangiogenic MicroRNA-17–92 Cluster in Endothelial Cells. *Arterioscler Thromb Vasc Biol*. 2013;33(3):533-543. doi:10.1161/ATVBAHA.112.300415
89. Chatterjee TK, Idelman G, Blanco V, et al. Histone Deacetylase 9 Is a Negative Regulator of Adipogenic Differentiation. *Journal of Biological Chemistry*. 2011;286(31):27836-27847. doi:10.1074/jbc.M111.262964
90. Chatterjee TK, Basford JE, Knoll E, et al. HDAC9 Knockout Mice Are Protected From Adipose Tissue Dysfunction and Systemic Metabolic Disease During High-Fat Feeding. *Diabetes*. 2014;63(1):176-187. doi:10.2337/db13-1148

91. Cao Q, Rong S, Repa JJ, Clair R St., Parks JS, Mishra N. Histone Deacetylase 9 Represses Cholesterol Efflux and Alternatively Activated Macrophages in Atherosclerosis Development. *Arterioscler Thromb Vasc Biol*. 2014;34(9):1871-1879. doi:10.1161/ATVBAHA.114.303393
92. Shen Z, Bei Y, Lin H, et al. The role of class IIa histone deacetylases in regulating endothelial function. *Front Physiol*. 2023;14. doi:10.3389/fphys.2023.1091794
93. McKinsey TA, Zhang CL, Olson EN. MEF2: a calcium-dependent regulator of cell division, differentiation and death. *Trends Biochem Sci*. 2002;27(1):40-47. doi:10.1016/S0968-0004(01)02031-X
94. Sacilotto N, Chouliaras KM, Nikitenko LL, et al. MEF2 transcription factors are key regulators of sprouting angiogenesis. *Genes Dev*. 2016;30(20):2297-2309. doi:10.1101/gad.290619.116
95. Anderson CM, Hu J, Thomas R, et al. Cooperative activation of cardiac transcription through myocardin bridging of paired MEF2 sites. *Development*. 2017;144(7):1235-1241. doi:10.1242/dev.138487
96. Zhou X, Marks PA, Rifkind RA, Richon VM. Cloning and characterization of a histone deacetylase, HDAC9. *Proceedings of the National Academy of Sciences*. 2001;98(19):10572-10577. doi:10.1073/pnas.191375098
97. Sparrow DB, Miska EA, Langley E, et al. MEF-2 function is modified by a novel co-repressor, MITR. *EMBO J*. 1999;18(18):5085-5098. doi:10.1093/emboj/18.18.5085
98. Zhang CL, McKinsey TA, Olson EN. The transcriptional corepressor MITR is a signal-responsive inhibitor of myogenesis. *Proceedings of the National Academy of Sciences*. 2001;98(13):7354-7359. doi:10.1073/pnas.131198498
99. Zhang CL, McKinsey TA, Lu J rong, Olson EN. Association of COOH-terminal-binding Protein (CtBP) and MEF2-interacting Transcription Repressor (MITR) Contributes to Transcriptional Repression of the MEF2 Transcription Factor. *Journal of Biological Chemistry*. 2001;276(1):35-39. doi:10.1074/jbc.M007364200
100. Li X, Zhang Q, Ding Y, et al. Methyltransferase Dnmt3a upregulates HDAC9 to deacetylate the kinase TBK1 for activation of antiviral innate immunity. *Nat Immunol*. 2016;17(7):806-815. doi:10.1038/ni.3464
101. de Zoeten EF, Wang L, Sai H, Dillmann WH, Hancock WW. Inhibition of HDAC9 Increases T Regulatory Cell Function and Prevents Colitis in Mice. *Gastroenterology*. 2010;138(2):583-594. doi:10.1053/j.gastro.2009.10.037
102. Li B, Samanta A, Song X, et al. FOXP3 interactions with histone acetyltransferase and class II histone deacetylases are required for repression. *Proceedings of the National Academy of Sciences*. 2007;104(11):4571-4576. doi:10.1073/pnas.0700298104
103. Wang X bin, Han Y di, Sabina S, et al. HDAC9 Variant Rs2107595 Modifies Susceptibility to Coronary Artery Disease and the Severity of Coronary Atherosclerosis in a Chinese Han Population. *PLoS One*. 2016;11(8):e0160449. doi:10.1371/journal.pone.0160449
104. Han X, Han X, Wang Z, Shen J, Dong Q. HDAC9 regulates ox-LDL-induced endothelial cell apoptosis by participating in inflammatory reactions. *Front Biosci (Landmark Ed)*. 2016;21(5):907-917. doi:10.2741/4428

105. Suraweera A, O'Byrne KJ, Richard DJ. Combination Therapy With Histone Deacetylase Inhibitors (HDACi) for the Treatment of Cancer: Achieving the Full Therapeutic Potential of HDACi. *Front Oncol*. 2018;8. doi:10.3389/fonc.2018.00092
106. Phiel CJ, Zhang F, Huang EY, Guenther MG, Lazar MA, Klein PS. Histone Deacetylase Is a Direct Target of Valproic Acid, a Potent Anticonvulsant, Mood Stabilizer, and Teratogen. *Journal of Biological Chemistry*. 2001;276(39):36734-36741. doi:10.1074/jbc.M101287200
107. Göttlicher M, Minucci S, Zhu P, et al. Valproic acid defines a novel class of HDAC inhibitors inducing differentiation of transformed cells. *EMBO J*. 2001;20(24):6969-6978. doi:10.1093/emboj/20.24.6969
108. Choi JH, Nam KH, Kim J, et al. Trichostatin A Exacerbates Atherosclerosis in Low Density Lipoprotein Receptor–Deficient Mice. *Arterioscler Thromb Vasc Biol*. 2005;25(11):2404-2409. doi:10.1161/01.ATV.0000184758.07257.88
109. Lobera M, Madauss KP, Pohlhaus DT, et al. Selective class IIa histone deacetylase inhibition via a nonchelating zinc-binding group. *Nat Chem Biol*. 2013;9(5):319-325. doi:10.1038/nchembio.1223
110. Guerriero JL, Sotayo A, Ponichtera HE, et al. Class IIa HDAC inhibition reduces breast tumours and metastases through anti-tumour macrophages. *Nature*. 2017;543(7645):428-432. doi:10.1038/nature21409
111. Han Y, Sun J, Yang Y, et al. TMP195 Exerts Antitumor Effects on Colorectal Cancer by Promoting M1 Macrophages Polarization. *Int J Biol Sci*. 2022;18(15):5653-5666. doi:10.7150/ijbs.73264
112. Barnes PJ, Karin M. Nuclear Factor-κB — A Pivotal Transcription Factor in Chronic Inflammatory Diseases. *New England Journal of Medicine*. 1997;336(15):1066-1071. doi:10.1056/NEJM199704103361506
113. de Winther MPJ, Kanters E, Kraal G, Hofker MH. Nuclear Factor κB Signaling in Atherogenesis. *Arterioscler Thromb Vasc Biol*. 2005;25(5):904-914. doi:10.1161/01.ATV.0000160340.72641.87
114. Karin M. Nuclear factor-κB in cancer development and progression. *Nature*. 2006;441(7092):431-436. doi:10.1038/nature04870
115. Courtois G, Gilmore TD. Mutations in the NF-κB signaling pathway: implications for human disease. *Oncogene*. 2006;25(51):6831-6843. doi:10.1038/sj.onc.1209939
116. Hayden MS, Ghosh S. Shared Principles in NF-κB Signaling. *Cell*. 2008;132(3):344-362. doi:10.1016/j.cell.2008.01.020
117. Ghosh S, Karin M. Missing Pieces in the NF-κB Puzzle. *Cell*. 2002;109(2):S81-S96. doi:10.1016/S0092-8674(02)00703-1
118. DiDonato JA, Hayakawa M, Rothwarf DM, Zandi E, Karin M. A cytokine-responsive IκB kinase that activates the transcription factor NF-κB. *Nature*. 1997;388(6642):548-554. doi:10.1038/41493
119. Christian F, Smith E, Carmody R. The Regulation of NF-κB Subunits by Phosphorylation. *Cells*. 2016;5(1):12. doi:10.3390/cells5010012

120. Moreno R, Sobotzik JM, Schultz C, Schmitz ML. Specification of the NF-κB transcriptional response by p65 phosphorylation and TNF-induced nuclear translocation of IKKε. *Nucleic Acids Res*. 2010;38(18):6029-6044. doi:10.1093/nar/gkq439
121. Rothwarf DM, Zandi E, Natoli G, Karin M. IKK-γ is an essential regulatory subunit of the IκB kinase complex. *Nature*. 1998;395(6699):297-300. doi:10.1038/26261
122. Mittal R, Peak-Chew SY, McMahon HT. Acetylation of MEK2 and IκB kinase (IKK) activation loop residues by YopJ inhibits signaling. *Proceedings of the National Academy of Sciences*. 2006;103(49):18574-18579. doi:10.1073/pnas.0608995103
123. Mercurio F, Zhu H, Murray BW, et al. IKK-1 and IKK-2: Cytokine-Activated IκB Kinases Essential for NF-κB Activation. *Science (1979)*. 1997;278(5339):860-866. doi:10.1126/science.278.5339.860
124. Marienfeld RB, Palkowitsch L, Ghosh S. Dimerization of the IκB Kinase-Binding Domain of NEMO Is Required for Tumor Necrosis Factor Alpha-Induced NF-κB Activity. *Mol Cell Biol*. 2006;26(24):9209-9219. doi:10.1128/MCB.00478-06
125. Palkowitsch L, Leidner J, Ghosh S, Marienfeld RB. Phosphorylation of Serine 68 in the IκB Kinase (IKK)-binding Domain of NEMO Interferes with the Structure of the IKK Complex and Tumor Necrosis Factor-α-induced NF-κB Activity. *Journal of Biological Chemistry*. 2008;283(1):76-86. doi:10.1074/jbc.M708856200
126. Sethi JK, Hotamisligil GS. Metabolic Messengers: tumour necrosis factor. *Nat Metab*. 2021;3(10):1302-1312. doi:10.1038/s42255-021-00470-z
127. Hsu H, Huang J, Shu HB, Baichwal V, Goeddel D V. TNF-Dependent Recruitment of the Protein Kinase RIP to the TNF Receptor-1 Signaling Complex. *Immunity*. 1996;4(4):387-396. doi:10.1016/S1074-7613(00)80252-6
128. Devin A, Lin Y, Yamaoka S, Li Z, Karin M, Liu Z gang. The α and β Subunits of IκB Kinase (IKK) Mediate TRAF2-Dependent IKK Recruitment to Tumor Necrosis Factor (TNF) Receptor 1 in Response to TNF. *Mol Cell Biol*. 2001;21(12):3986-3994. doi:10.1128/MCB.21.12.3986-3994.2001
129. Blonska M, Shambharkar PB, Kobayashi M, et al. TAK1 Is Recruited to the Tumor Necrosis Factor-α (TNF-α) Receptor 1 Complex in a Receptor-interacting Protein (RIP)-dependent Manner and Cooperates with MEKK3 Leading to NF-κB Activation. *Journal of Biological Chemistry*. 2005;280(52):43056-43063. doi:10.1074/jbc.M507807200
130. Zhang SQ, Kovalenko A, Cantarella G, Wallach D. Recruitment of the IKK Signalosome to the p55 TNF Receptor. *Immunity*. 2000;12(3):301-311. doi:10.1016/S1074-7613(00)80183-1
131. Inohara N, Koseki T, Lin J, et al. An Induced Proximity Model for NF-κB Activation in the Nod1/RICK and RIP Signaling Pathways. *Journal of Biological Chemistry*. 2000;275(36):27823-27831. doi:10.1074/jbc.M003415200
132. Lee TH, Shank J, Cusson N, Kelliher MA. The Kinase Activity of Rip1 Is Not Required for Tumor Necrosis Factor-α-induced IκB Kinase or p38 MAP Kinase Activation or for the Ubiquitination of Rip1 by Traf2. *Journal of Biological Chemistry*. 2004;279(32):33185-33191. doi:10.1074/jbc.M404206200

133. Silverman N, Zhou R, Erlich RL, et al. Immune Activation of NF-κB and JNK Requires Drosophila TAK1. *Journal of Biological Chemistry*. 2003;278(49):48928-48934. doi:10.1074/jbc.M304802200
134. Takaesu G, Surabhi RM, Park KJ, Ninomiya-Tsuji J, Matsumoto K, Gaynor RB. TAK1 is Critical for IκB Kinase-mediated Activation of the NF-κB Pathway. *J Mol Biol*. 2003;326(1):105-115. doi:10.1016/S0022-2836(02)01404-3
135. Delhase M, Hayakawa M, Chen Y, Karin M. Positive and Negative Regulation of IκB Kinase Activity Through IKKβ Subunit Phosphorylation. *Science (1979)*. 1999;284(5412):309-313. doi:10.1126/science.284.5412.309
136. Li ZW, Chu W, Hu Y, et al. The IKKβ Subunit of IκB Kinase (IKK) is Essential for Nuclear Factor κB Activation and Prevention of Apoptosis. *J Exp Med*. 1999;189(11):1839-1845. doi:10.1084/jem.189.11.1839
137. Solt LA, Madge LA, Orange JS, May MJ. Interleukin-1-induced NF-κB Activation Is NEMO-dependent but Does Not Require IKKβ. *Journal of Biological Chemistry*. 2007;282(12):8724-8733. doi:10.1074/jbc.M609613200
138. Prescott JA, Balmanno K, Mitchell JP, Okkenhaug H, Cook SJ. IKKα plays a major role in canonical NF-κB signalling in colorectal cells. *Biochemical Journal*. 2022;479(3):305-325. doi:10.1042/BCJ20210783
139. Ling L, Cao Z, Goeddel D V. NF-κB-inducing kinase activates IKK-α by phosphorylation of Ser-176. *Proceedings of the National Academy of Sciences*. 1998;95(7):3792-3797. doi:10.1073/pnas.95.7.3792
140. Häcker H, Karin M. Regulation and Function of IKK and IKK-Related Kinases. *Science's STKE*. 2006;2006(357). doi:10.1126/stke.3572006re13
141. Karin M, Ben-Neriah Y. Phosphorylation Meets Ubiquitination: The Control of NF-κB Activity. *Annu Rev Immunol*. 2000;18(1):621-663. doi:10.1146/annurev.immunol.18.1.621
142. Chen Z, Hagler J, Palombella VJ, et al. Signal-induced site-specific phosphorylation targets I kappa B alpha to the ubiquitin-proteasome pathway. *Genes Dev*. 1995;9(13):1586-1597. doi:10.1101/gad.9.13.1586
143. Chen ZJ. Ubiquitin signalling in the NF-κB pathway. *Nat Cell Biol*. 2005;7(8):758-765. doi:10.1038/ncb0805-758
144. Senftleben U, Cao Y, Xiao G, et al. Activation by IKKα of a Second, Evolutionary Conserved, NF-κB Signaling Pathway. *Science (1979)*. 2001;293(5534):1495-1499. doi:10.1126/science.1062677
145. Ashburner BP, Westerheide SD, Baldwin AS. The p65 (RelA) Subunit of NF-κB Interacts with the Histone Deacetylase (HDAC) Corepressors HDAC1 and HDAC2 To Negatively Regulate Gene Expression. *Mol Cell Biol*. 2001;21(20):7065-7077. doi:10.1128/MCB.21.20.7065-7077.2001
146. Chen L feng, Fischle W, Verdin E, Greene WC. Duration of Nuclear NF-κB Action Regulated by Reversible Acetylation. *Science (1979)*. 2001;293(5535):1653-1657. doi:10.1126/science.1062374

147. Sun SC, Ganchi PA, Ballard DW, Greene WC. NF-κB Controls Expression of Inhibitor IκBα: Evidence for an Inducible Autoregulatory Pathway. *Science (1979)*. 1993;259(5103):1912-1915. doi:10.1126/science.8096091
148. Arenzana-Seisdedos F, Thompson J, Rodriguez MS, Bachelerie F, Thomas D, Hay RT. Inducible Nuclear Expression of Newly Synthesized IκBα Negatively Regulates DNA-Binding and Transcriptional Activities of NF-κB. *Mol Cell Biol*. 1995;15(5):2689-2696. doi:10.1128/MCB.15.5.2689
149. Sun SC. Non-canonical NF-κB signaling pathway. *Cell Res*. 2011;21(1):71-85. doi:10.1038/cr.2010.177
150. Buss H, Dörrie A, Schmitz ML, Hoffmann E, Resch K, Kracht M. Constitutive and Interleukin-1-inducible Phosphorylation of p65 NF-κB at Serine 536 Is Mediated by Multiple Protein Kinases Including IκB Kinase (IKK)-α, IKKβ, IKKε, TRAF Family Member-associated (TANK)-binding Kinase 1 (TBK1), and an Unknown Kinase and Couples p65 to TATA-binding Protein-associated Factor II31-mediated Interleukin-8 Transcription. *Journal of Biological Chemistry*. 2004;279(53):55633-55643. doi:10.1074/jbc.M409825200
151. Buss H, Dörrie A, Schmitz ML, et al. Phosphorylation of Serine 468 by GSK-3β Negatively Regulates Basal p65 NF-κB Activity. *Journal of Biological Chemistry*. 2004;279(48):49571-49574. doi:10.1074/jbc.C400442200
152. Mattioli I, Geng H, Sebald A, et al. Inducible Phosphorylation of NF-κB p65 at Serine 468 by T Cell Costimulation Is Mediated by IKKε. *Journal of Biological Chemistry*. 2006;281(10):6175-6183. doi:10.1074/jbc.M508045200
153. Peters RT, Liao SM, Maniatis T. IKKε Is Part of a Novel PMA-Inducible IκB Kinase Complex. *Mol Cell*. 2000;5(3):513-522. doi:10.1016/S1097-2765(00)80445-1
154. Hemmi H, Takeuchi O, Sato S, et al. The Roles of Two IκB Kinase-related Kinases in Lipopolysaccharide and Double Stranded RNA Signaling and Viral Infection. *J Exp Med*. 2004;199(12):1641-1650. doi:10.1084/jem.20040520
155. Oeckinghaus A, Hayden MS, Ghosh S. Crosstalk in NF-κB signaling pathways. *Nat Immunol*. 2011;12(8):695-708. doi:10.1038/ni.2065
156. Ziesché E, Kettner-Buhrow D, Weber A, et al. The coactivator role of histone deacetylase 3 in IL-1-signaling involves deacetylation of p65 NF-κB. *Nucleic Acids Res*. 2013;41(1):90-109. doi:10.1093/nar/gks916
157. Johnson LN, Noble MEM, Owen DJ. Active and Inactive Protein Kinases: Structural Basis for Regulation. *Cell*. 1996;85(2):149-158. doi:10.1016/S0092-8674(00)81092-2
158. Hu Y, Baud V, Delhase M, et al. Abnormal Morphogenesis But Intact IKK Activation in Mice Lacking the IKKα Subunit of IκB Kinase. *Science (1979)*. 1999;284(5412):316-320. doi:10.1126/science.284.5412.316
159. Schesser K, Spiik AK, Dukuzumuremyi JM, Neurath MF, Pettersson S, Wolf-Watz H. The yopJ locus is required for Yersinia-mediated inhibition of NF-kappaB activation and cytokine expression: YopJ contains a eukaryotic SH2-like domain that is essential for its repressive activity. *Mol Microbiol*. 1998;28(6):1067-1079. doi:10.1046/j.1365-2958.1998.00851.x

160. Vermeulen L, De Wilde G, Van Damme P, Vanden Berghe W, Haegeman G. Transcriptional activation of the NF-kappaB p65 subunit by mitogen- and stress-activated protein kinase-1 (MSK1). *EMBO J*. 2003;22(6):1313-1324. doi:10.1093/emboj/cdg139
161. Zhong H, SuYang H, Erdjument-Bromage H, Tempst P, Ghosh S. The Transcriptional Activity of NF-κB Is Regulated by the IκB-Associated PKAc Subunit through a Cyclic AMP–Independent Mechanism. *Cell*. 1997;89(3):413-424. doi:10.1016/S0092-8674(00)80222-6
162. Nihira K, Ando Y, Yamaguchi T, Kagami Y, Miki Y, Yoshida K. Pim-1 controls NF-κB signalling by stabilizing RelA/p65. *Cell Death Differ*. 2010;17(4):689-698. doi:10.1038/cdd.2009.174
163. Geng H, Wittwer T, Dittrich-Breiholz O, Kracht M, Schmitz ML. Phosphorylation of NF-κB p65 at Ser468 controls its COMMD1-dependent ubiquitination and target gene-specific proteasomal elimination. *EMBO Rep*. 2009;10(4):381-386. doi:10.1038/embor.2009.10
164. Schwabe RF, Sakurai H. IKKβ phosphorylates p65 at S468 in transactivaton domain 2. *The FASEB Journal*. 2005;19(12):1758-1760. doi:10.1096/fj.05-3736fje
165. Rothgiesser KM, Fey M, Hottiger MO. Acetylation of p65 at lysine 314 is important for late NF-κB-dependent gene expression. *BMC Genomics*. 2010;11(1):22. doi:10.1186/1471-2164-11-22
166. Rothgiesser KM, Erener S, Waibel S, Lüscher B, Hottiger MO. SIRT2 regulates NF-κB-dependent gene expression through deacetylation of p65 Lys310. *J Cell Sci*. 2010;123(24):4251-4258. doi:10.1242/jcs.073783
167. Chen LF, Williams SA, Mu Y, et al. NF-κB RelA Phosphorylation Regulates RelA Acetylation. *Mol Cell Biol*. 2005;25(18):7966-7975. doi:10.1128/MCB.25.18.7966-7975.2005
168. Tang ED, Nuñez G, Barr FG, Guan KL. Negative Regulation of the Forkhead Transcription Factor FKHR by Akt. *Journal of Biological Chemistry*. 1999;274(24):16741-16746. doi:10.1074/jbc.274.24.16741
169. Sun SC, Elwood J, Greene WC. Both Amino- and Carboxyl-Terminal Sequences within IκBα Regulate Its Inducible Degradation. *Mol Cell Biol*. 1996;16(3):1058-1065. doi:10.1128/MCB.16.3.1058
170. Richards SA, Dreisbach VC, Murphy LO, Blenis J. Characterization of Regulatory Events Associated with Membrane Targeting of p90 Ribosomal S6 Kinase 1. *Mol Cell Biol*. 2001;21(21):7470-7480. doi:10.1128/MCB.21.21.7470-7480.2001
171. He X, Saint-Jeannet JP, Woodgett JR, Varmus HE, Dawid IB. Glycogen synthase kinase-3 and dorsoventral patterning in Xenopus embryos. *Nature*. 1995;374(6523):617-622. doi:10.1038/374617a0
172. Fitzgerald KA, McWhirter SM, Faia KL, et al. IKKε and TBK1 are essential components of the IRF3 signaling pathway. *Nat Immunol*. 2003;4(5):491-496. doi:10.1038/ni921
173. Dalton AC, Barton WA. Over-expression of secreted proteins from mammalian cell lines. *Protein Science*. 2014;23(5):517-525. doi:10.1002/pro.2439
174. Román R, Miret J, Scalia F, Casablancas A, Lecina M, Cairó JJ. Enhancing heterologous protein expression and secretion in HEK293 cells by means of combination of CMV promoter and IFNα2 signal peptide. *J Biotechnol*. 2016;239:57-60. doi:10.1016/j.jbiotec.2016.10.005

175. Sakurai H, Chiba H, Miyoshi H, Sugita T, Toriumi W. IκB Kinases Phosphorylate NF-κB p65 Subunit on Serine 536 in the Transactivation Domain. *Journal of Biological Chemistry*. 1999;274(43):30353-30356. doi:10.1074/jbc.274.43.30353
176. Lawrence T, Bebien M, Liu GY, Nizet V, Karin M. IKKα limits macrophage NF-κB activation and contributes to the resolution of inflammation. *Nature*. 2005;434(7037):1138-1143. doi:10.1038/nature03491
177. Yu H, Lin L, Zhang Z, Zhang H, Hu H. Targeting NF-κB pathway for the therapy of diseases: mechanism and clinical study. *Signal Transduct Target Ther*. 2020;5(1):209. doi:10.1038/s41392-020-00312-6
178. Anjum R, Blenis J. The RSK family of kinases: emerging roles in cellular signalling. *Nat Rev Mol Cell Biol*. 2008;9(10):747-758. doi:10.1038/nrm2509
179. Ghoda L, Lin X, Greene WC. The 90-kDa Ribosomal S6 Kinase (pp90rsk) Phosphorylates the N-terminal Regulatory Domain of IκBα and Stimulates Its Degradation in Vitro. *Journal of Biological Chemistry*. 1997;272(34):21281-21288. doi:10.1074/jbc.272.34.21281
180. Schouten GJ. Ikappa Balpha is a target for the mitogen-activated 90kDa ribosomal S6 kinase. *EMBO J*. 1997;16(11):3133-3144. doi:10.1093/emboj/16.11.3133
181. Beurel E, Grieco SF, Jope RS. Glycogen synthase kinase-3 (GSK3): Regulation, actions, and diseases. *Pharmacol Ther*. 2015;148:114-131. doi:10.1016/j.pharmthera.2014.11.016
182. Peters RT, Liao SM, Maniatis T. IKKε Is Part of a Novel PMA-Inducible IκB Kinase Complex. *Mol Cell*. 2000;5(3):513-522. doi:10.1016/S1097-2765(00)80445-1
183. Tojima Y, Fujimoto A, Delhase M, et al. NAK is an IκB kinase-activating kinase. *Nature*. 2000;404(6779):778-782. doi:10.1038/35008109
184. Hayden MS, Ghosh S. Regulation of NF-κB by TNF family cytokines. *Semin Immunol*. 2014;26(3):253-266. doi:10.1016/j.smim.2014.05.004
185. Arkin MR, Wells JA. Small-molecule inhibitors of protein–protein interactions: progressing towards the dream. *Nat Rev Drug Discov*. 2004;3(4):301-317. doi:10.1038/nrd1343
186. Azzarito V, Long K, Murphy NS, Wilson AJ. Inhibition of α-helix-mediated protein–protein interactions using designed molecules. *Nat Chem*. 2013;5(3):161-173. doi:10.1038/nchem.1568
187. Berg T. Modulation of Protein–Protein Interactions with Small Organic Molecules. *Angewandte Chemie International Edition*. 2003;42(22):2462-2481. doi:10.1002/anie.200200558
188. Wells JA, McClendon CL. Reaching for high-hanging fruit in drug discovery at protein–protein interfaces. *Nature*. 2007;450(7172):1001-1009. doi:10.1038/nature06526
189. Hodges RS, Heaton RJ, Parker JM, Molday L, Molday RS. Antigen-antibody interaction. Synthetic peptides define linear antigenic determinants recognized by monoclonal antibodies directed to the cytoplasmic carboxyl terminus of rhodopsin. *J Biol Chem*. 1988;263(24):11768-11775.
190. Suryadevara N, Shrihari S, Gilchuk P, et al. Neutralizing and protective human monoclonal antibodies recognizing the N-terminal domain of the SARS-CoV-2 spike protein. *Cell*. 2021;184(9):2316-2331.e15. doi:10.1016/j.cell.2021.03.029

191. Lian W, Upadhyaya P, Rhodes CA, Liu Y, Pei D. Screening Bicyclic Peptide Libraries for Protein–Protein Interaction Inhibitors: Discovery of a Tumor Necrosis Factor-α Antagonist. *J Am Chem Soc*. 2013;135(32):11990-11995. doi:10.1021/ja405106u
192. Cunningham AD, Qvit N, Mochly-Rosen D. Peptides and peptidomimetics as regulators of protein–protein interactions. *Curr Opin Struct Biol*. 2017;44:59-66. doi:10.1016/j.sbi.2016.12.009
193. Bruzzoni-Giovanelli H, Alezra V, Wolff N, Dong CZ, Tuffery P, Rebollo A. Interfering peptides targeting protein–protein interactions: the next generation of drugs? *Drug Discov Today*. 2018;23(2):272-285. doi:10.1016/j.drudis.2017.10.016
194. Sun Y, Xu Y, Roy K, Price BD. DNA Damage-Induced Acetylation of Lysine 3016 of ATM Activates ATM Kinase Activity. *Mol Cell Biol*. 2007;27(24):8502-8509. doi:10.1128/MCB.01382-07
195. Sanguigno L, Guida N, Anzilotti S, et al. Stroke by inducing HDAC9-dependent deacetylation of HIF-1 and Sp1, promotes TfR1 transcription and GPX4 reduction, thus determining ferroptotic neuronal death. *Int J Biol Sci*. 2023;19(9):2695-2710. doi:10.7150/ijbs.80735
196. Iaconelli J, Lalonde J, Watmuff B, et al. Lysine Deacetylation by HDAC6 Regulates the Kinase Activity of AKT in Human Neural Progenitor Cells. *ACS Chem Biol*. 2017;12(8):2139-2148. doi:10.1021/acschembio.6b01014
197. Sundaresan NR, Pillai VB, Wolfgeher D, et al. The Deacetylase SIRT1 Promotes Membrane Localization and Activation of Akt and PDK1 During Tumorigenesis and Cardiac Hypertrophy. *Sci Signal*. 2011;4(182). doi:10.1126/scisignal.2001465
198. Zhong H, Voll RE, Ghosh S. Phosphorylation of NF-κB p65 by PKA Stimulates Transcriptional Activity by Promoting a Novel Bivalent Interaction with the Coactivator CBP/p300. *Mol Cell*. 1998;1(5):661-671. doi:10.1016/S1097-2765(00)80066-0
199. Richmond A. NF-κB, chemokine gene transcription and tumour growth. *Nat Rev Immunol*. 2002;2(9):664-674. doi:10.1038/nri887
200. Bu Y, Cai G, Shen Y, et al. Targeting NF-κB RelA/p65 phosphorylation overcomes RITA resistance. *Cancer Lett*. 2016;383(2):261-271. doi:10.1016/j.canlet.2016.10.006
201. Sutcliffe AM, Clarke DL, Bradbury DA, Corbett LM, Patel JA, Knox AJ. Transcriptional regulation of monocyte chemotactic protein-1 release by endothelin-1 in human airway smooth muscle cells involves NF-κB and AP-1. *Br J Pharmacol*. 2009;157(3):436-450. doi:10.1111/j.1476-5381.2009.00143.x
202. Bolognesi B, Lehner B. Reaching the limit. *Elife*. 2018;7. doi:10.7554/eLife.39804
203. Geiler-Samerotte KA, Dion MF, Budnik BA, Wang SM, Hartl DL, Drummond DA. Misfolded proteins impose a dosage-dependent fitness cost and trigger a cytosolic unfolded protein response in yeast. *Proceedings of the National Academy of Sciences*. 2011;108(2):680-685. doi:10.1073/pnas.1017570108
204. Eguchi Y, Makanae K, Hasunuma T, Ishibashi Y, Kito K, Moriya H. Estimating the protein burden limit of yeast cells by measuring the expression limits of glycolytic proteins. *Elife*. 2018;7. doi:10.7554/eLife.34595

205. Stoebel DM, Dean AM, Dykhuizen DE. The Cost of Expression of Escherichia coli lac Operon Proteins Is in the Process, Not in the Products. *Genetics*. 2008;178(3):1653-1660. doi:10.1534/genetics.107.085399
206. Vavouri T, Semple JI, Garcia-Verdugo R, Lehner B. Intrinsic Protein Disorder and Interaction Promiscuity Are Widely Associated with Dosage Sensitivity. *Cell*. 2009;138(1):198-208. doi:10.1016/j.cell.2009.04.029
207. Papp B, Pál C, Hurst LD. Dosage sensitivity and the evolution of gene families in yeast. *Nature*. 2003;424(6945):194-197. doi:10.1038/nature01771
208. Xu C, Tang J, Yang Q, et al. Histone deacetylase 5 deacetylates the phosphatase PP2A for positively regulating NF-κB signaling. *Journal of Biological Chemistry*. 2021;297(6):101380. doi:10.1016/j.jbc.2021.101380
209. Ye J, Zhong S, Deng Y, et al. HDAC7 Activates IKK/NF-κB Signaling to Regulate Astrocyte-Mediated Inflammation. *Mol Neurobiol*. 2022;59(10):6141-6157. doi:10.1007/s12035-022-02965-6
210. Choi JH, Nam KH, Kim J, et al. Trichostatin A Exacerbates Atherosclerosis in Low Density Lipoprotein Receptor–Deficient Mice. *Arterioscler Thromb Vasc Biol*. 2005;25(11):2404-2409. doi:10.1161/01.ATV.0000184758.07257.88
211. Zhang W, Guan Y, Bayliss G, Zhuang S. Class IIa HDAC inhibitor TMP195 alleviates lipopolysaccharide-induced acute kidney injury. *American Journal of Physiology-Renal Physiology*. 2020;319(6):F1015-F1026. doi:10.1152/ajprenal.00405.2020
212. Chen X, Li C, Zhao J, et al. mPPTMP195 nanoparticles enhance fracture recovery through HDAC4 nuclear translocation inhibition. *J Nanobiotechnology*. 2024;22(1):261. doi:10.1186/s12951-024-02436-1